Electronic Supplementary Information

Phosphorescent Cyclometalated Ir(III) Complexes Comprising Chelating Thiolate Ligands as pH-Activatable Sensors

Sareh Paziresh,[a] Reza Babadi Aghakhanpour,[a,b] Hamid R. Shahsavari,*[a] Vahideh Dolatyari,[a] Irene Ara,[c] and S. Masoud Nabavizadeh*[b]

[a]Department of Chemistry, Institute for Advanced Studies in Basic Sciences (IASBS), Zanjan 45137-66731, Iran. *E-mail: shahsavari@iasbs.ac.ir.

[b]Professor Rashidi Laboratory of Organometallic Chemistry, Department of Chemistry, College of Sciences, Shiraz University, Shiraz 71467-13565, Iran. *E-mail: nabavizadeh@shirazu.ac.ir.

[c]Departamento de Química Inorgánica, Facultad de Ciencias, Instituto de Síntesis Química y Catálisis Homogénea (ISQCH), CSIC - Universidad de Zaragoza, Pedro Cerbuna 12, 50009 Zaragoza, Spain.

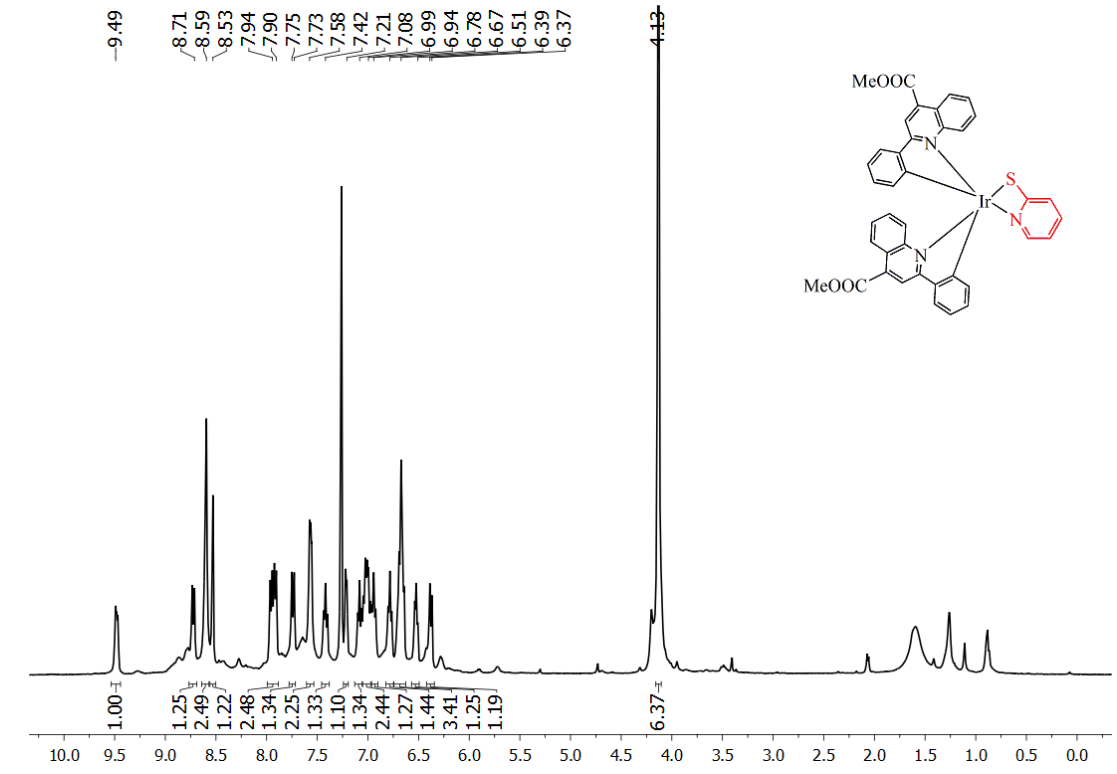

Figure S1. ^{1}H NMR spectrum of **B1** in $CDCl_3$.

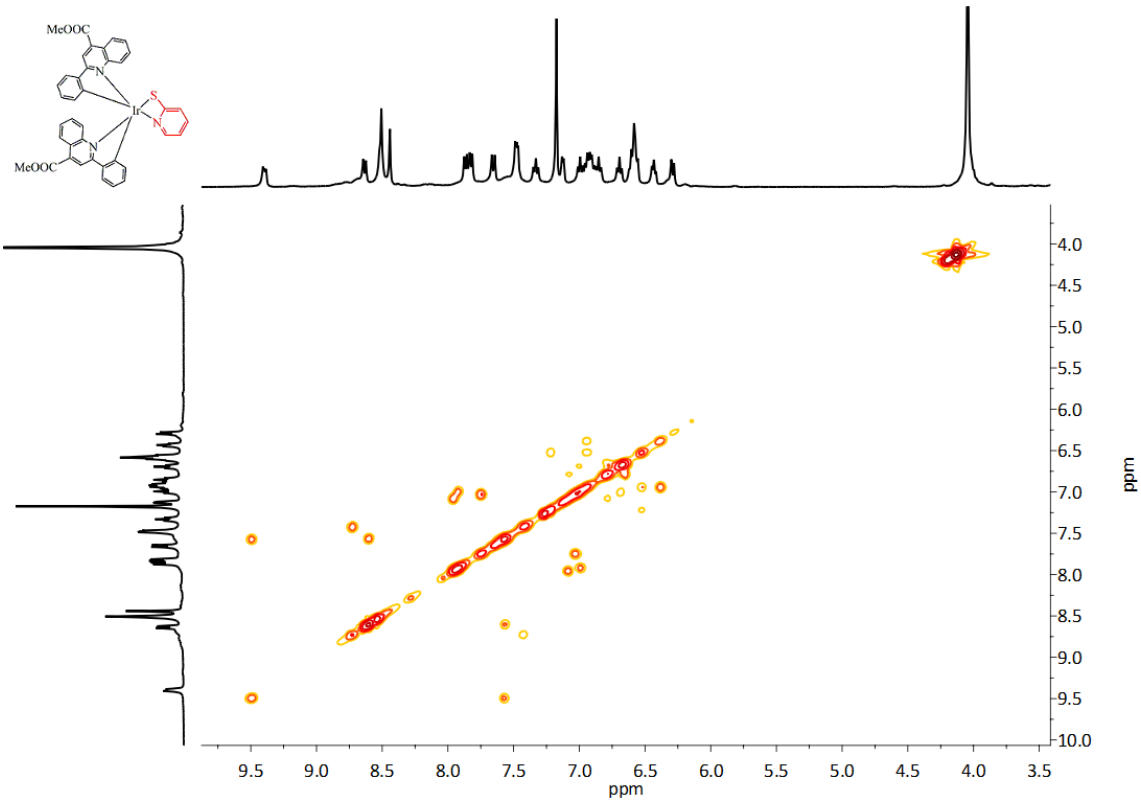

Figure S2. ^{1}H^{1}H COSY NMR spectrum of **B1** in $CDCl_3$.

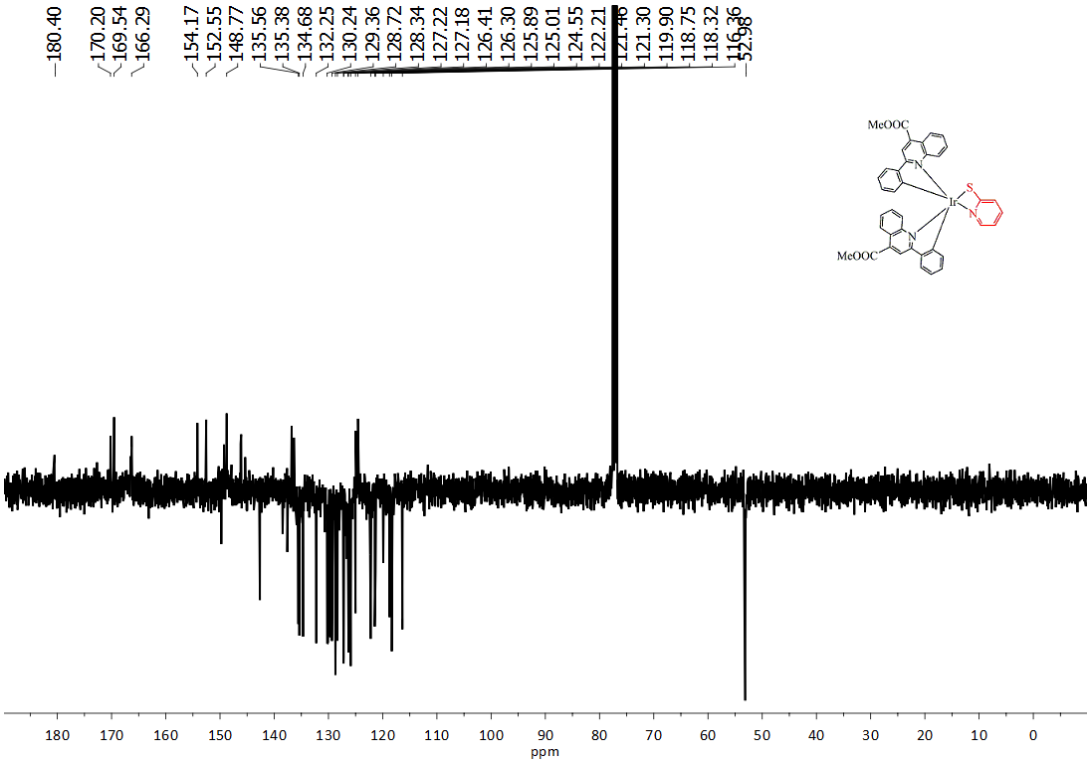

Figure S3. $^{13}C\{^{1}H\}$ APT NMR spectrum of **B1** in $CDCl_3$.

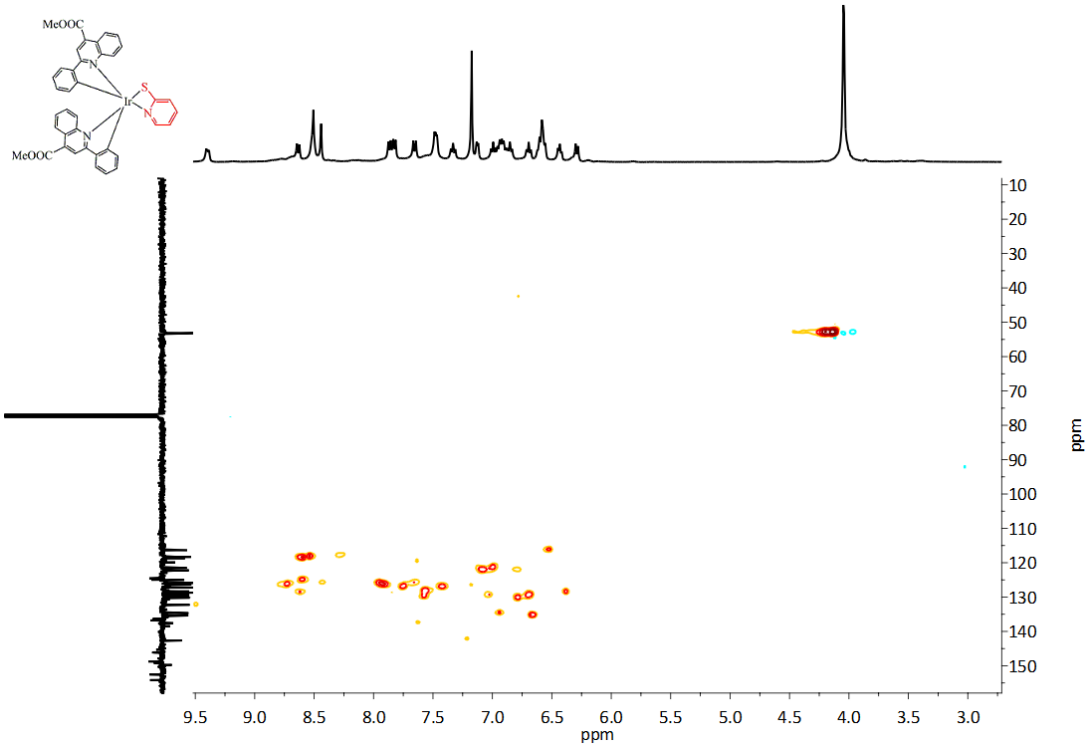

Figure S4. HSQC NMR spectrum of **B1** in $CDCl_3$.

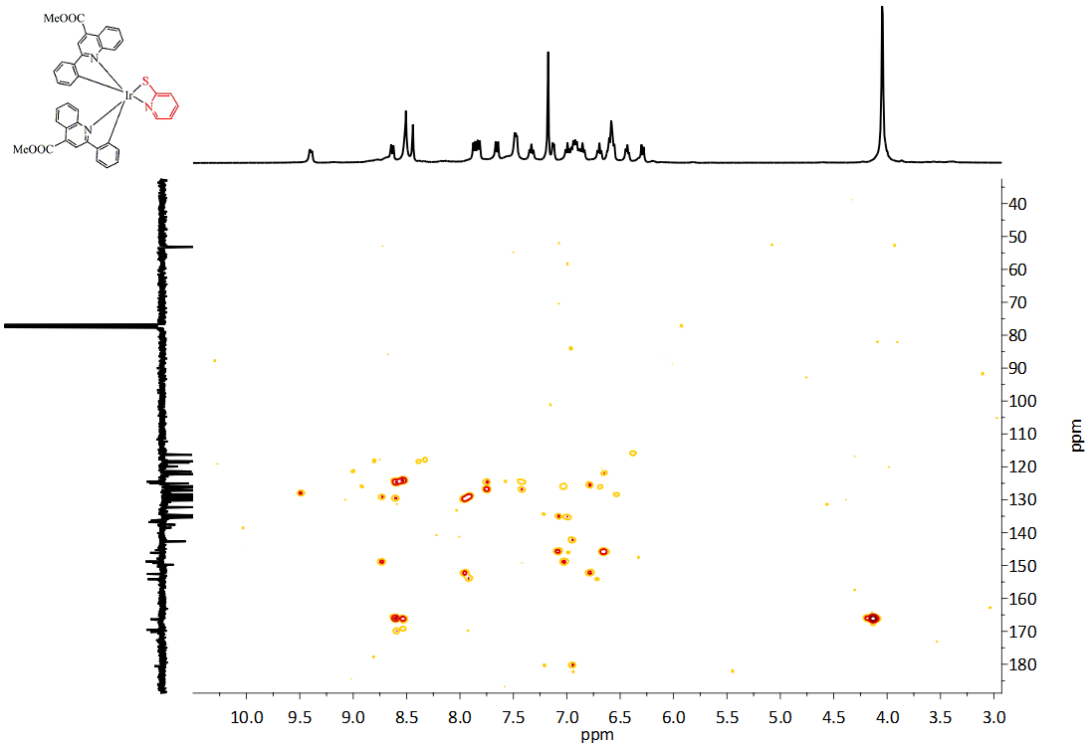

Figure S5. HMBC NMR spectrum of **B1** in $CDCl_3$.

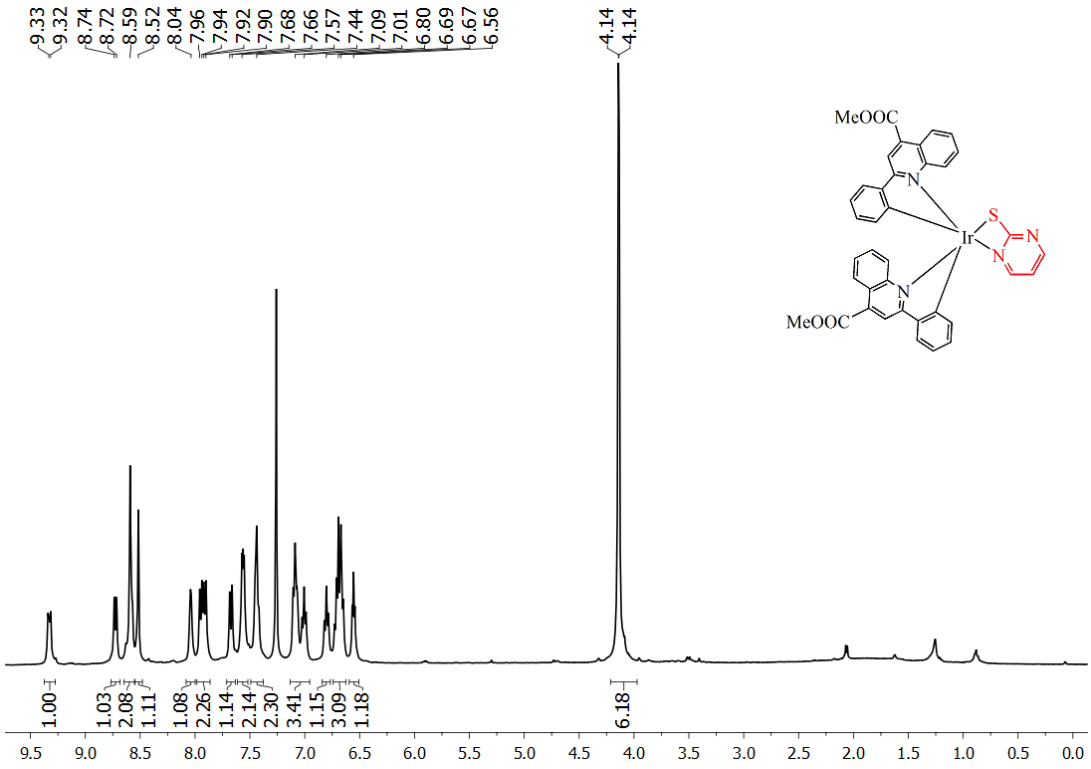

Figure S6. ^1H NMR spectrum of **B2** in $CDCl_3$.

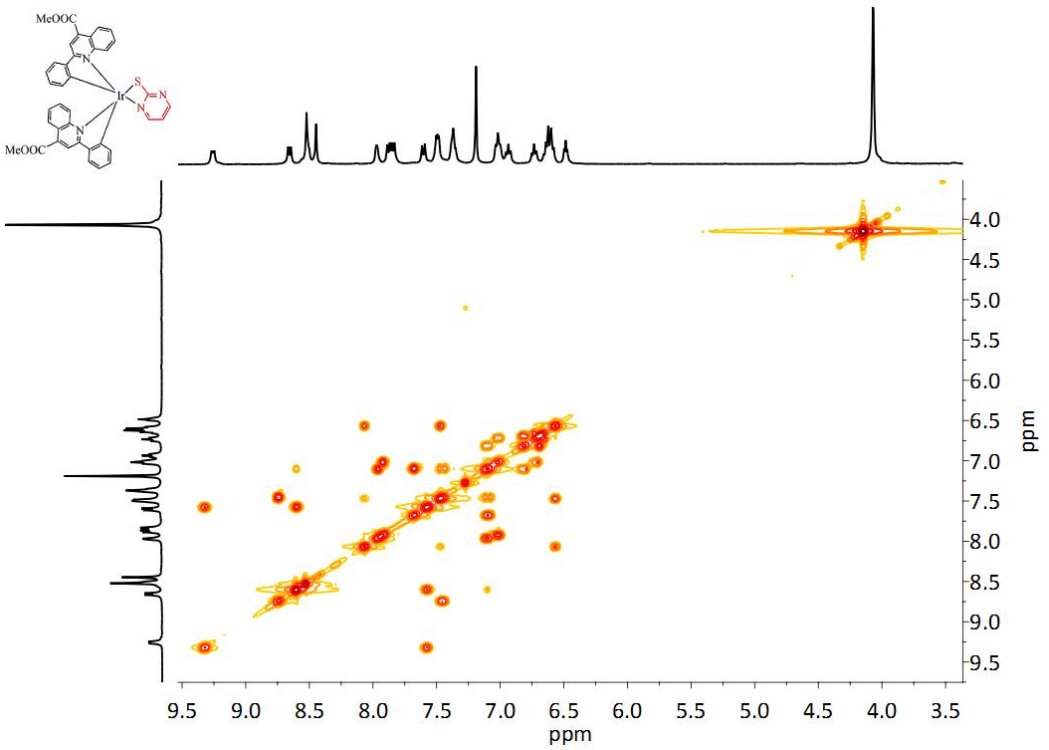

Figure S7. $^{1}H^{1}H$ COSY NMR spectrum of **B2** in $CDCl_3$.

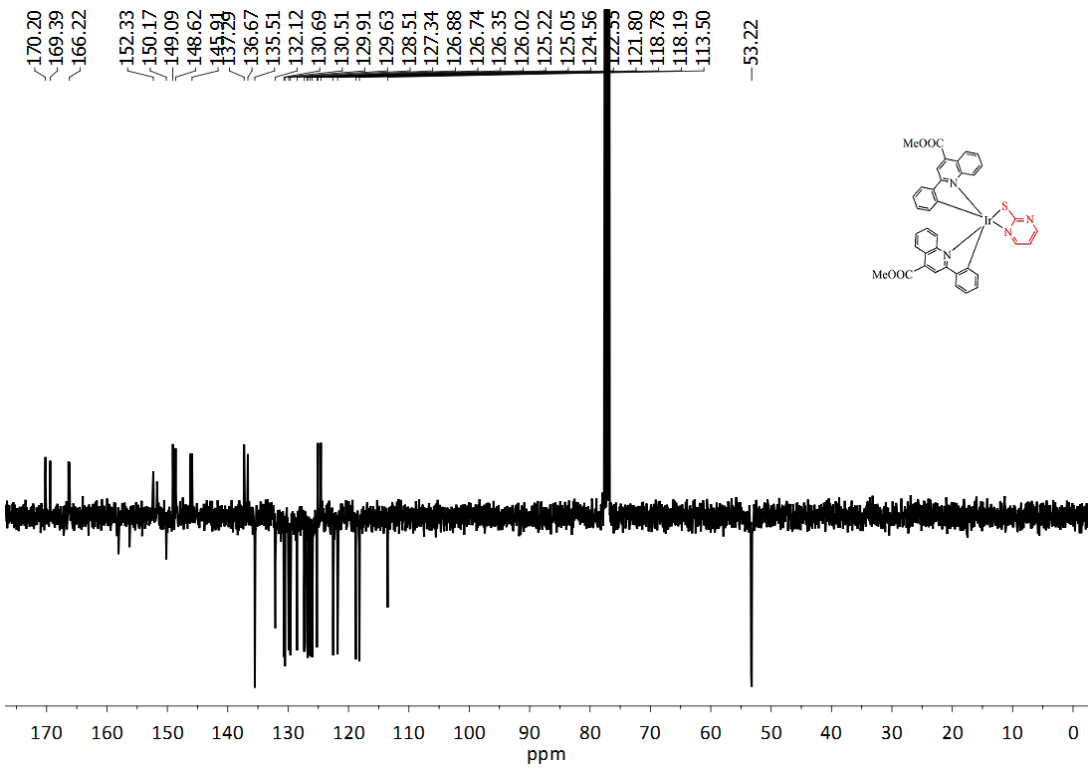

Figure S8. $^{13}C\{^{1}H\}$ APT NMR spectrum of **B2** in $CDCl_3$.

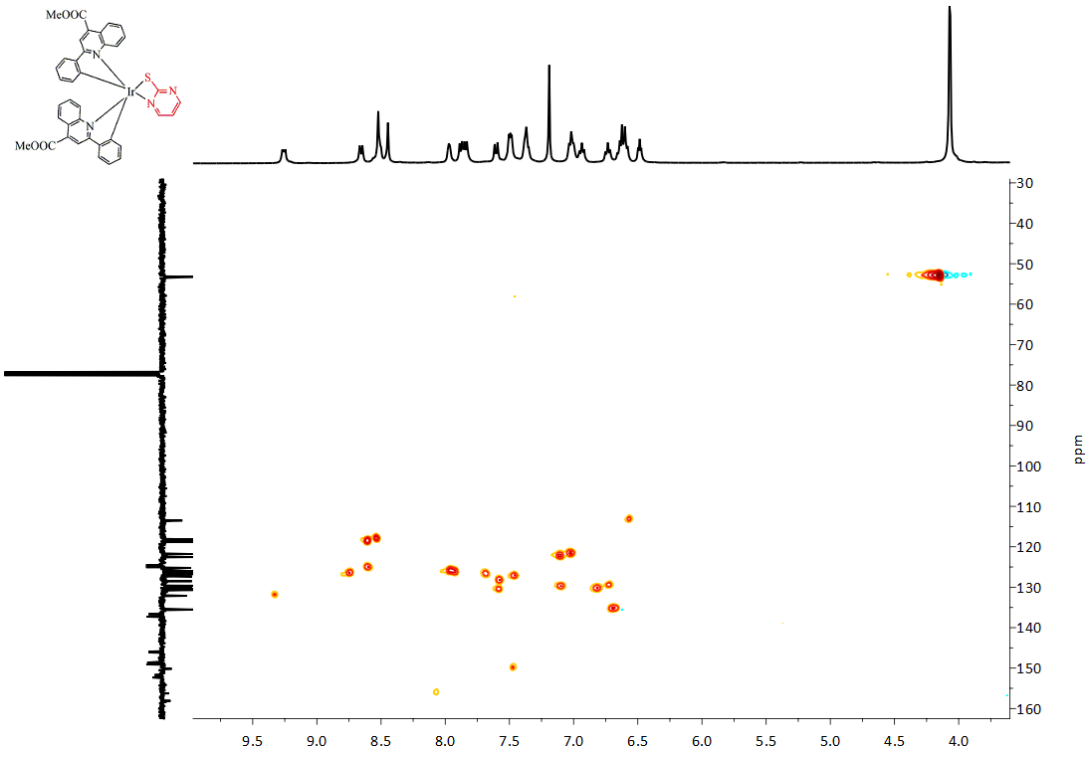

Figure S9. HSQC NMR spectrum of **B2** in $CDCl_3$.

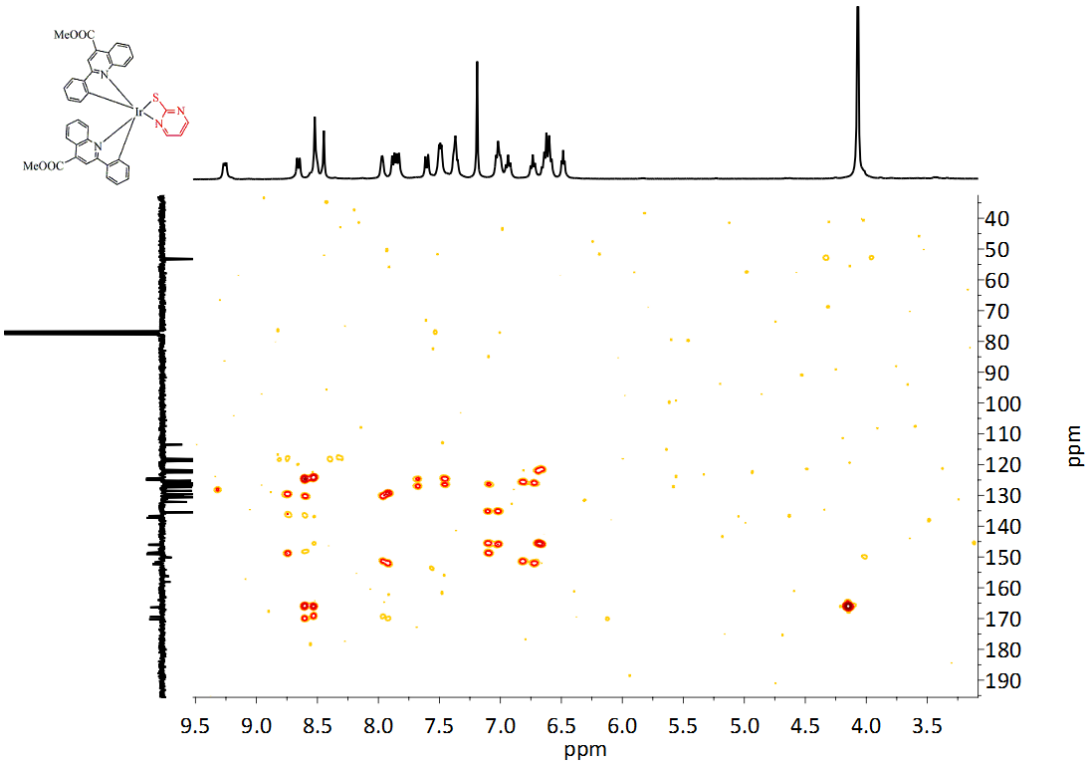

Figure S10. HMBC NMR spectrum of **B2** in $CDCl_3$.

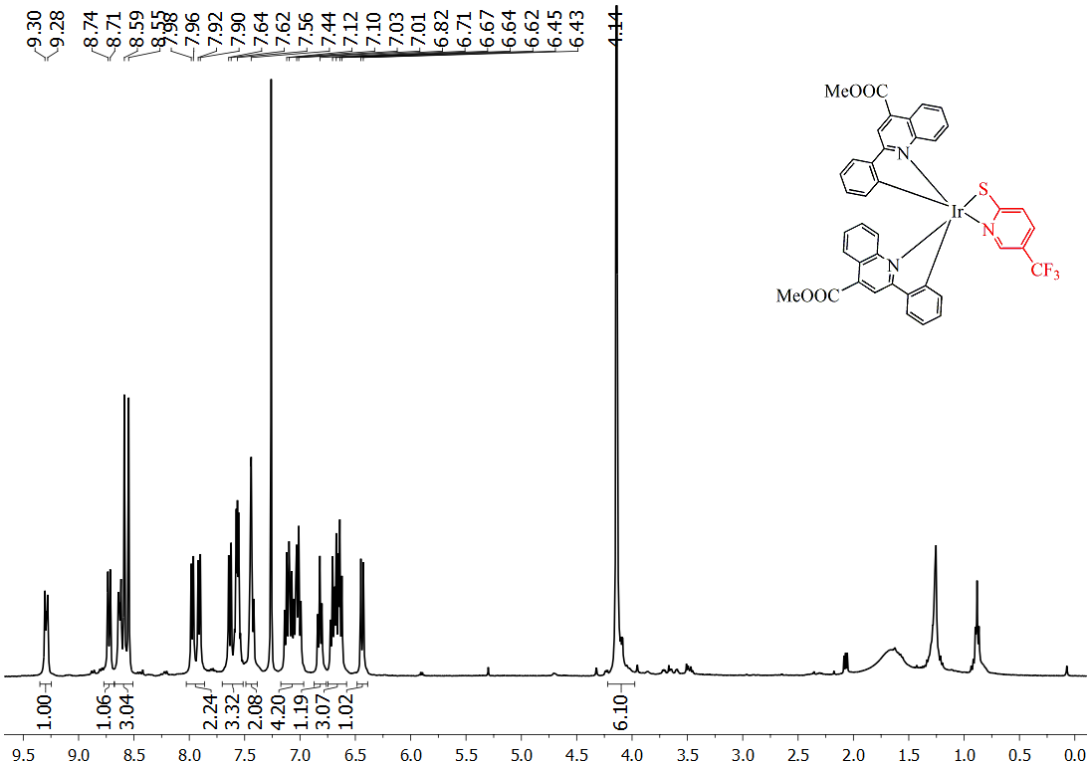

Figure S11. ^{1}H NMR spectrum of **B3** in $CDCl_3$.

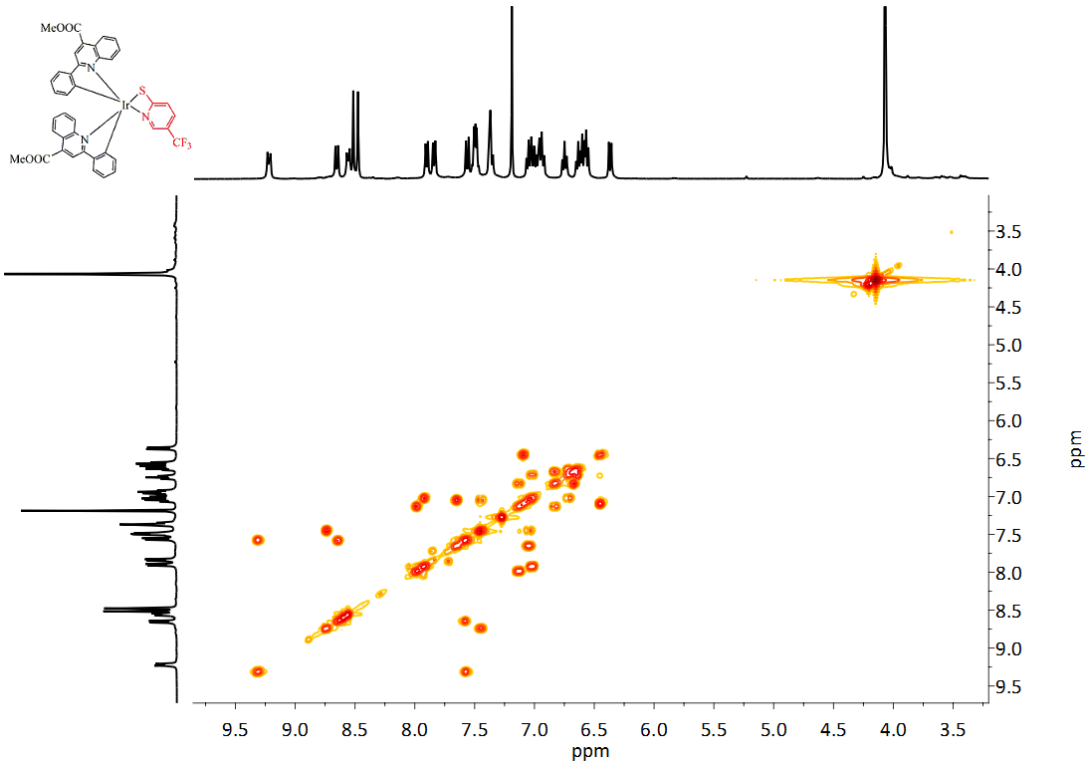

Figure S12. ^{1}H^{1}H COSY NMR spectrum of **B3** in $CDCl_3$.

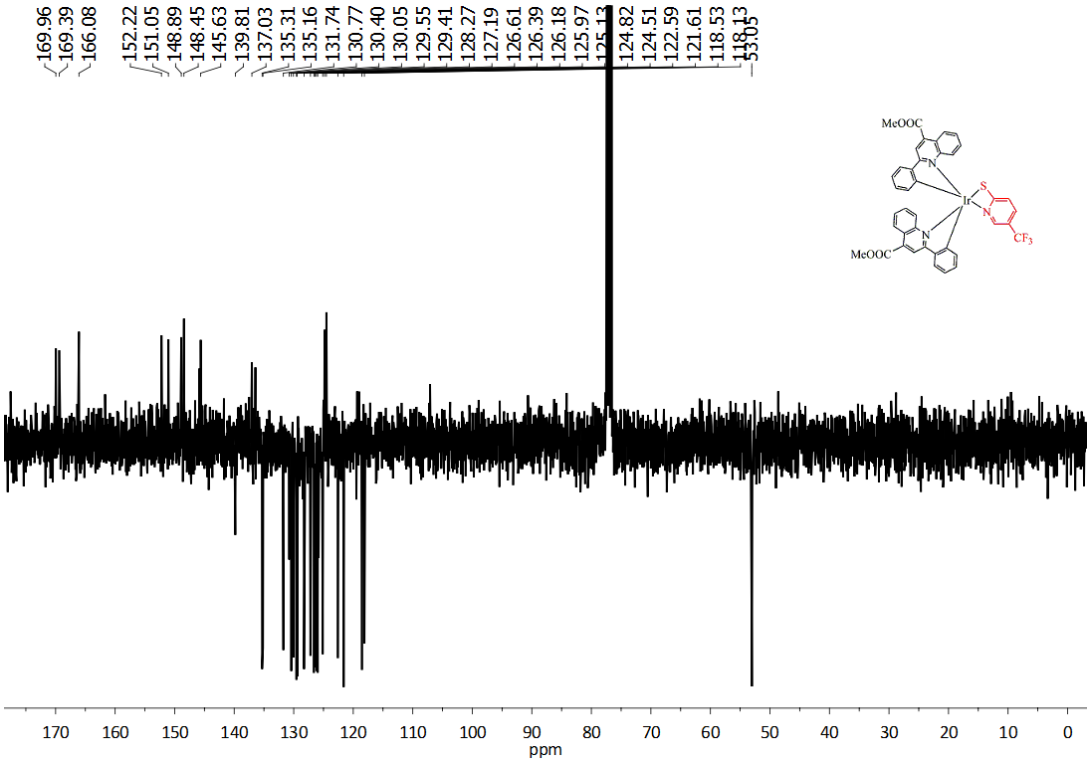

Figure S13. $^{13}C\{^{1}H\}$ APT NMR spectrum of **B3** in $CDCl_3$.

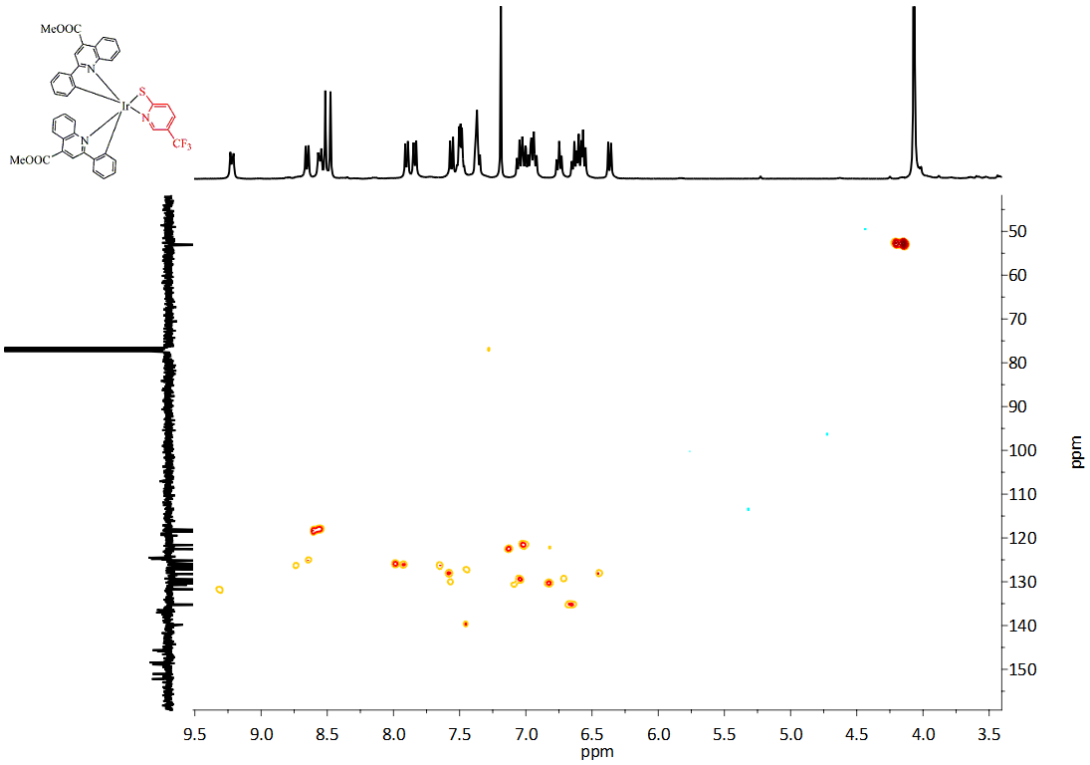

Figure S14. HSQC NMR spectrum of **B3** in $CDCl_3$.

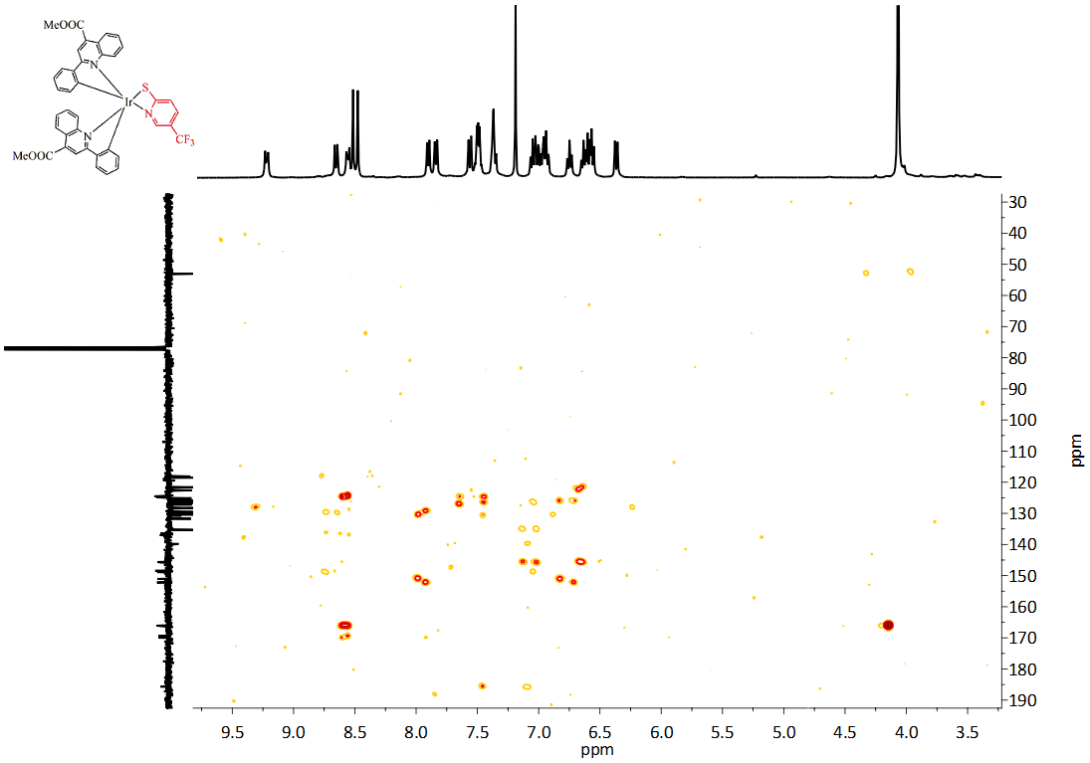

Figure S15. HMBC NMR spectrum of **B3** in $CDCl_3$.

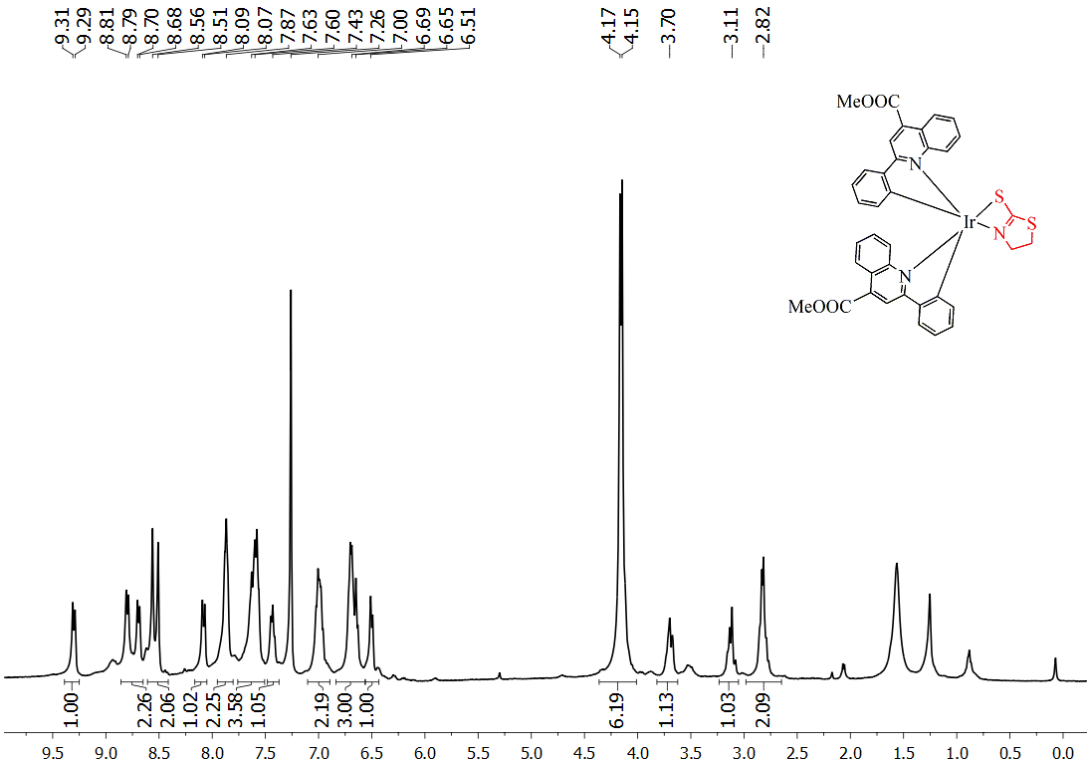

Figure S16. ^1H NMR spectrum of **B4** in $CDCl_3$.

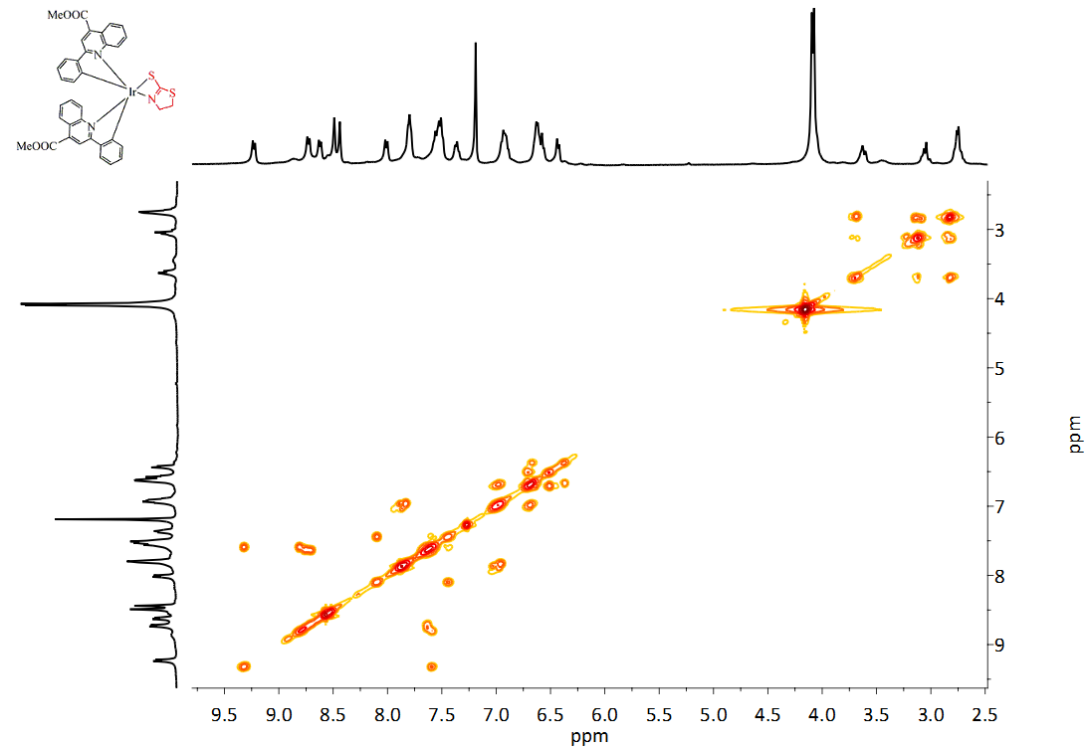

Figure S17. $^{1}H^{1}H$ COSY NMR spectrum of **B4** in $CDCl_3$.

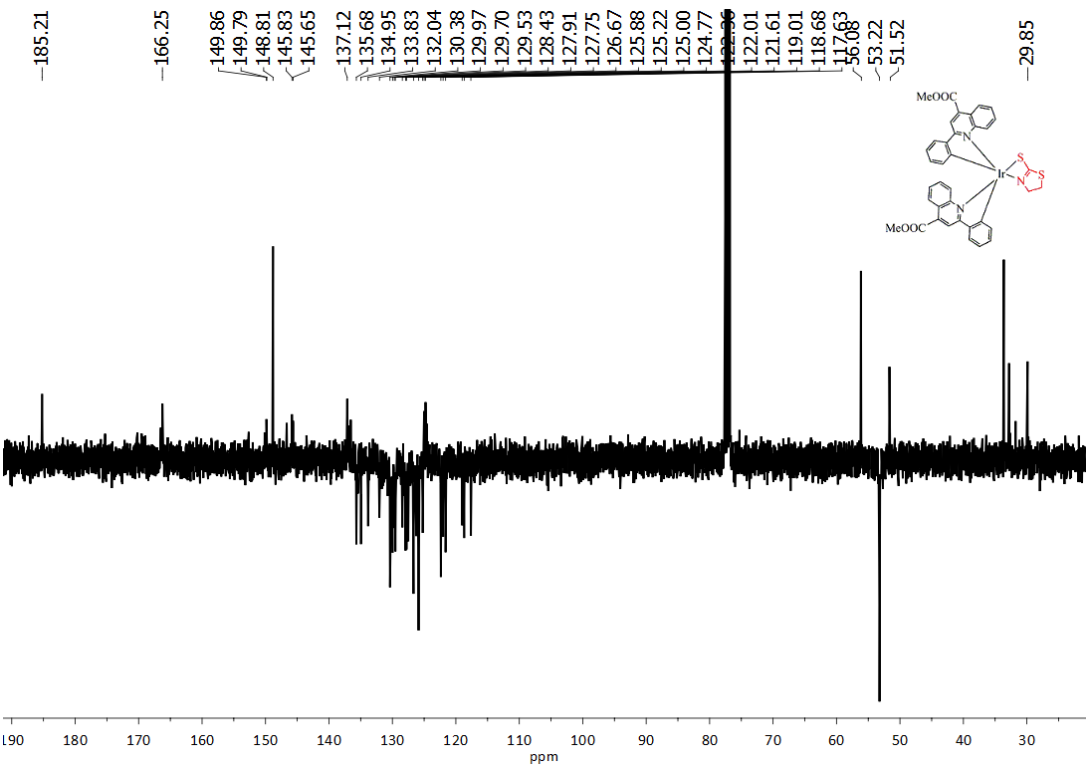

Figure S18. $^{13}C\{^{1}H\}$ APT NMR spectrum of **B4** in $CDCl_3$.

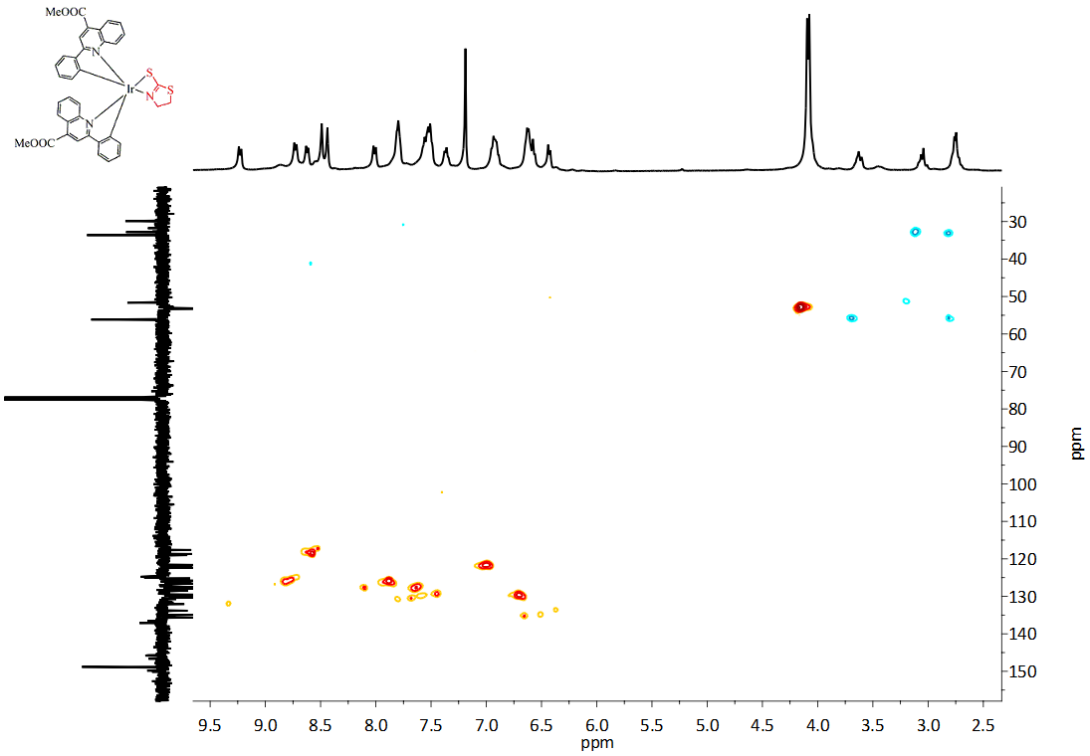

Figure S19. HSQC NMR spectrum of **B4** in $CDCl_3$.

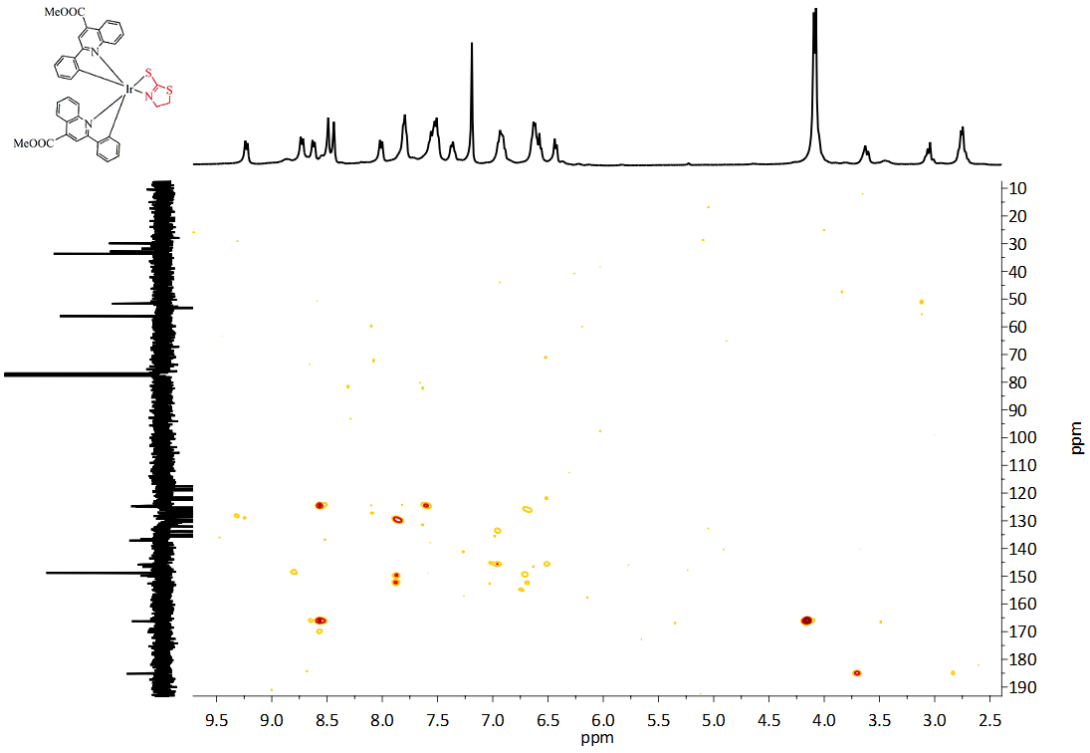

Figure S20. HMBC NMR spectrum of **B4** in $CDCl_3$.

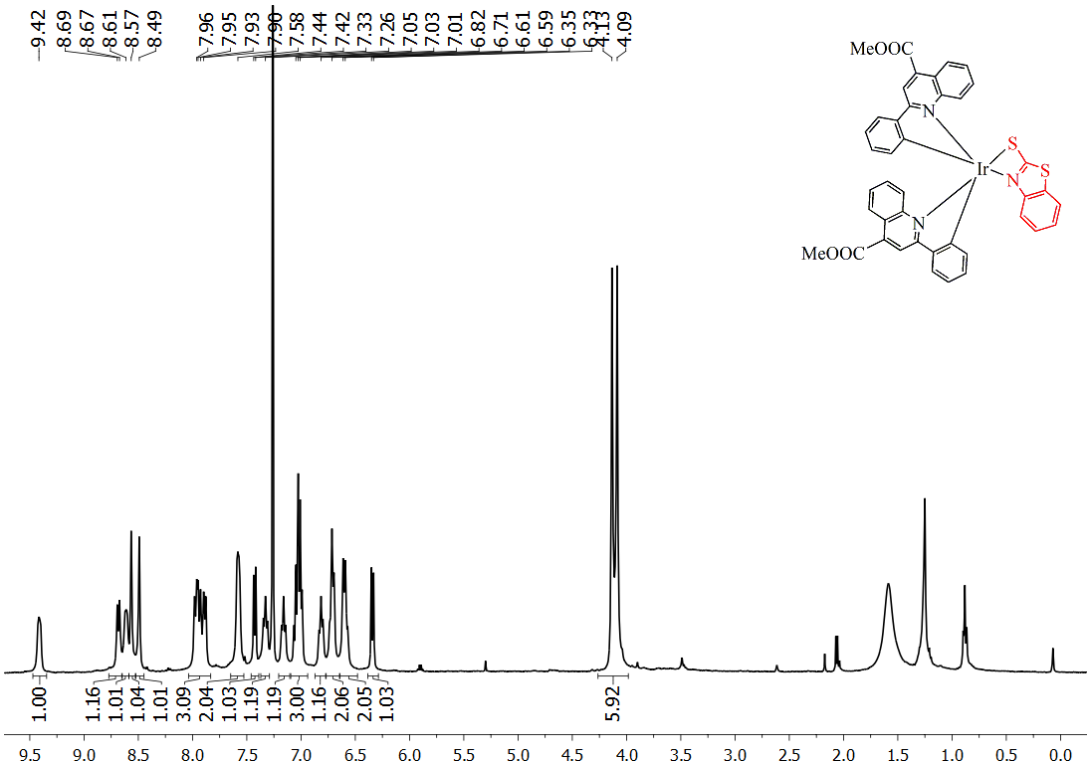

Figure S21. ^{1}H NMR spectrum of **B5** in $CDCl_3$.

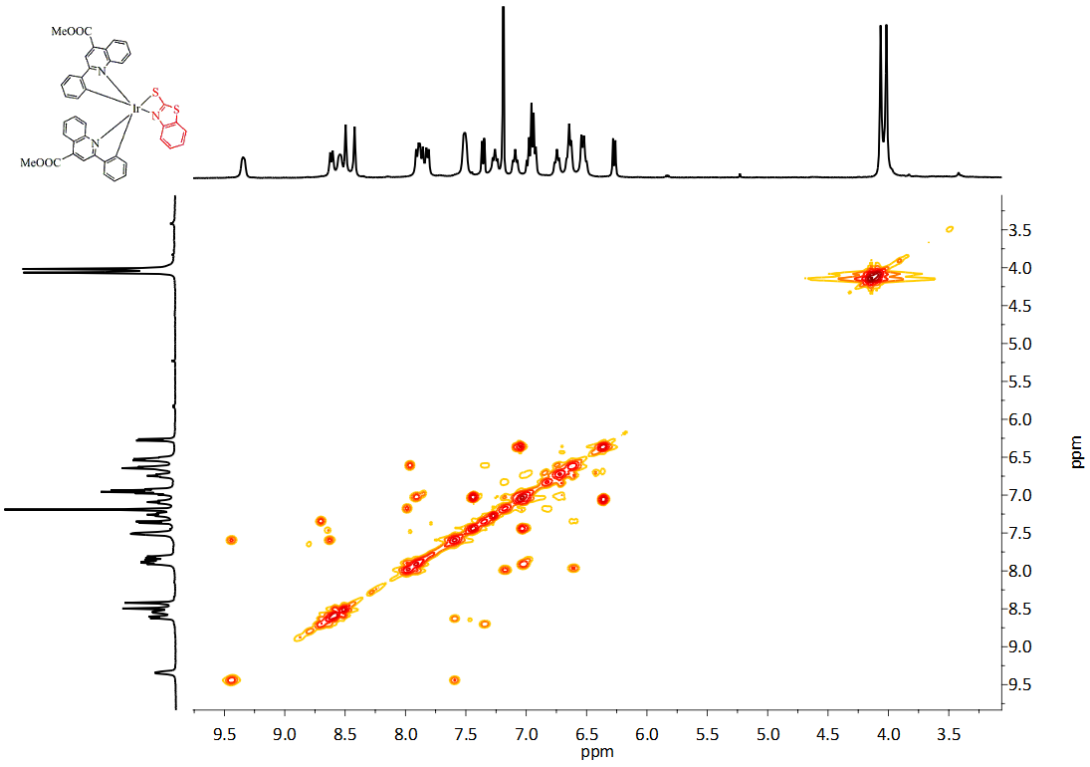

Figure S22. $^{1}H^{1}H$ COSY NMR spectrum of **B5** in $CDCl_3$.

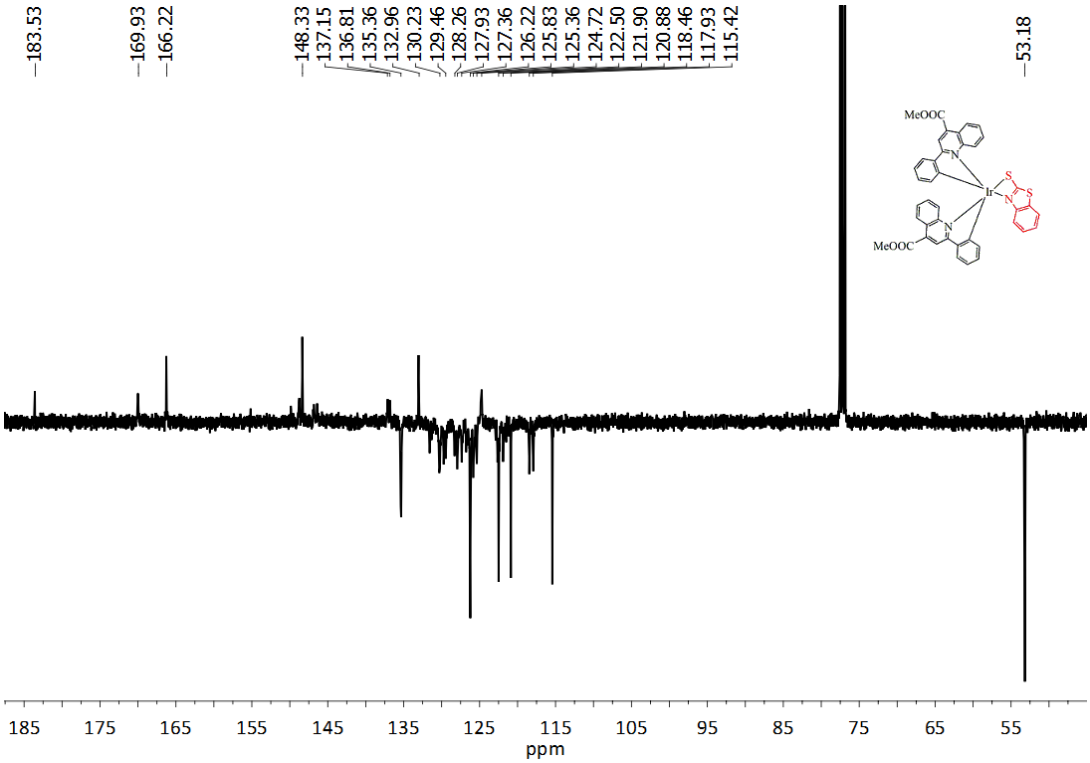

Figure S23. $^{13}C\{^{1}H\}$ APT NMR spectrum of **B5** in $CDCl_3$.

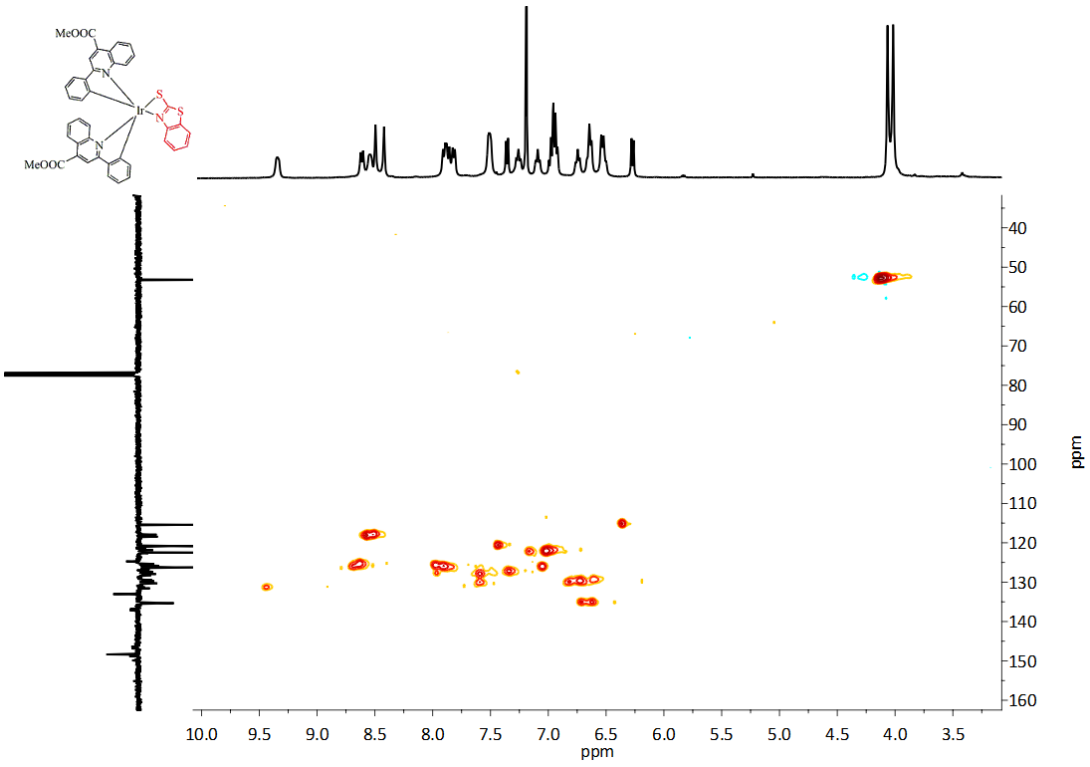

Figure S24. HSQC NMR spectrum of **B5** in $CDCl_3$.

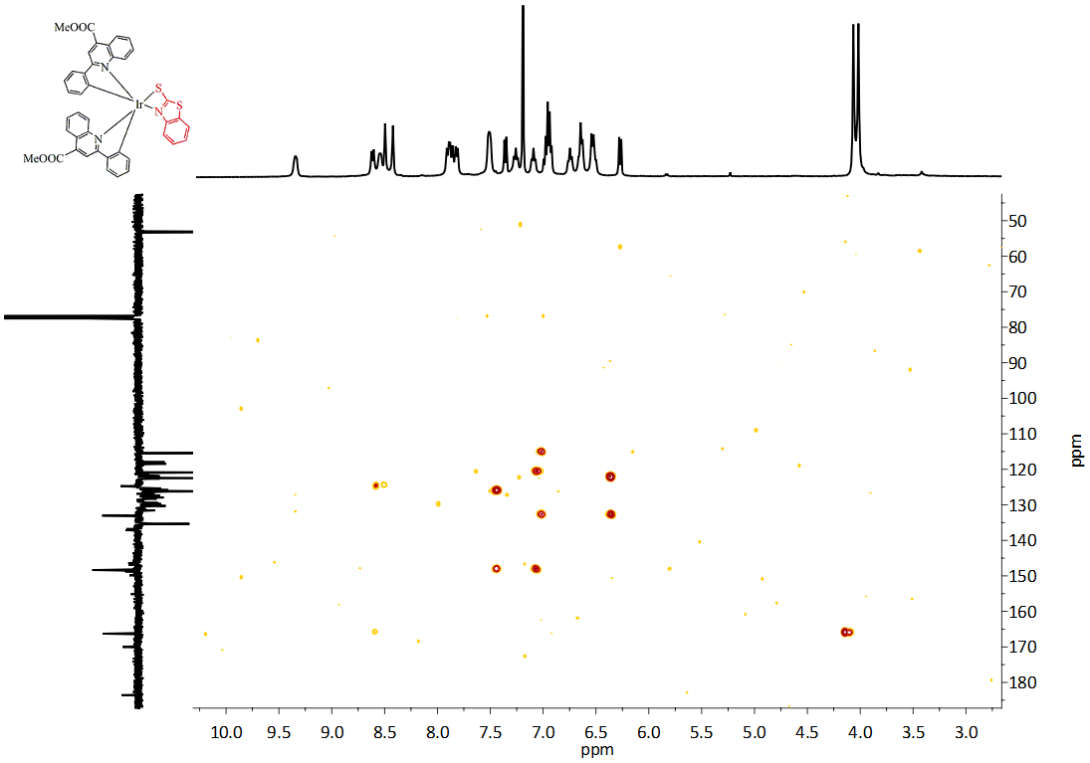

Figure S25. HMBC NMR spectrum of **B5** in $CDCl_3$.

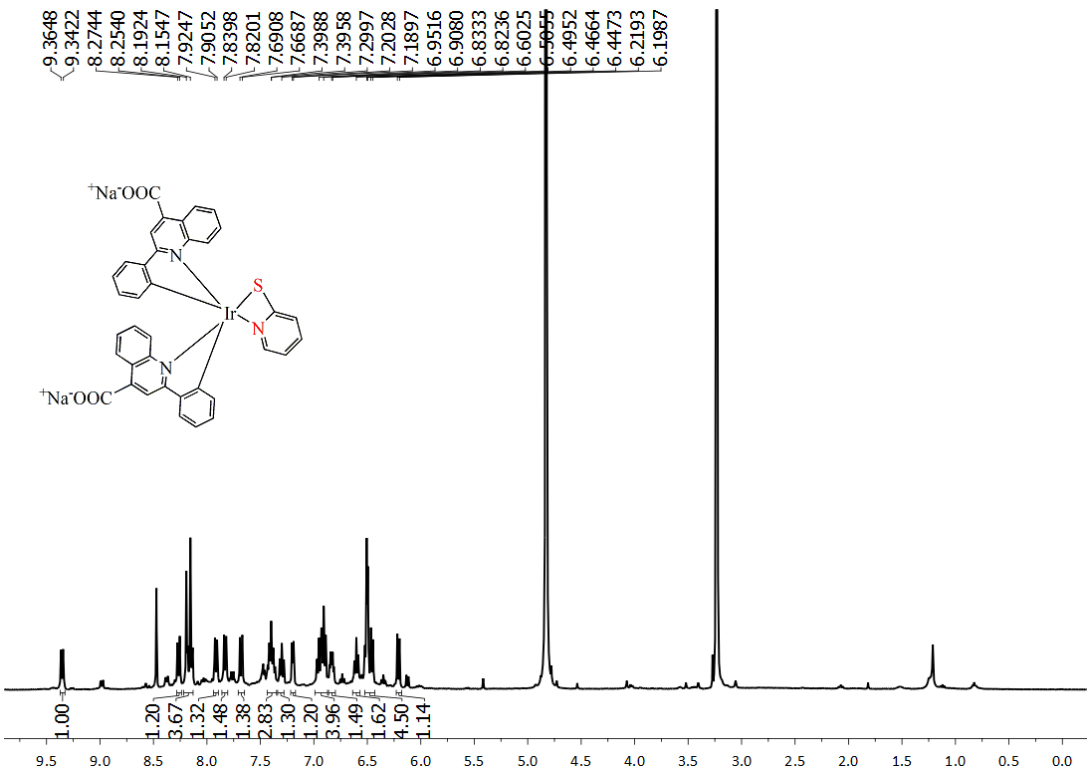

Figure S26. ^{1}H NMR spectrum of **C1** in CD_3OD-d_4.

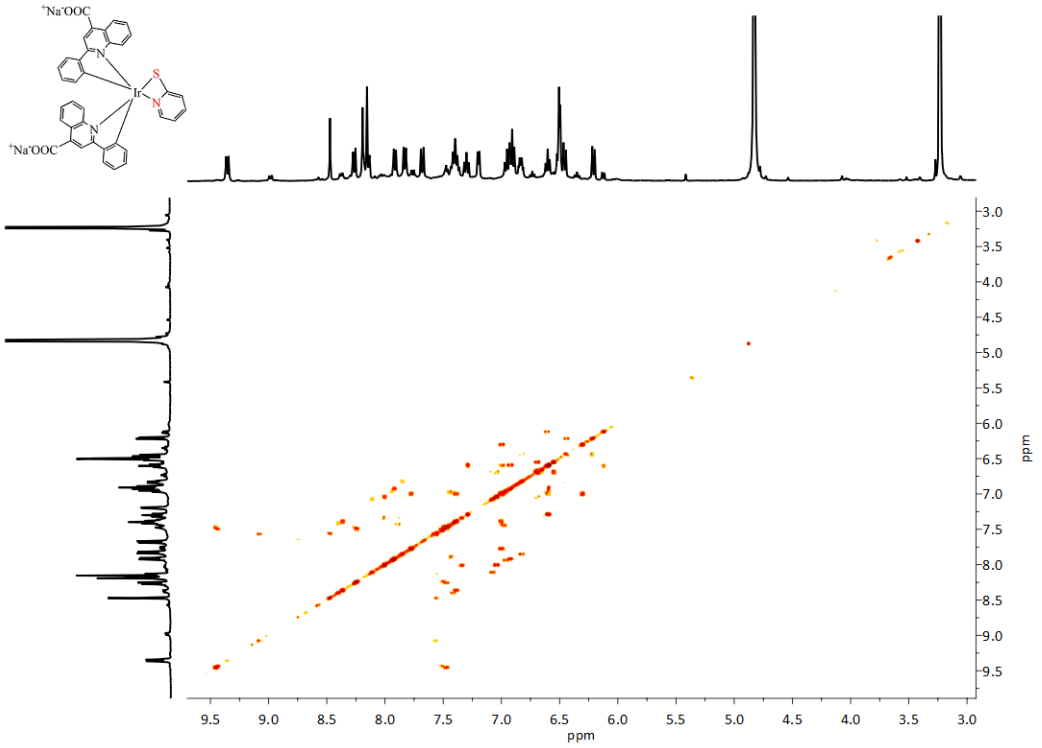

Figure S27. $^{1}H^{1}H$ COSY NMR spectrum of **C1** in CD_3OD-d_4.

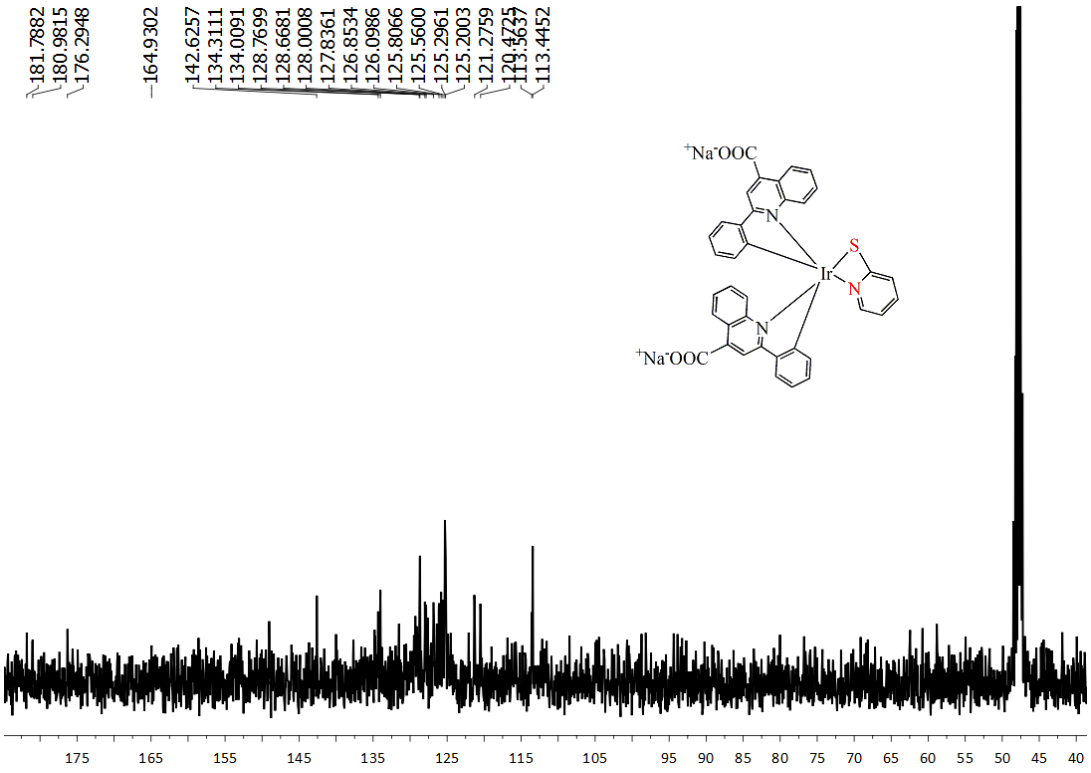

Figure S28. $^{13}C\{^{1}H\}$ NMR spectrum of **C1** in CD_3OD-d_4.

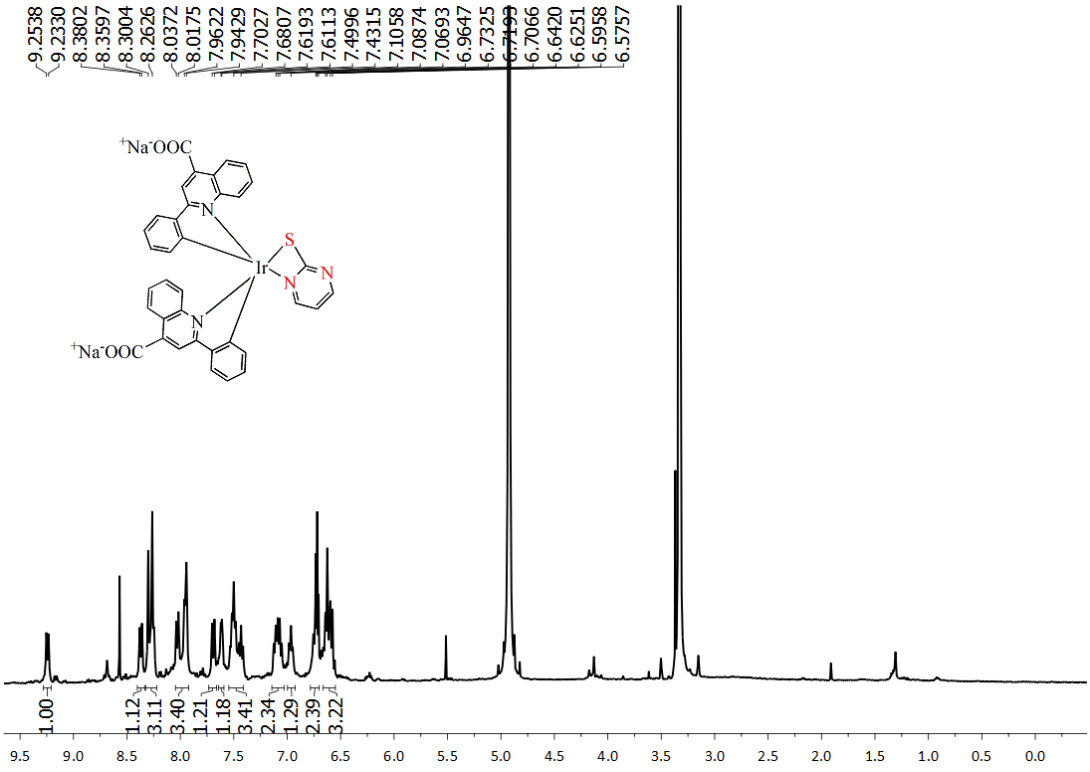

Figure S29. ^{1}H NMR spectrum of **C2** in CD_3OD-d_4.

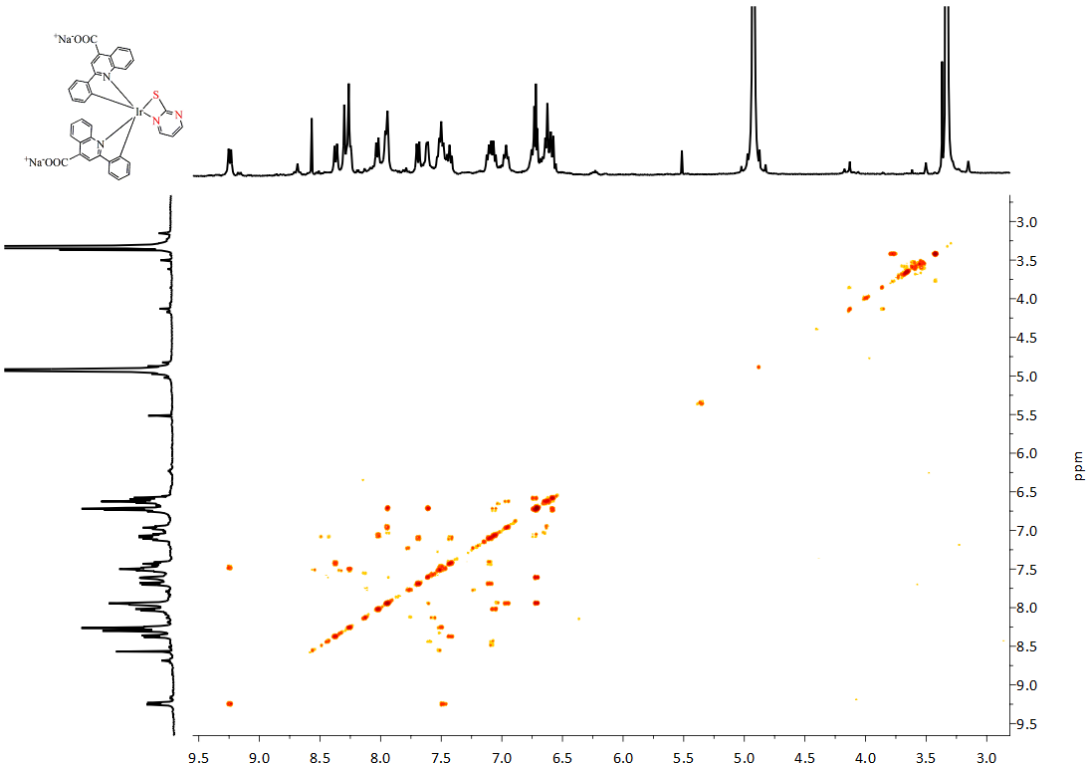

Figure S30. ^{1}H^{1}H COSY NMR spectrum of **C2** in CD_3OD-d_4.

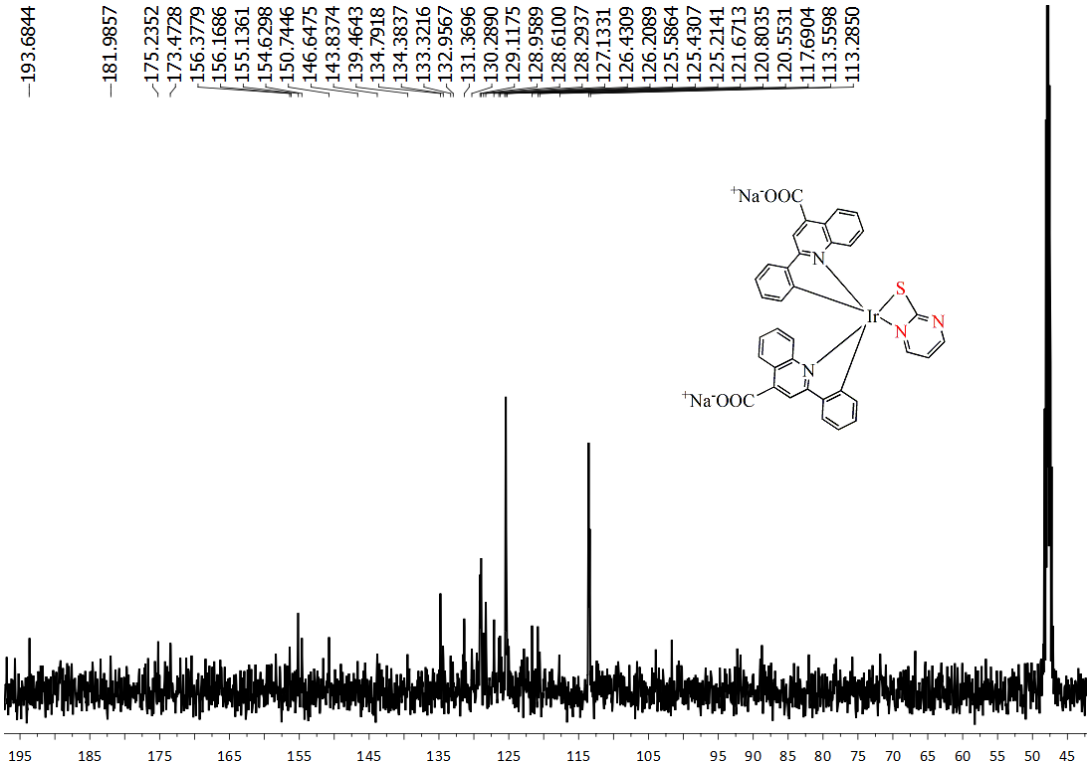

Figure S31. $^{13}C\{^{1}H\}$ NMR spectrum of **C2** in CD_3OD-d_4.

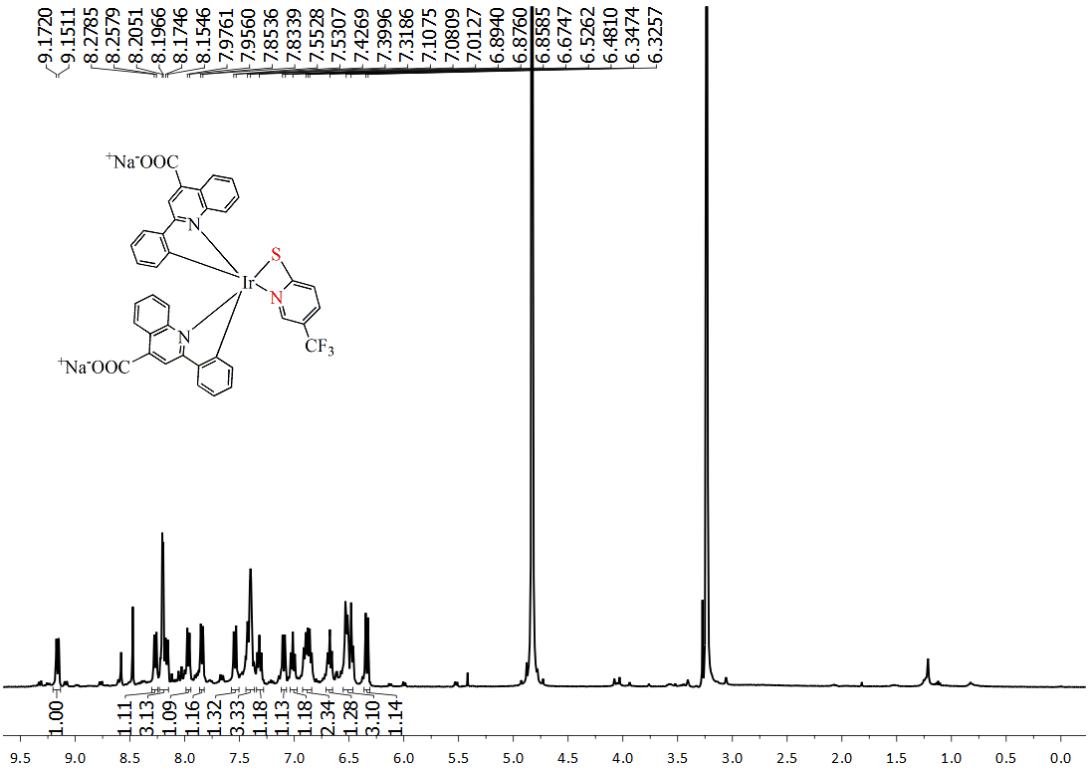

Figure S32. ^{1}H NMR spectrum of **C3** in CD_3OD-d_4.

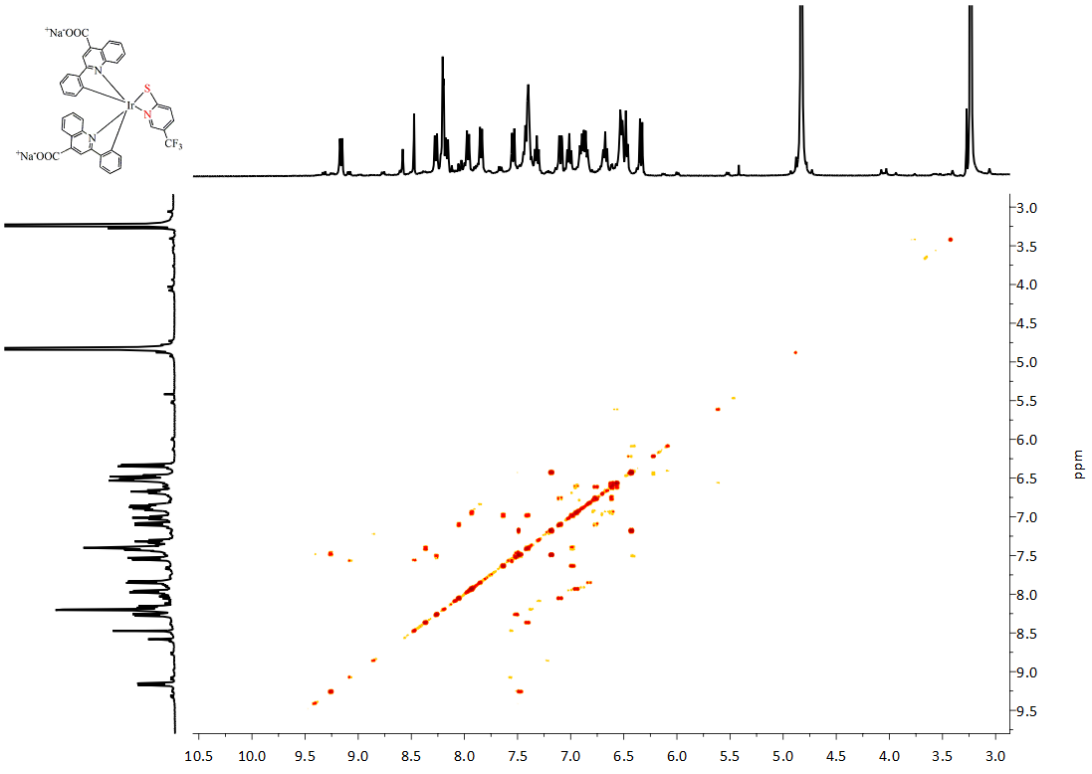

Figure S33. $^{1}H^{1}H$ COSY NMR spectrum of **C3** in CD_3OD-d_4.

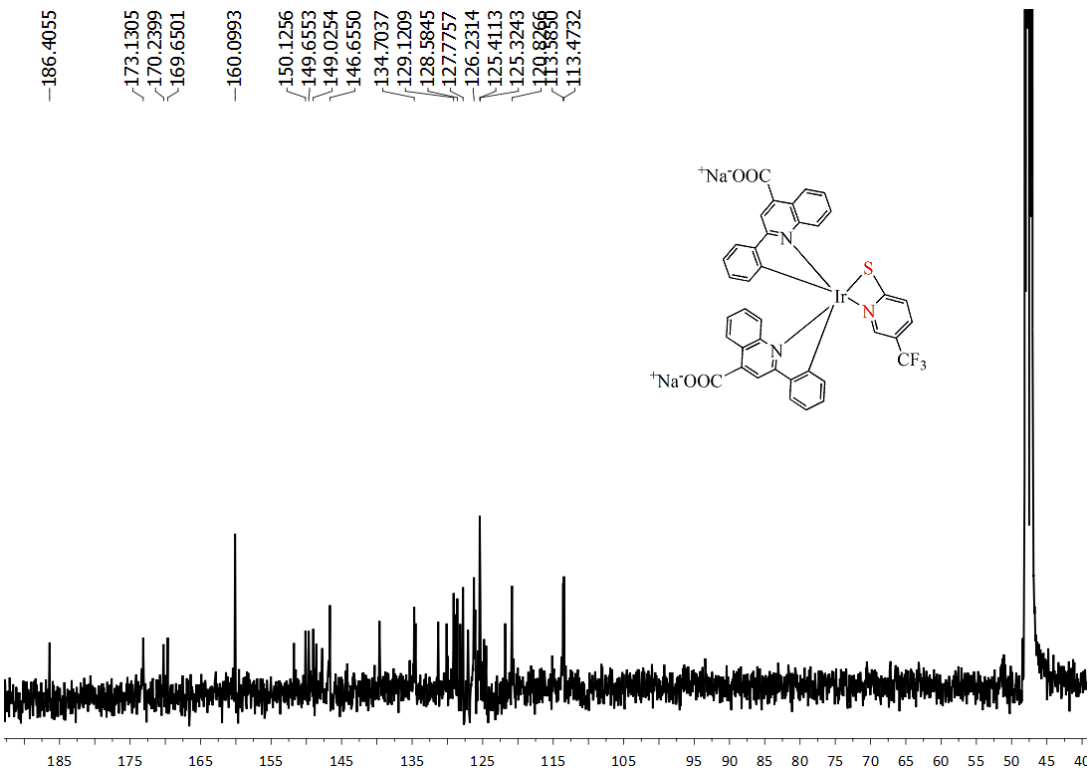

Figure S34. $^{13}C\{^{1}H\}$ NMR spectrum of **C3** in CD_3OD-d_4.

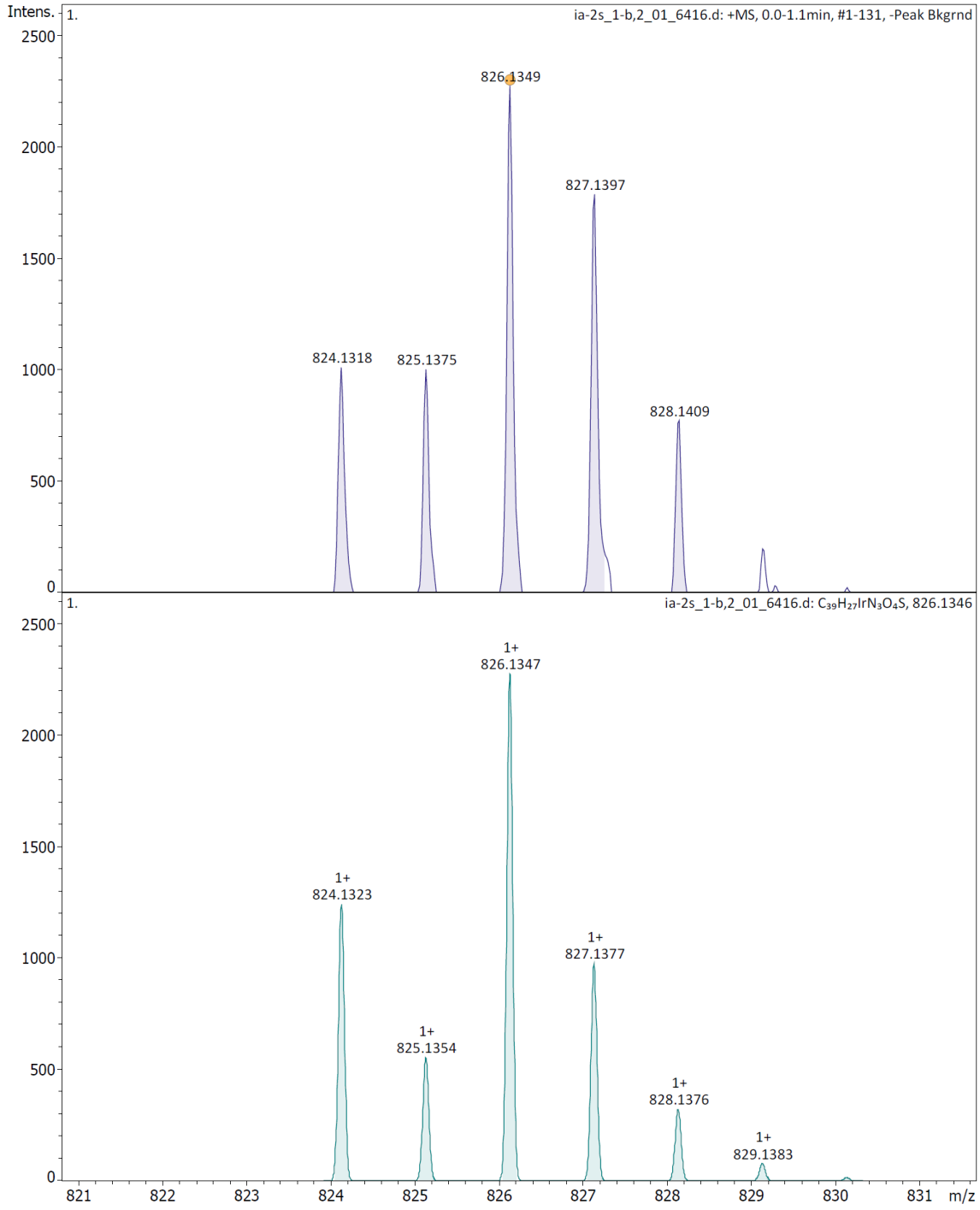

Figure S35. HR Mass spectrum of **B1**.

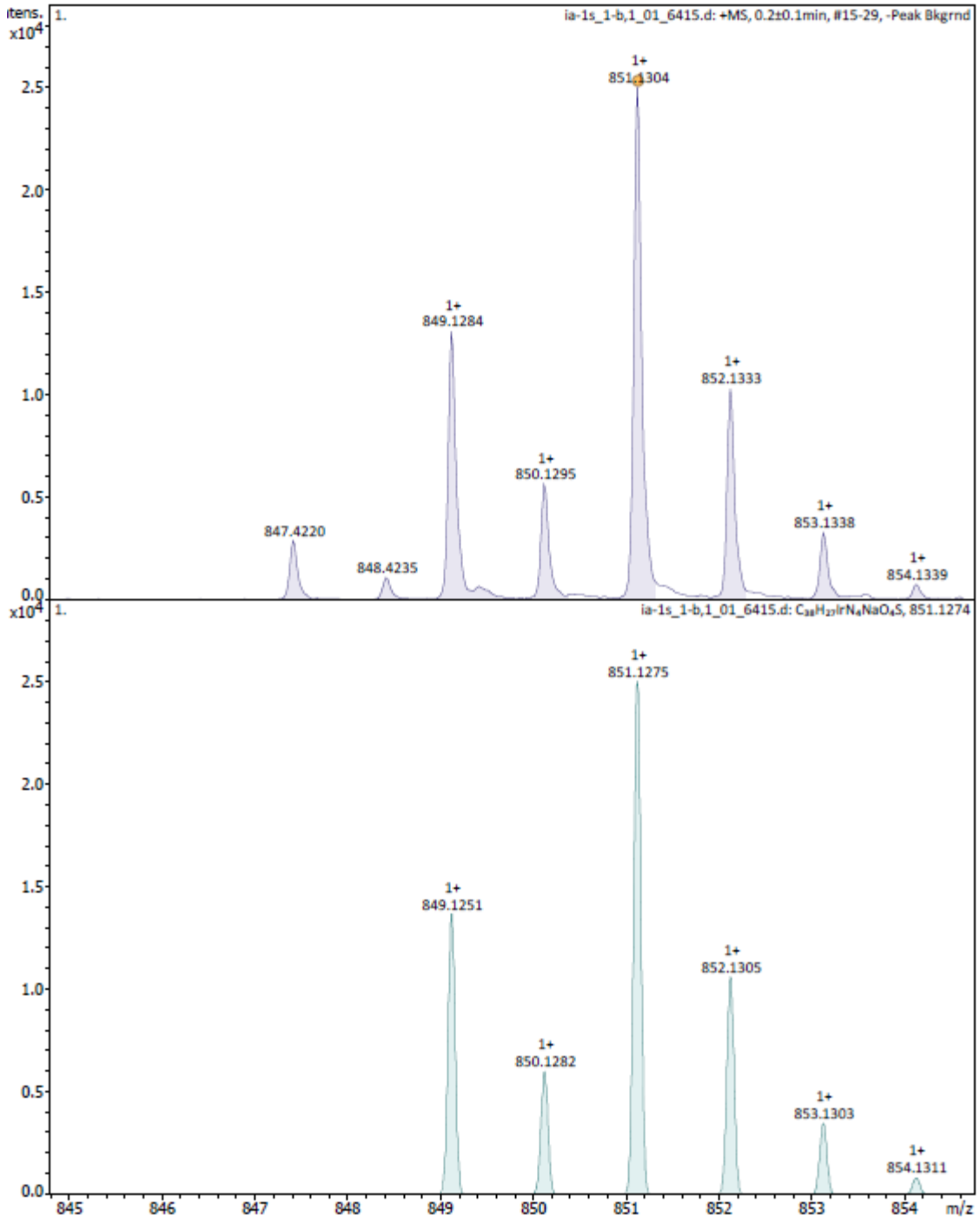

Figure S36. HR Mass spectrum of **B2**.

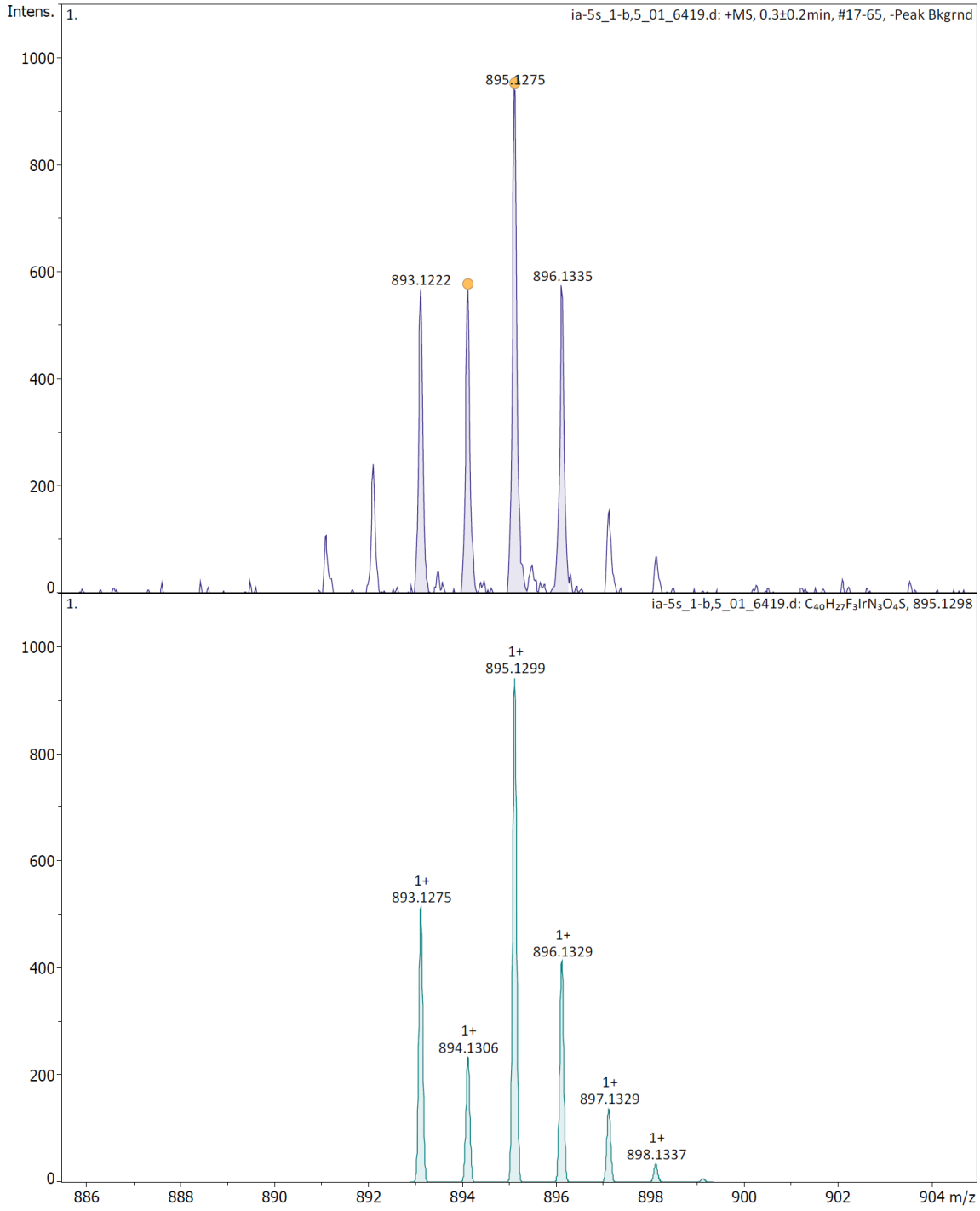

Figure S37. HR Mass spectrum of **B3**.

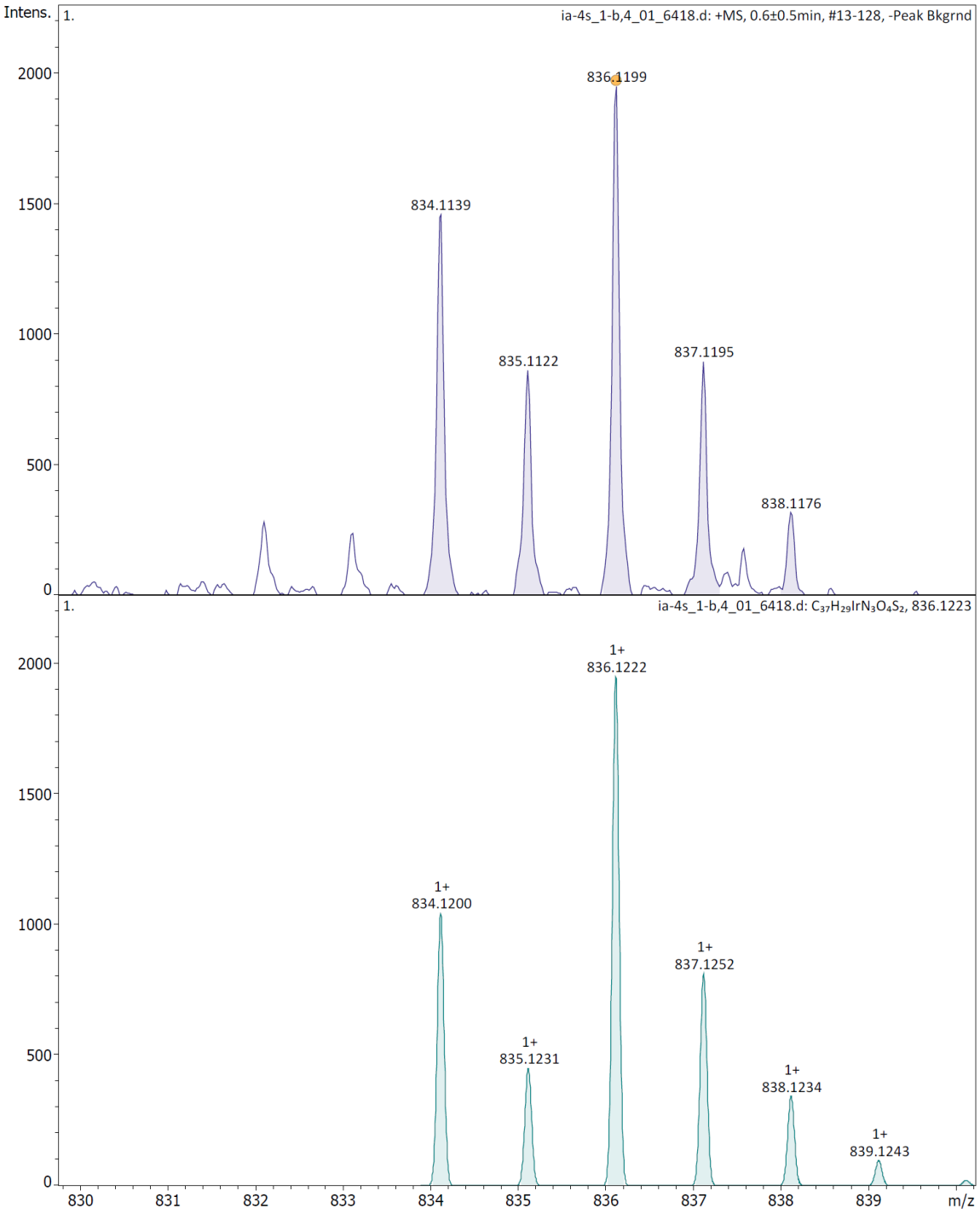

Figure S38. HR Mass spectrum of **B4**.

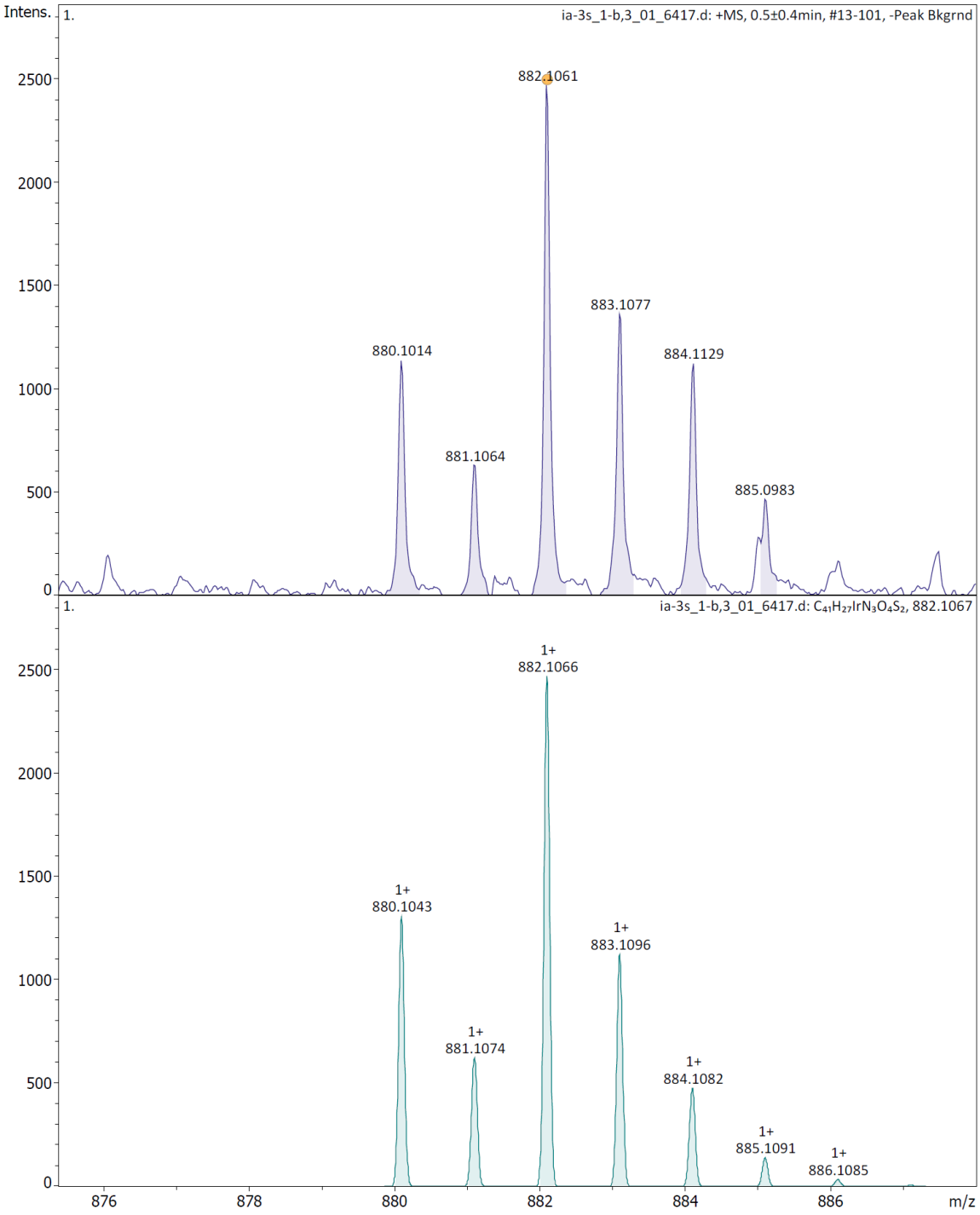

Figure S39. HR Mass spectrum of **B5**.

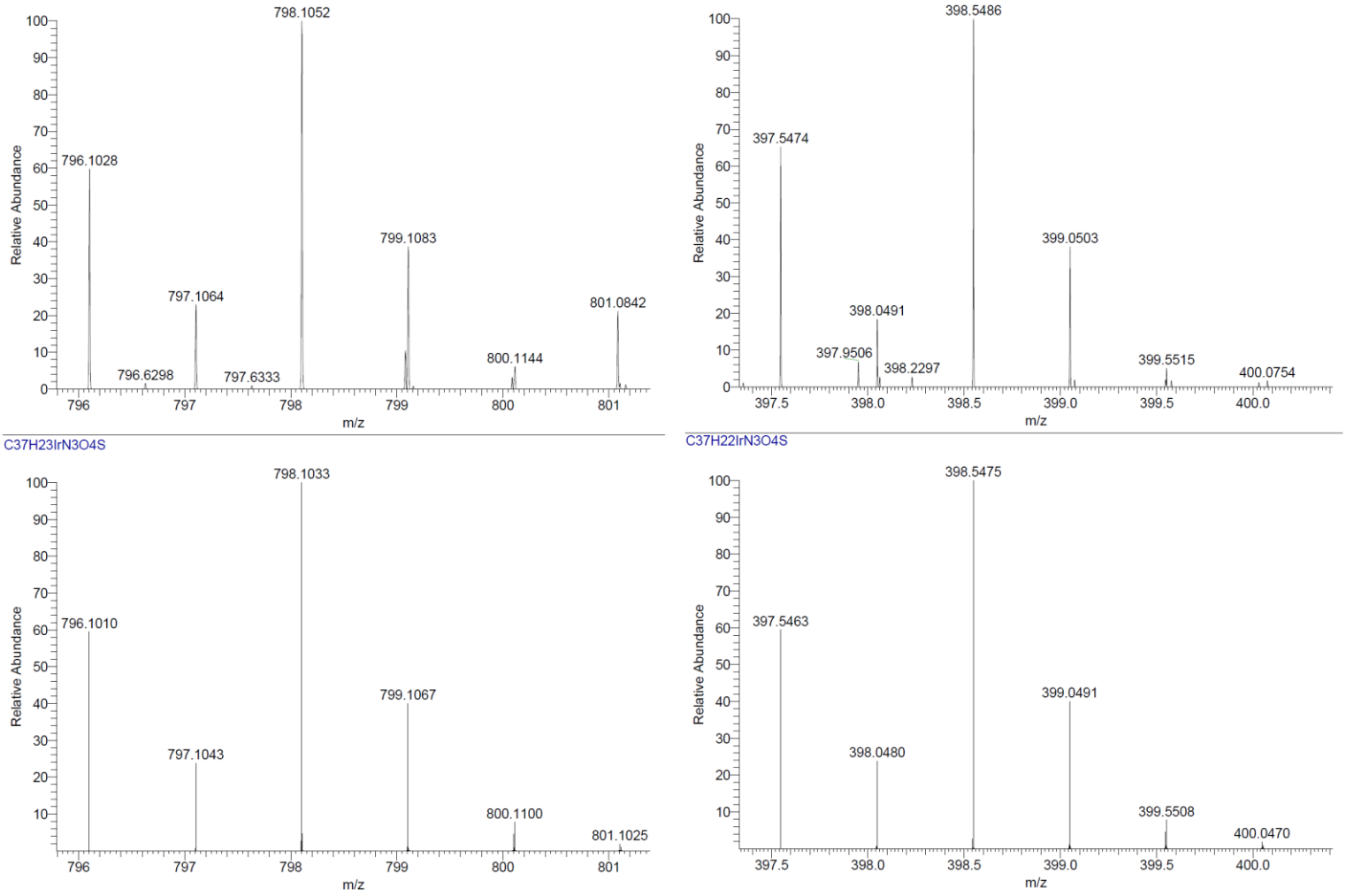

Figure S40. HR Mass spectrum of **C1**.

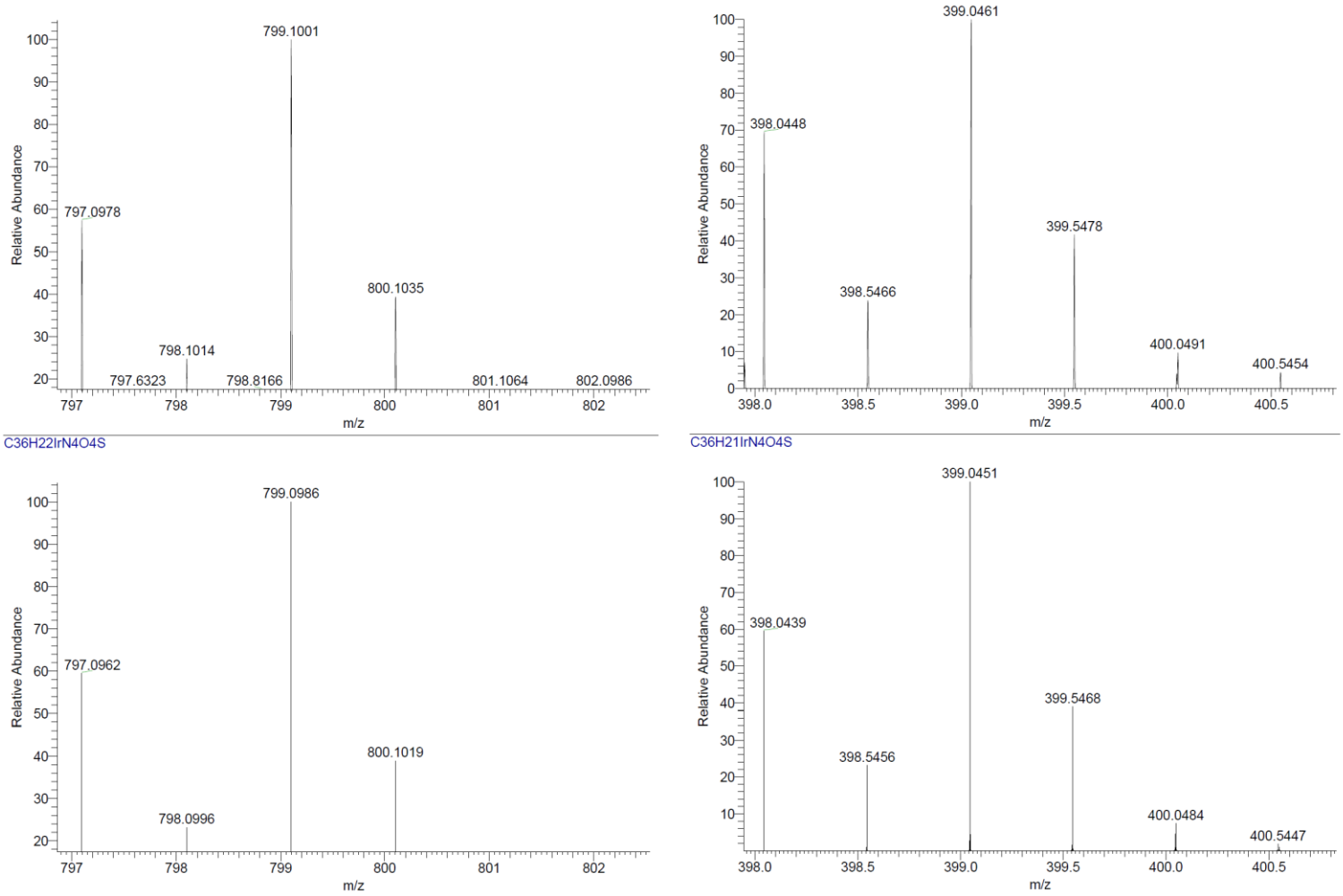

Figure S41. HR Mass spectrum of **C2**.

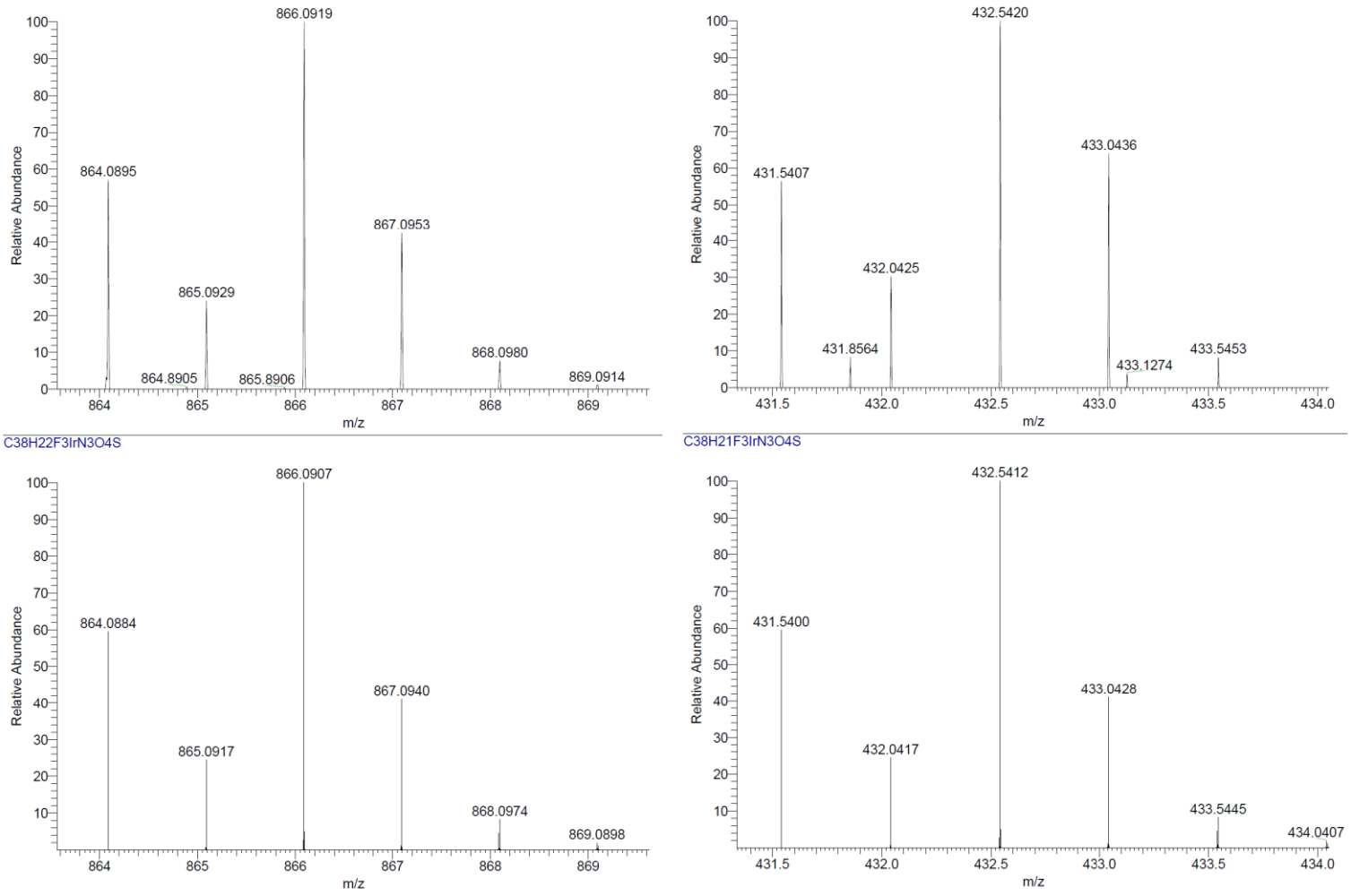

Figure S42. HR Mass spectrum of **C3**.

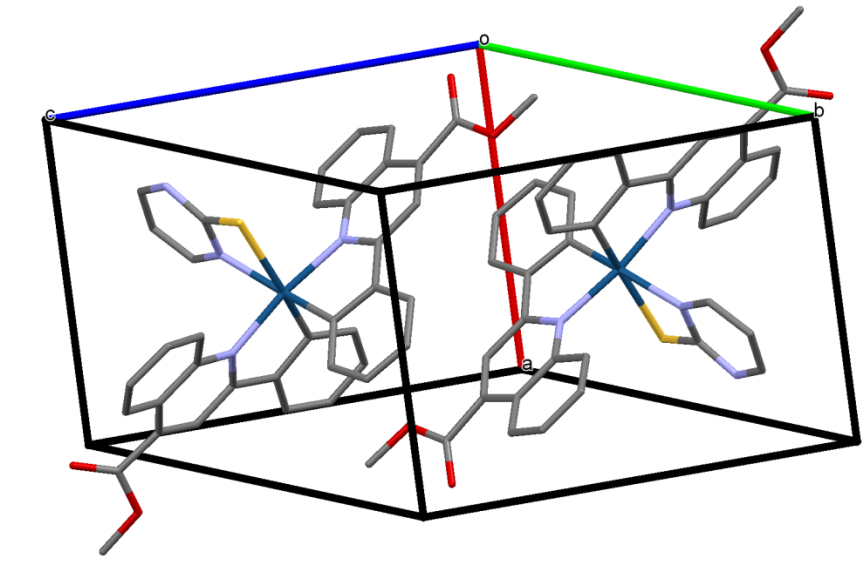

Figure S43. Crystal packing view for **B2**.

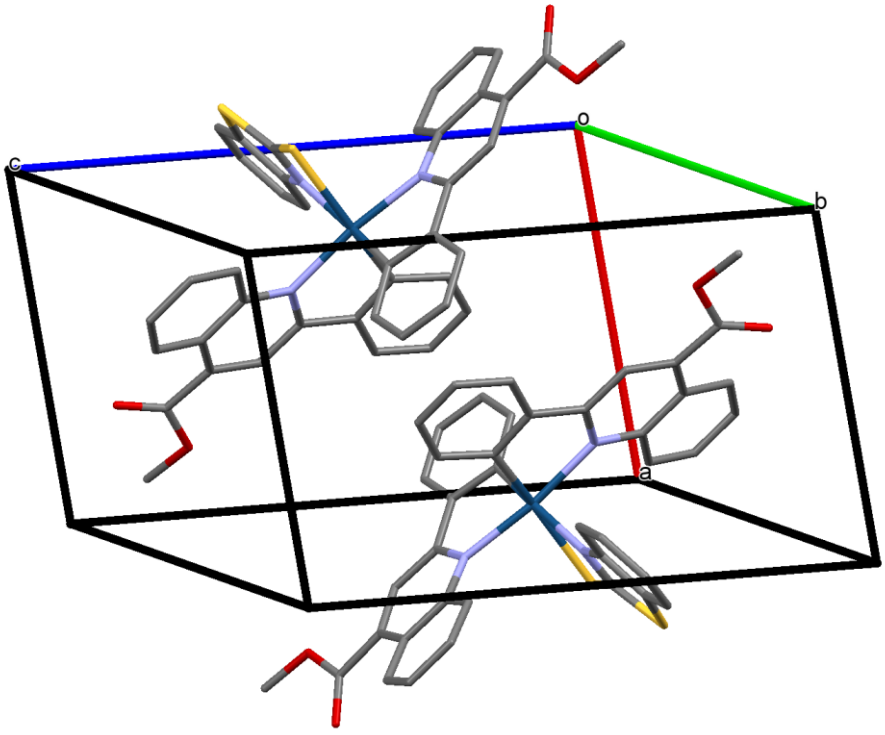

Figure S44. Crystal packing view for **B5**.

Table S1. Selected geometrical parameters (bond lengths [Å] and angles [°]) for the crystal structures of **B2** and **B5**.

B2		**B5**	
Ir1—C17 (1.998(4))	C34—Ir1—N4 (79.86(17))	Ir1—C24 (1.989 (2))	C24—Ir1—N2 (80.05 (6))
Ir1—C34 (1.996(5))	C17—Ir1—N3 (80.26(16))	Ir1—C41 (1.990 (2))	C41—Ir1—N3 (80.40 (6))
Ir1—N4 (2.076(4))	N1—Ir1—S1 (65.36(10))	Ir1—N2 (2.073 (1))	N1—Ir1—S1 (65.05 (4))
Ir1—N3 (2.086(4))	N4—Ir1—N3 (172.45(15))	Ir1—N3 (2.077 (1))	N2—Ir1—N3 (173.04 (5))
Ir1—N1 (2.178(4))	C17—Ir1—N1 (166.82(15))	Ir1—N1 (2.199 (1))	C24—Ir1—N1 (169.23 (6))
Ir1—S1 (2.5250(11))	C34—Ir1—S1 (163.17(13))	Ir1—S1 (2.579 (1))	C41—Ir1—S1 (161.88 (4))

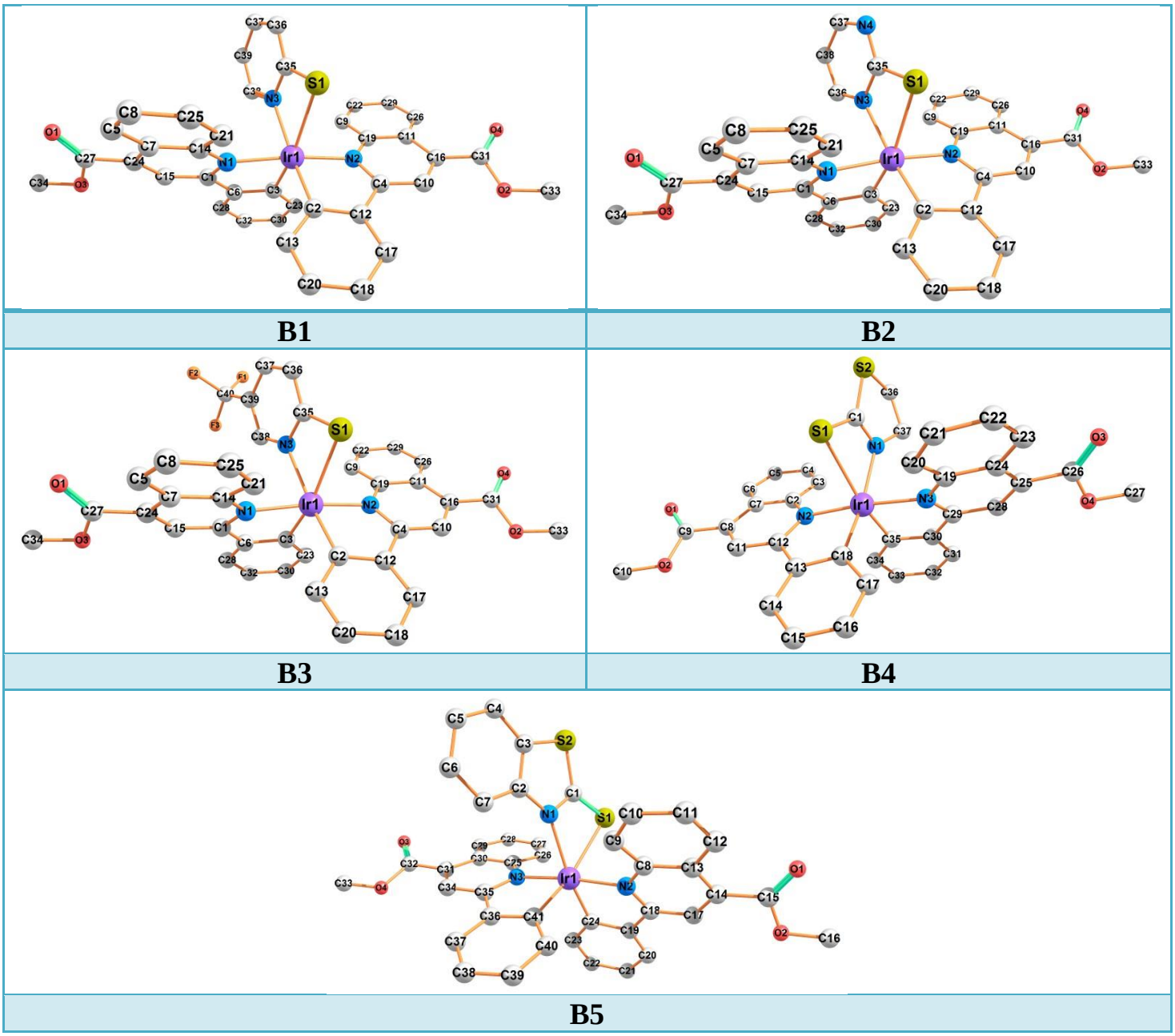

Figure S45. DFT-optimized structures of **B1–B5** in CH_2Cl_2 solvent.

Table S2. Selected geometrical parameters (bond length [Å] and angle [°]) for the DFT-optimized structures of **B1**–**B5** in CH_2Cl_2.

B1	B2	B3	B4	B5
Ir1-S1	Ir1-S1	Ir1-S1	Ir1-S1	Ir1-S1
(2.647)	(2.639)	(2.655)	(2.721)	(2.711)
Ir1-N3	Ir1-N3	Ir1-N3	Ir1-N1	Ir1-N1
(2.253)	(2.253)	(2.259)	(2.263)	(2.306)
Ir1-C2	Ir1-C2	Ir1-C2	Ir1-C35	Ir1-C24
(2.005)	(2.004)	(2.004)	(2.001)	(1.999)
Ir1-C3	Ir1-C3	Ir1-C3	Ir1-C18	Ir1-C41
(2.007)	(2.008)	(2.006)	(2.003)	(2.003)
Ir1-N2	Ir1-N2	Ir1-N2	Ir1-N3	Ir1-N3
(2.121)	(2.120)	(2.119)	(2.115)	(2.113)
Ir1-N1	Ir1-N1	Ir1-N1	Ir1-N2	Ir1-N2
(2.116)	(2.117)	(2.117)	(2.112)	(2.117)
N3-Ir1-S1	N3-Ir1-S1	N3-Ir1-S1	N1-Ir1-S1	N1-Ir1-S1
(63.416)	(63.421)	(63.124)	(62.346)	(62.557)
N2-Ir1-C2	N2-Ir1-C2	N2-Ir1-C2	N2-Ir1-C18	N2-Ir1-C24
(79.632)	(79.654)	(79.692)	(79.952)	(79.969)
N1-Ir1-C3	N1-Ir1-C3	N1-Ir1-C3	N3-Ir1-C35	N3-Ir1-C41
(79.884)	(79.864)	(79.879)	(79.920)	(79.923)
S1-Ir1-C3	S1-Ir1-C3	S1-Ir1-C3	S1-Ir1-C35	S1-Ir1-C41
(160.93)	(161.09)	(160.95)	(160.95)	(162.67)
N3-Ir1-C2	N3-Ir1-C2	N3-Ir1-C2	N1-Ir1-C18	N1-Ir1-C24
(167.42)	(167.34)	(167.27)	(166.56)	(165.74)
N1-Ir1-N2	N1-Ir1-N2	N1-Ir1-N2	N2-Ir1-N3	N2-Ir1-N3
(174.12)	(174.20)	(174.12)	(174.70)	(174.49)

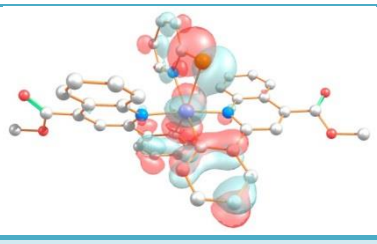	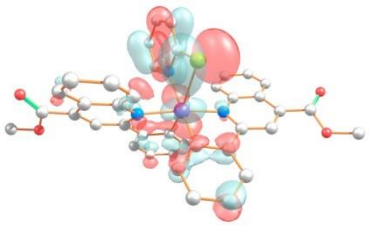	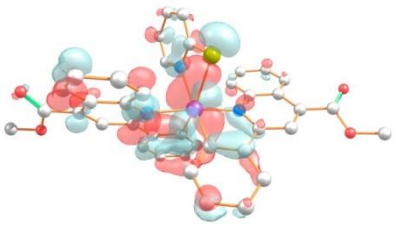
HOMO (-5.284 eV) Ir(36%), S^N(30%), C^N(34%)	HOMO-1 (-5.424 eV) Ir(16%), S^N(63%), C^N(21%)	HOMO-2 (-6.038 eV) Ir(35%), S^N(14%), C^N(51%)
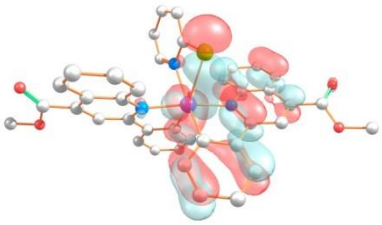	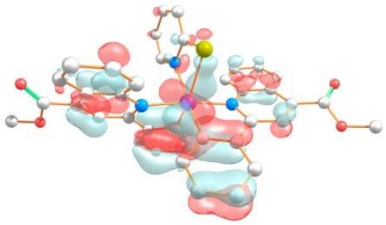	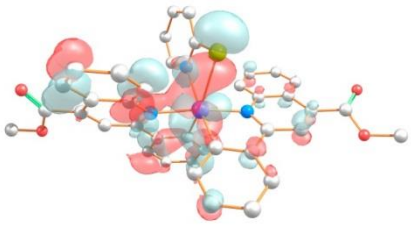
HOMO-3 (-6.152 eV) Ir(23%), S^N(17%), C^N(60%)	HOMO-4 (-6.350 eV) Ir(29%), S^N(7%), C^N(64%)	HOMO-5 (-6.463 eV) Ir(26%), S^N(23%), C^N(52%)
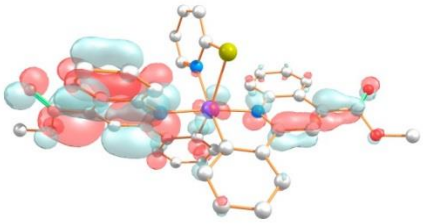	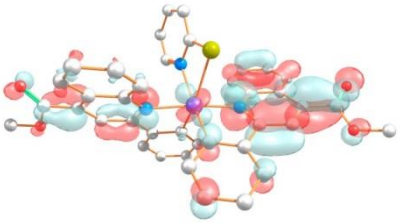	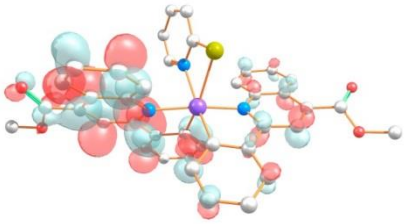
LUMO (-2.514 eV) Ir(4%), S^N(2%), C^N(94%)	LUMO+1 (-2.450 eV) Ir(5%), S^N(2%), C^N(93%)	LUMO+2 (-1.218 eV) Ir(1%), S^N(1%), C^N(98%)
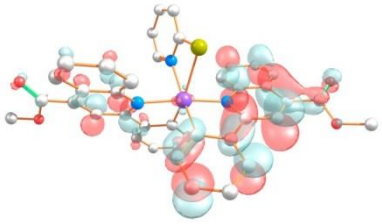	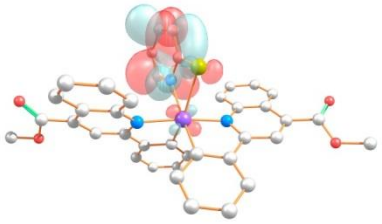	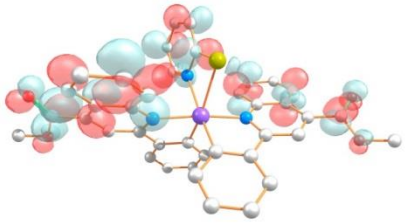
LUMO+3 (-1.139 eV) Ir(1%), S^N(1%), C^N(98%)	LUMO+4 (-0.917 eV) Ir(5%), S^N(88%), C^N(7%)	LUMO+5 (-0.401 eV) Ir(1%), S^N(26%), C^N(73%)

Figure S46. Molecular orbital plots for the optimized structure of **B1** in CH_2Cl_2 solution.

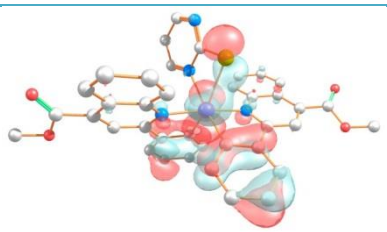	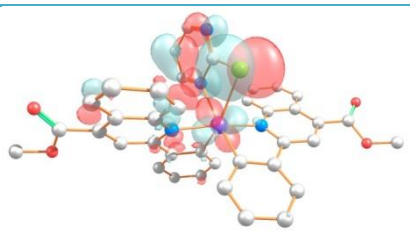	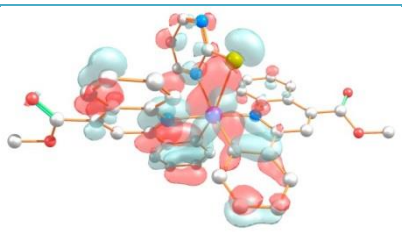
HOMO (-5.358 eV) Ir(44%), S^N(11%), C^N(45%)	HOMO-1 (-5.666 eV) Ir(14%), S^N(72%), C^N(13%)	HOMO-2 (-6.113 eV) Ir(30%), S^N(16%), C^N(54%)
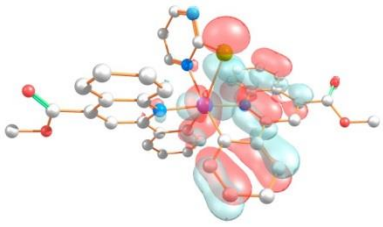	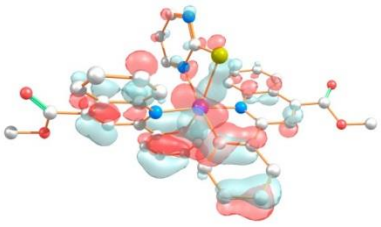	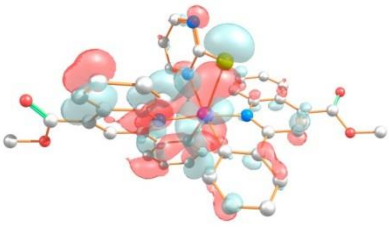
HOMO-3 (-6.200 eV) Ir(12%), S^N(16%), C^N(63%)	HOMO-4 (-6.394 eV) Ir(30%), S^N(9%), C^N(61%)	HOMO-5 (-6.518 eV) Ir(23%), S^N(22%), C^N(55%)
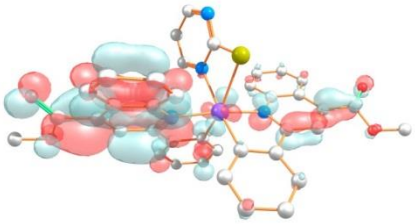	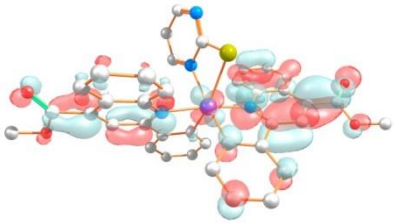	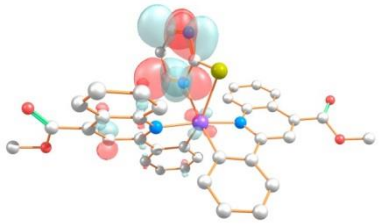
LUMO (-2.545 eV) Ir(4%), S^N(2%), C^N(94%)	LUMO+1 (-2.478 eV) Ir(4%), S^N(2%), C^N(94%)	LUMO+2 (-1.352 eV) Ir(3%), S^N(84%), C^N(13%)
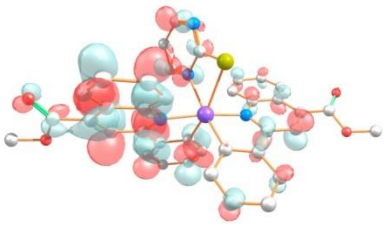	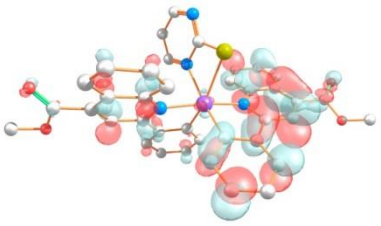	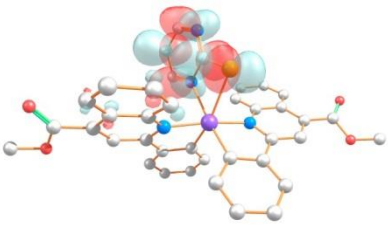
LUMO+3 (-1.236 eV) Ir(1%), S^N(10%), C^N(89%)	LUMO+4 (-1.163 eV) Ir(1%), S^N(3%), C^N(96%)	LUMO+5 (-0.716 eV) Ir(1%), S^N(86%), C^N(13%)

Figure S47. Molecular orbital plots for the optimized structure of **B2** in CH_2Cl_2 solution.

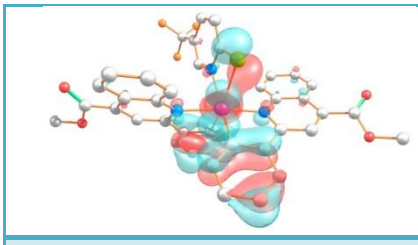	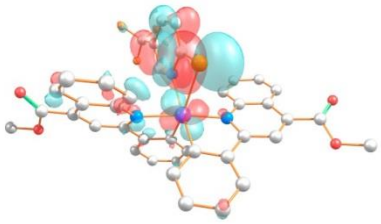	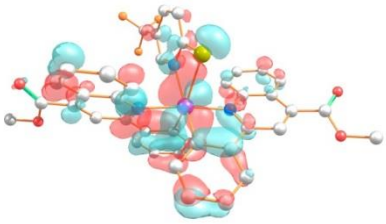
HOMO (-5.373 eV) Ir(44%), S^N(12%), C^N(44%)	HOMO-1 (-5.630 eV) Ir(12%), S^N(75%), C^N(13%)	HOMO-2 (-6.117 eV) Ir(31%), S^N(13%), C^N(56%)
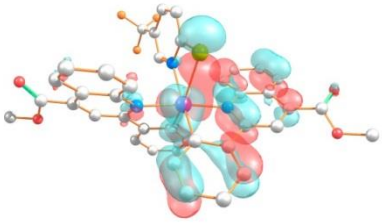	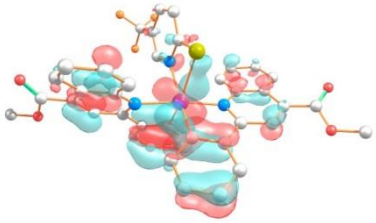	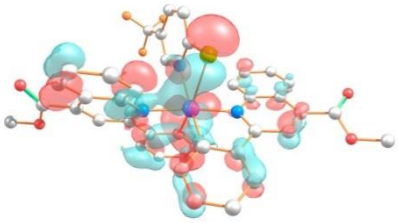
HOMO-3 (-6.218 eV) Ir(24%), S^N(16%), C^N(60%)	HOMO-4 (-6.409 eV) Ir(31%), S^N(7%), C^N(62%)	HOMO-5 (-6.539 eV) Ir(23%), S^N(23%), C^N(54%)
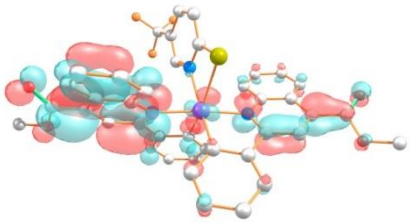	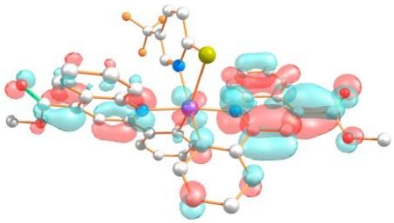	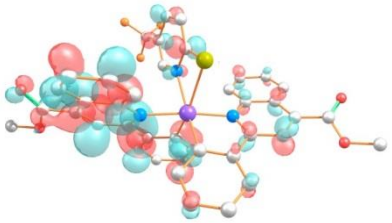
LUMO (-2.550 eV) Ir(4%), S^N(2%), C^N(94%)	LUMO+1 (-2.491 eV) Ir(5%), S^N(2%), C^N(93%)	LUMO+2 (-1.260 eV) Ir(0%), S^N(10%), C^N(90%)
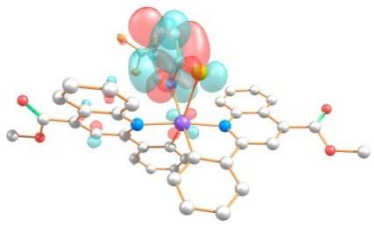	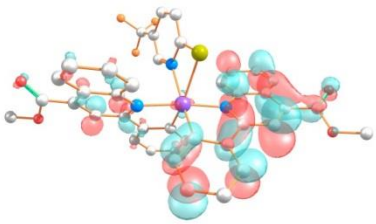	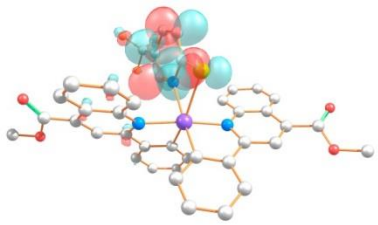
LUMO+3 (-1.233 eV) Ir(3%), S^N(87%), C^N(10%)	LUMO+4 (-1.175 eV) Ir(1%), S^N(2%), C^N(97%)	LUMO+5 (-0.831 eV) Ir(4%), S^N(85%), C^N(11%)

Figure S48. Molecular orbital plots for the optimized structure of **B3** in CH_2Cl_2 solution.

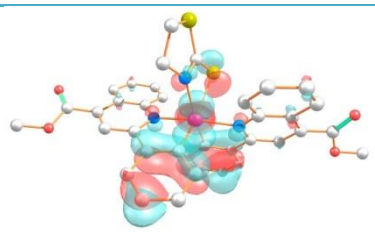	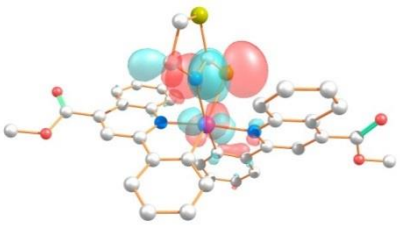	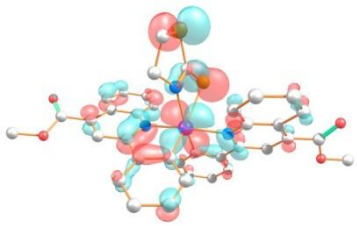
HOMO (-5.345 eV) Ir(46%), S^N(8%), C^N(46%)	HOMO-1 (-5.824 eV) Ir(11%), S^N(77%), C^N(12%)	HOMO-2 (-5.919 eV) Ir(40%), S^N(28%), C^N(32%)
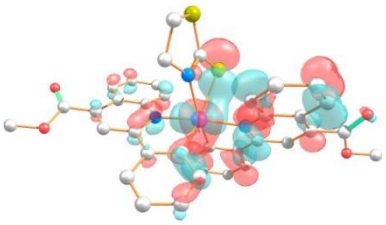	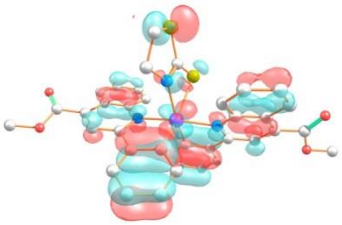	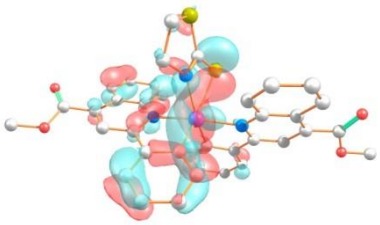
HOMO-3 (-6.205 eV) Ir(25%), S^N(17%), C^N(57%)	HOMO-4 (-6.290 eV) Ir(8%), S^N(19%), C^N(73%)	HOMO-5 (-6.447 eV) Ir(20%), S^N(30%), C^N(50%)
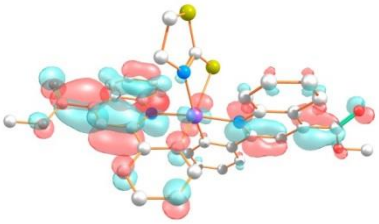	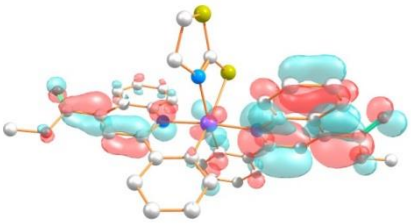	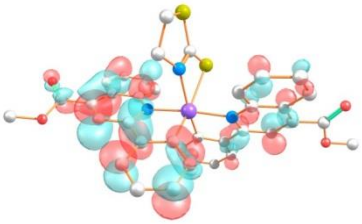
LUMO (-2.530 eV) Ir(4%), S^N(2%), C^N(94%)	LUMO+1 (-2.472 eV) Ir(5%), S^N(2%), C^N(93%)	LUMO+2 (-1.231 eV) Ir(1%), S^N(1%), C^N(98%)
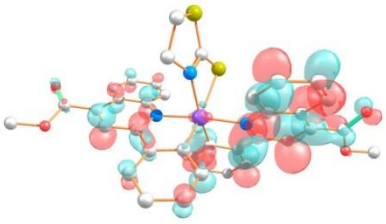	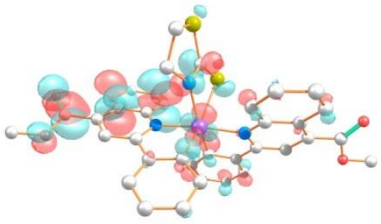	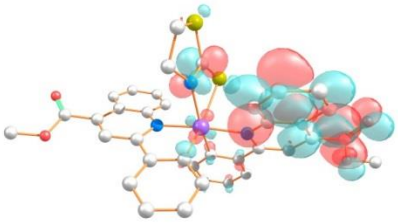
LUMO+3 (-1.157 eV) Ir(2%), S^N(1%), C^N(97%)	LUMO+4 (-0.396 eV) Ir(6%), S^N(13%), C^N(80%)	LUMO+5 (-0.377 eV) Ir(3%), S^N(15%), C^N(82%)

Figure S49. Molecular orbital plots for the optimized structure of **B4** in CH_2Cl_2 solution.

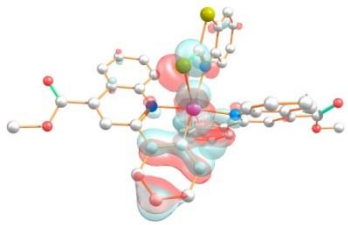	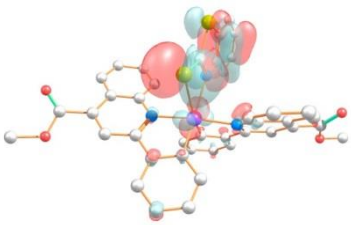	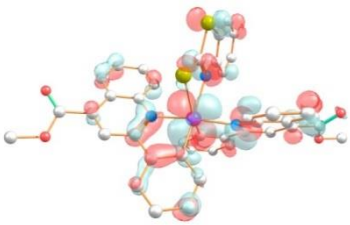
HOMO (-5.411 eV) Ir(44%), S^N(14%), C^N(42%)	HOMO-1 (-5.585 eV) Ir(7%), S^N(82%), C^N(11%)	HOMO-2 (-6.043 eV) Ir(41%), S^N(16%), C^N(43%)
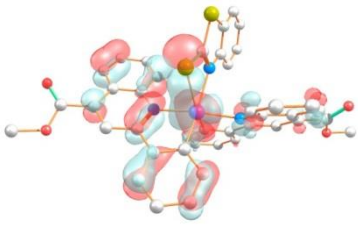	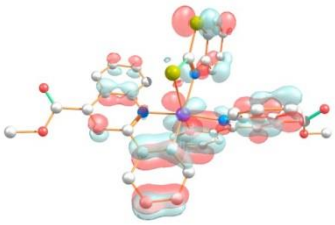	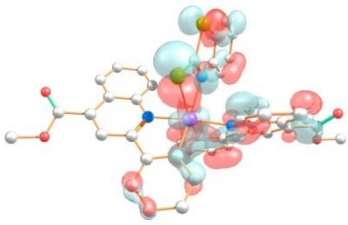
HOMO-3 (-6.260 eV) Ir(32%), S^N(12%), C^N(56%)	HOMO-4 (-6.347 eV) Ir(12%), S^N(23%), C^N(65%)	HOMO-5 (-6.515 eV) Ir(8%), S^N(40%), C^N(52%)
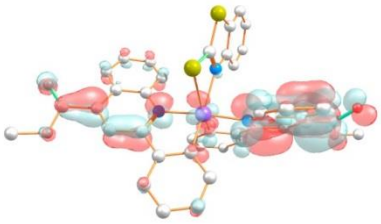	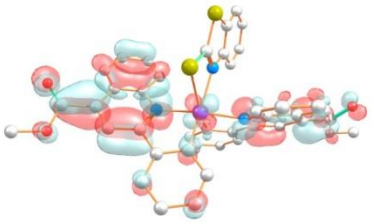	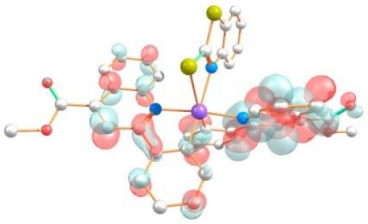
LUMO (-2.550 eV) Ir(4%), S^N(2%), C^N(94%)	LUMO+1 (-2.498 eV) Ir(5%), S^N(2%), C^N(93%)	LUMO+2 (-1.253 eV) Ir(0%), S^N(2%), C^N(98%)
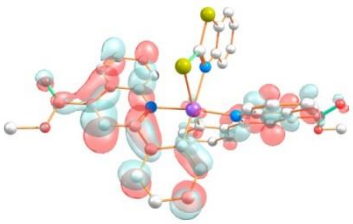	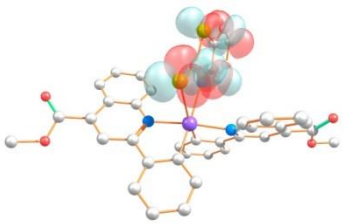	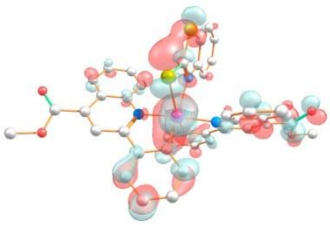
LUMO+3 (-1.184 eV) Ir(2%), S^N(1%), C^N(97%)	LUMO+4 (-0.923 eV) Ir(1%), S^N(93%), C^N(6%)	LUMO+5 (-0.420 eV) Ir(20%), S^N(29%), C^N(51%)

Figure S50. Molecular orbital plots for the optimized structure of **B5** in CH_2Cl_2 solution.

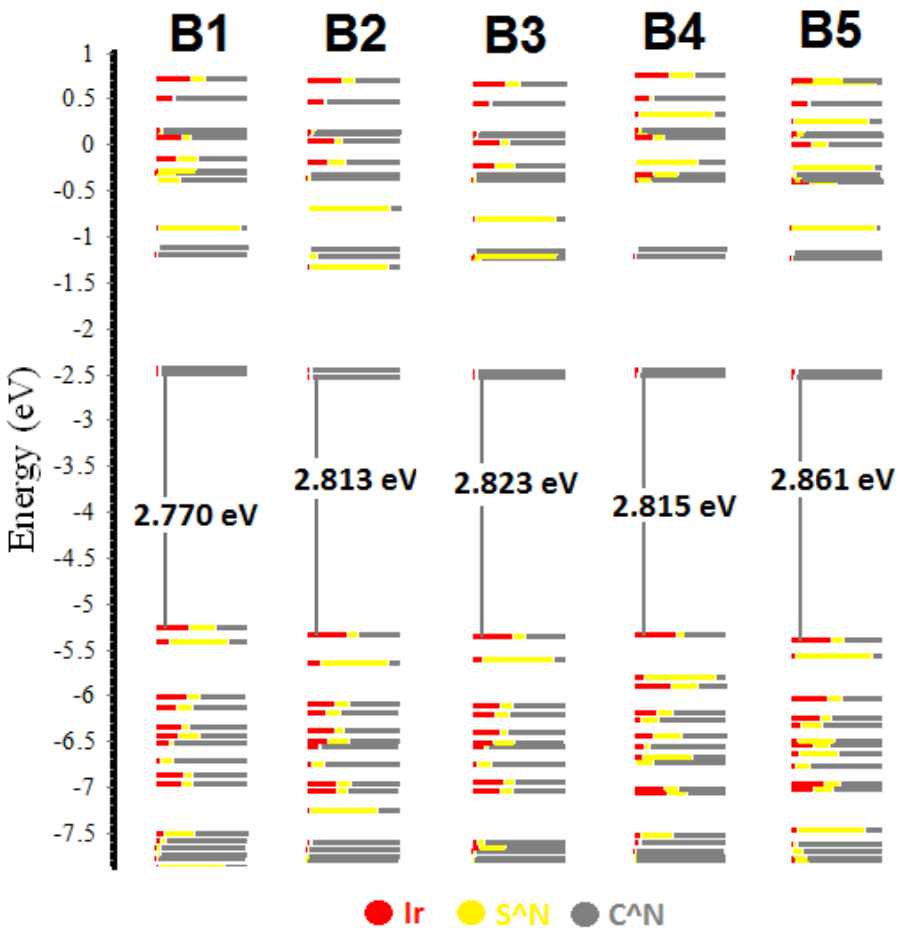

Figure S51. Comparative energy diagram for the molecular orbitals of **B1**–**B5**.

Table S3. Wavelengths and the nature of transitions for **B1** where M = Ir, L = C^N and L′ = S^N.

Excited state	Calculated λ (nm)	Oscillator strength	Transitions (Major Contribution)	Assignment
1	576.42	0.0147	HOMO→LUMO (96%)	ILCT/MLCT/L′LCT
2	571.35	0.0438	HOMO→L+1 (98%)	ILCT/MLCT/L′LCT
3	536.46	0.0199	H-1→LUMO (97%)	L′LCT/ILCT/MLCT
4	523.42	0.0148	H-1→L+1 (97%)	L′LCT/ILCT/MLCT
5	428.78	0.0515	H-2→LUMO (76%)	ILCT/MLCT/L′LCT
			H-2→L+1 (14%)	ILCT/MLCT/L′LCT
6	418.89	0.0316	H-2→LUMO (16%)	ILCT/MLCT/L′LCT
			H-2→L+1 (69%)	ILCT/MLCT/L′LCT
8	393.64	0.1839	H-3→L+1 (74%)	ILCT/MLCT/L′LCT
9	380.94	0.1333	H-5→LUMO (11%)	ILCT/MLCT/L′LCT
			H-4→LUMO (76%)	ILCT/MLCT/L′LCT
16	349.15	0.1244	H-6→L+1 (47%)	ILCT/MLCT
			HOMO→L+3 (39%)	ILCT/MLCT/L′LCT
28	296.90	0.1349	H-2→L+2 (76%)	ILCT/MLCT/L′LCT
34	286.64	0.1435	H-3→L+2 (25%)	ILCT/MLCT/L′LCT
			H-3→L+3 (24%)	ILCT/MLCT/L′LCT

Table S4. Wavelengths and the nature of transitions for **B2** where M = Ir, L = C^N and L′ = S^N.

Excited state	Calculated λ (nm)	Oscillator strength	Transitions (Major Contribution)	Assignment
1	568.05	0.0184	HOMO→LUMO (93%)	ILCT/MLCT/L′LCT
2	559.54	0.0445	HOMO→L+1 (93%)	ILCT/MLCT/L′LCT
3	493.72	0.0344	H-1→LUMO (98%)	L′LCT/ILCT
5	421.06	0.0358	H-2→LUMO (70%)	ILCT/MLCT/L′LCT
			H-2→L+1 (16%)	ILCT/MLCT/L′LCT
6	412.19	0.039	H-3→L+1 (11%)	ILCT/L′LCT
			H-2→LUMO (18%)	ILCT/MLCT/L′LCT
			H-2→L+1 (64%)	ILCT/MLCT/L′LCT
8	389.97	0.1807	H-3→L+1 (73%)	ILCT/L′LCT
			H-2→L+1 (10%)	ILCT/MLCT/L′LCT
9	379.82	0.1454	H-4→LUMO (81%)	ILCT/MLCT
13	359.79	0.0874	H-5→L+1 (65%)	ILCT/MLCT/L′LCT
15	354.49	0.0949	H-6→LUMO (37%)	ILCT/MLCT
			HOMO→L+3 (47%)	ILCT/MLCT
16	349.21	0.1098	H-6→L+1 (62%)	ILCT/MLCT
			H-5→L+1 (11%)	ILCT/MLCT/L′LCT
33	291.95	0.068	H-3→L+2 (17%)	LL′CT/ML′CT
			H-2→L+3 (22%)	ILCT/MLCT/L′LCT
39	283.52	0.1112	H-3→L+3 (15%)	ILCT/MLCT
			H-3→L+4 (12%)	ILCT/MLCT
			H-1→L+5 (12%)	IL′CT/ML′CT

Table S5. Wavelengths and the nature of transitions for **B3** where M = Ir, L = C^N and L′ = S^N.

Excited state	Calculated λ (nm)	Oscillator strength	Transitions (Major Contribution)	Assignment
1	564.97	0.0177	HOMO→LUMO (92%)	ILCT/MLCT/L′LCT
2	559.54	0.0441	HOMO→L+1 (92%)	ILCT/MLCT/L′LCT
3	499.69	0.03	H-1→LUMO (98%)	L′LCT/MLCT
5	421.21	0.0379	H-2→LUMO (68%)	ILCT/MLCT/L′LCT
			H-2→L+1 (16%)	ILCT/MLCT/L′LCT
6	411.90	0.0452	H-3→L+1 (11%)	ILCT/MLCT/L′LCT
			H-2→LUMO (21%)	ILCT/MLCT/L′LCT
			H-2→L+1 (61%)	ILCT/MLCT/L′LCT
8	390.76	0.1768	H-3→L+1 (68%)	ILCT/MLCT/L′LCT
			H-2→L+1 (14%)	ILCT/MLCT/L′LCT
9	378.54	0.1609	H-4→LUMO (84%)	ILCT/MLCT
12	360.65	0.079	H-5→L+1 (57%)	ILCT/MLCT/L′LCT
			HOMO→L+3 (15%)	LL′CT/IL′CT/ML′CT
16	349.40	0.1145	H-6→L+1 (67%)	ILCT/MLCT
			HOMO→L+2 (10%)	ILCT/MLCT
22	325.38	0.0574	H-1→L+2 (81%)	L′LCT/MLCT
30	294.02	0.1266	H-2→L+2 (61%)	ILCT/MLCT
31	292.46	0.0952	H-2→L+3 (17%)	LL′CT/ML′CT
			H-1→L+5 (45%)	IL′CT/ML′CT
37	284.55	0.1365	H-3→L+2 (24%)	ILCT/MLCT
			H-3→L+4 (30%)	ILCT/MLCT/L′LCT

Table S6. Wavelengths and the nature of transitions for **B4** where M = Ir, L = C^N and L′ = S^N.

Excited state	Calculated λ (nm)	Oscillator strength	Transitions (Major Contribution)	Assignment
1	569.64	0.0224	HOMO→LUMO (82%)	ILCT/MLCT/L′LCT
			HOMO→L+1 (17%)	ILCT/MLCT/L′LCT
2	562.02	0.0383	HOMO→LUMO (17%)	ILCT/MLCT/L′LCT
			HOMO→L+1 (82%)	ILCT/MLCT/L′LCT
5	448.82	0.106	H-2→LUMO (92%)	MLCT/ILCT/L′LCT
8	393.51	0.1559	H-3→LUMO (13%)	ILCT/MLCT/L′LCT
			H-3→L+1 (73%)	ILCT/MLCT/L′LCT
9	384.88	0.1062	H-5→LUMO (16%)	ILCT/MLCT/L′LCT
			H-4→LUMO (78%)	ILCT/L′LCT
12	366.56	0.0782	H-5→L+1 (73%)	ILCT/L′LCT/MLCT
15	350.21	0.1238	H-6→L+1 (48%)	ILCT/MLCT/L′LCT
			HOMO→L+2 (13%)	MLCT/ILCT
			HOMO→L+3 (22%)	ILCT/MLCT
16	347.49	0.124	H-6→L+1 (26%)	ILCT/MLCT/L′LCT
			HOMO→L+3 (60%)	ILCT/MLCT
28	303.60	0.1033	H-2→L+2 (80%)	MLCT/ILCT/L′LCT
44	270.81	0.2077	H-4→L+3 (45%)	ILCT/L′LCT
			H-3→L+3 (11%)	MLCT/ILCT/L′LCT

Table S7. Wavelengths and the nature of transitions for **B5** where M = Ir, L = C^N and L′ = S^N.

Excited state	Calculated λ (nm)	Oscillator strength	Transitions (Major Contribution)	Assignment
1	556.90	0.0220	HOMO→LUMO (81%)	MLCT/ILCT/L′LCT
			HOMO→L+1 (17%)	ILCT/MLCT/L′LCT
2	552.85	0.0346	HOMO→LUMO (17%)	MLCT/ILCT/L′LCT
			HOMO→L+1 (81%)	ILCT/MLCT/L′LCT
5	432.88	0.0908	H-2→LUMO (88%)	ILCT/MLCT/L′LCT
8	391.72	0.1611	H-3→LUMO (19%)	ILCT/MLCT/L′LCT
			H-3→L+1 (63%)	ILCT/MLCT/L′LCT
9	380.78	0.1381	H-4→LUMO (88%)	ILCT/MLCT/L′LCT
12	360.94	0.1051	H-6→LUMO (10%)	ILCT/MLCT/L′LCT
			H-6→L+1 (28%)	ILCT/MLCT/L′LCT
			H-5→L+1 (45%)	ILCT/MLCT
16	348.28	0.2393	H-7→LUMO (25%)	L′LCT/MLCT/ILCT
			H-6→L+1 (15%)	ILCT/MLCT/L′LCT
			HOMO→L+2 (45%)	MLCT/ILCT/L′LCT
29	300.70	0.2152	H-1→L+4 (81%)	IL′CT/ML′CT
31	294.72	0.1691	H-2→L+3 (69%)	MLCT/ILCT/L′LCT

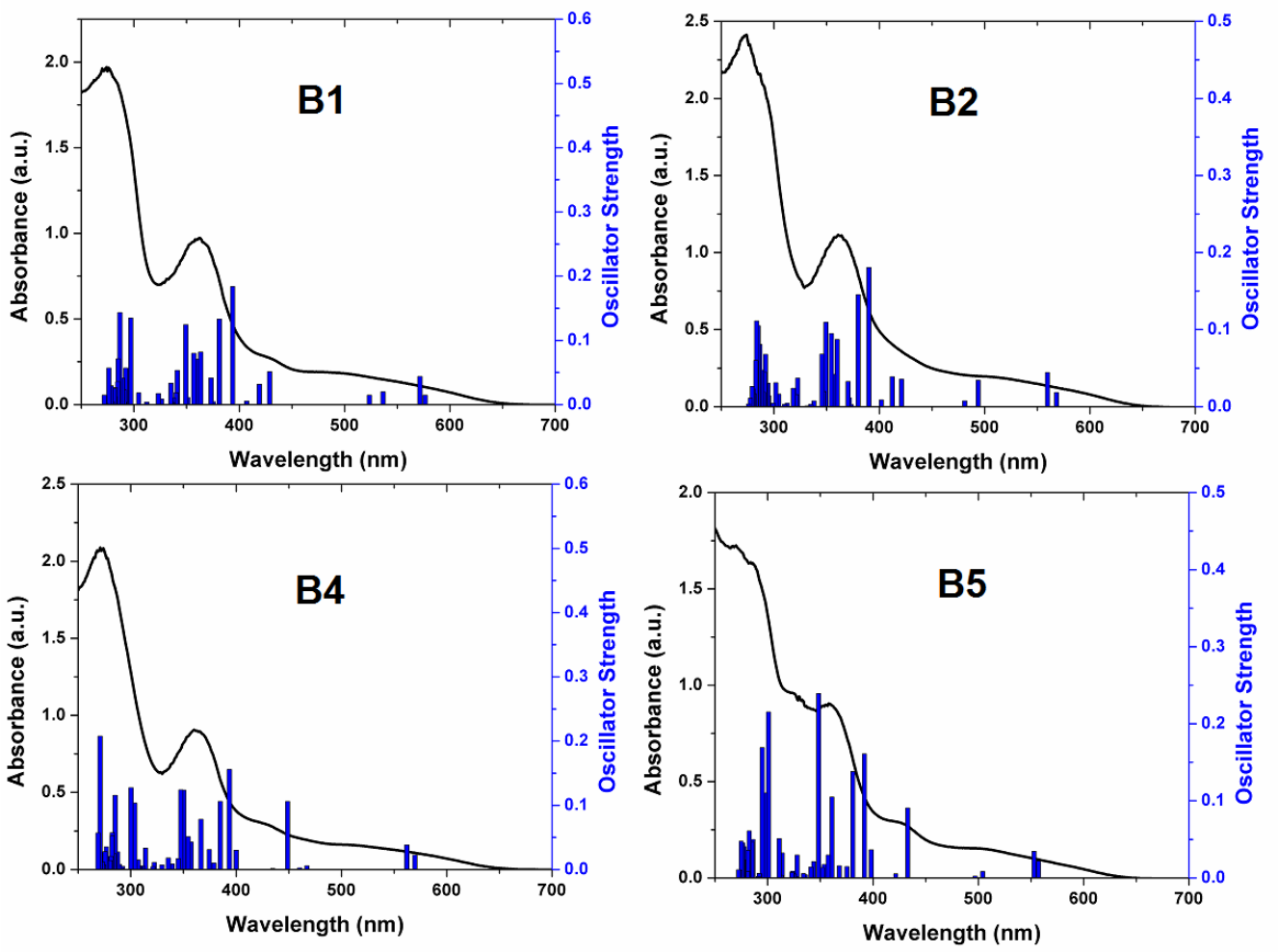

Figure S52. Overlaid experimental UV-Vis spectra and theoretical TD-DFT bars for **B1**, **B2**, **B4** and **B5**.

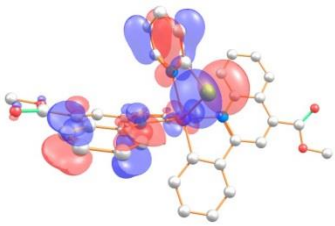	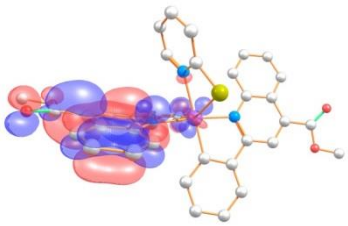
B1 LSOMO (-5.768 eV)	**B1** HSOMO (-3.496 eV)
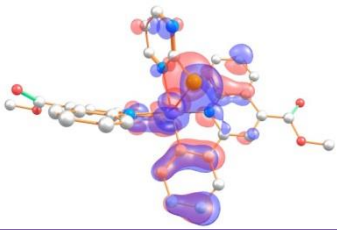	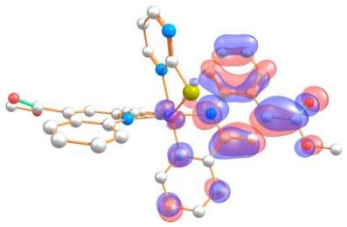
B2 LSOMO (-5.925 eV)	**B2** HSOMO (-3.558 eV)
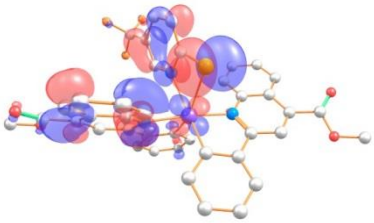	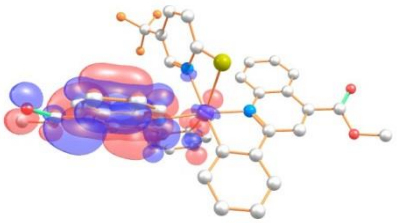
B3 LSOMO (-5.849 eV)	**B3** HSOMO (-3.562 eV)
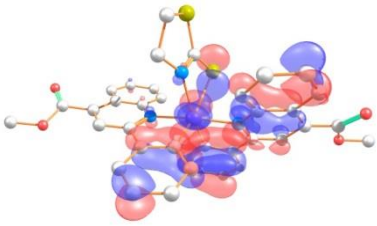	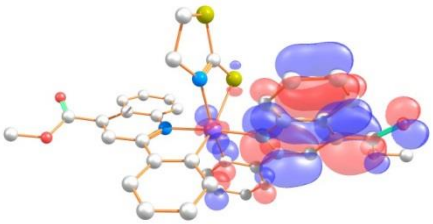
B4 LSOMO (-5.949 eV)	**B4** HSOMO (-3.571 eV)
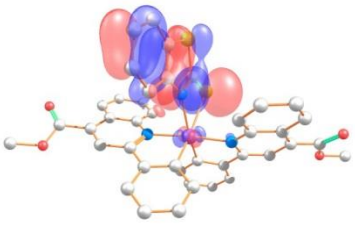	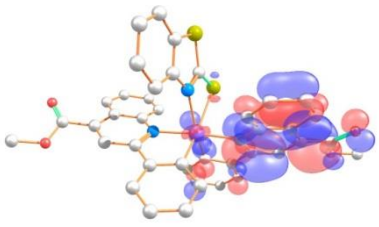
B5 LSOMO (-5.739 eV)	**B5** HSOMO (-3.650 eV)

Figure S53. LSOMO and HSOMO plots of **B1–B5** in T_1 states (CH_2Cl_2 solvent).

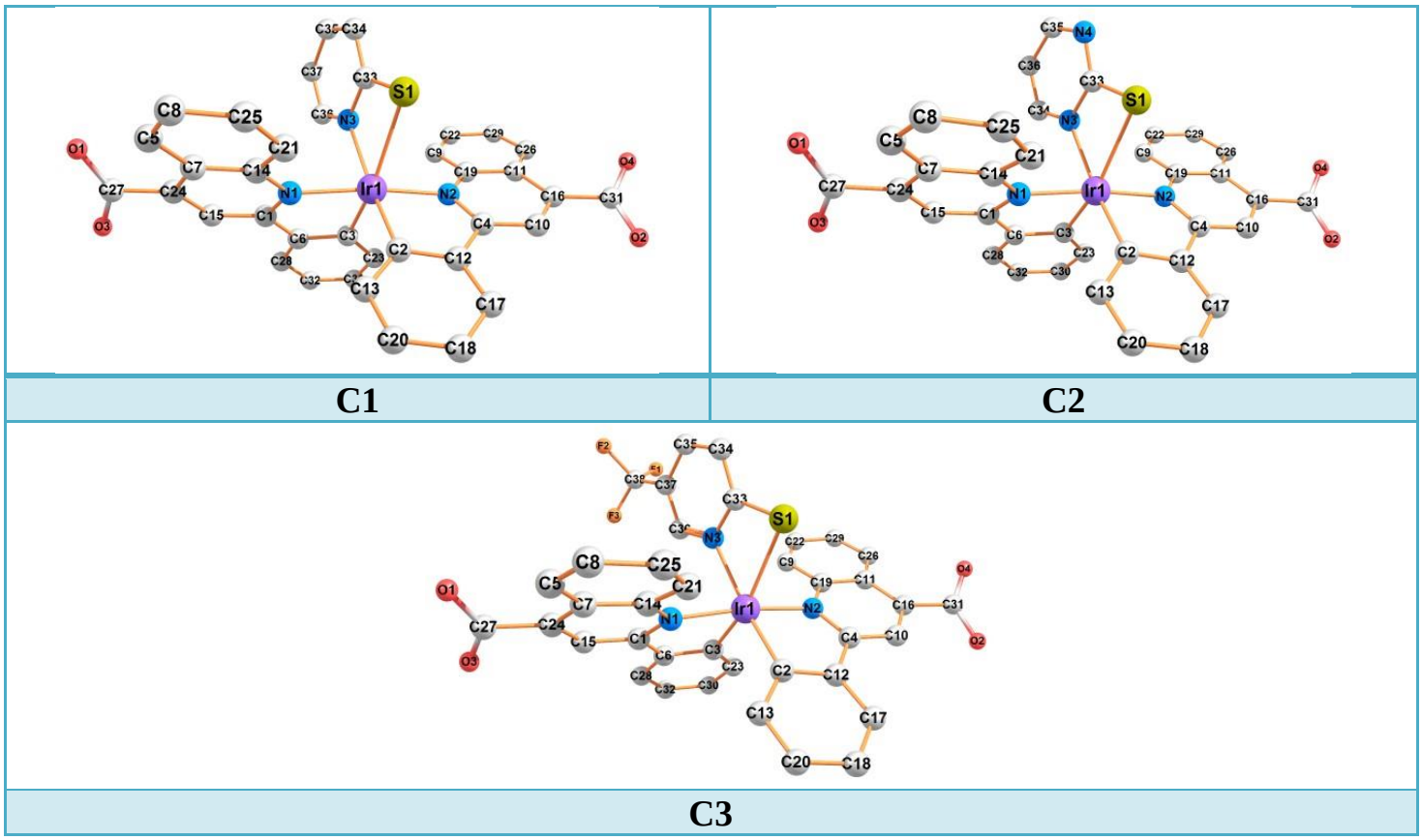

Figure S54. DFT-optimized structures of **C1–C3** in H_2O solvent.

Table S8. Selected geometrical parameters (bond length [Å] and angle [°]) for the DFT-optimized structures of **C1–C3** in H_2O.

C1	C2	C3
Ir1-S1 (2.673)	Ir1-S1 (2.665)	Ir1-S1 (2.680)
Ir1-N3 (2.249)	Ir1-N3 (2.247)	Ir1-N3 (2.253)
Ir1-C2 (2.007)	Ir1-C2 (2.006)	Ir1-C2 (2.005)
Ir1-C3 (2.004)	Ir1-C3 (2.005)	Ir1-C3 (2.003)
Ir1-N2 (2.127)	Ir1-N2 (2.127)	Ir1-N2 (2.128)
Ir1-N1 (2.123)	Ir1-N1 (2.123)	Ir1-N1 (2.123)
N3-Ir1-S1 (63.105)	N3-Ir1-S1 (63.112)	N3-Ir1-S1 (62.819)
N2-Ir1-C2 (79.565)	N2-Ir1-C2 (79.584)	N2-Ir1-C2 (79.584)
N1-Ir1-C3 (79.792)	N1-Ir1-C3 (79.786)	N1-Ir1-C3 (79.842)
S1-Ir1-C3 (160.68)	S1-Ir1-C3 (160.67)	S1-Ir1-C3 (160.36)
N3-Ir1-C2 (167.60)	N3-Ir1-C2 (167.64)	N3-Ir1-C2 (167.67)
N1-Ir1-N2 (173.62)	N1-Ir1-N2 (173.71)	N1-Ir1-N2 (173.66)

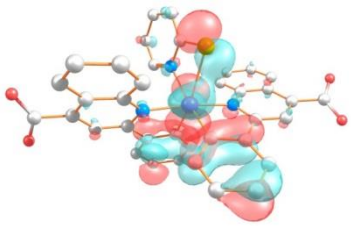	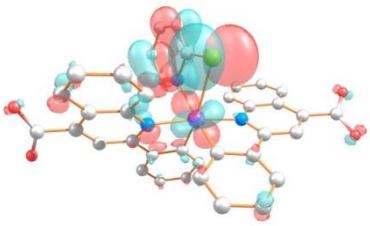	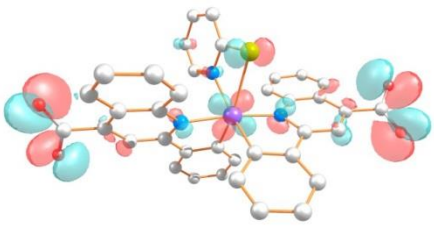
HOMO (-5.071 eV) Ir(44%), S^N(15%), C^N(41%)	HOMO-1 (-5.291 eV) Ir(14%), S^N(69%), C^N(16%)	HOMO-2 (-5.541 eV) Ir(6%), S^N(5%), C^N(89%)
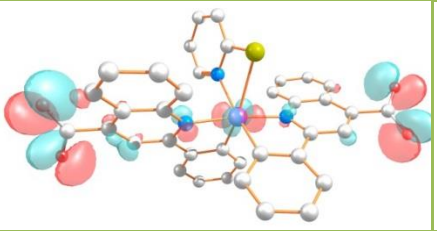	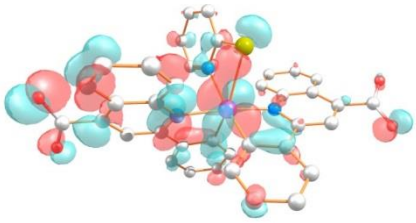	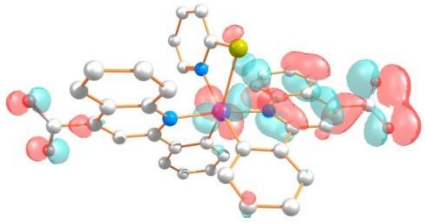
HOMO-3 (-5.556 eV) Ir(5%), S^N(1%), C^N(95%)	HOMO-4 (-5.775 eV) Ir(31%), S^N(10%), C^N(59%)	HOMO-5 (-5.816 eV) Ir(14%), S^N(4%), C^N(83%)
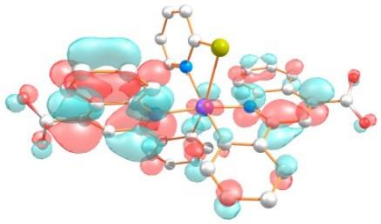	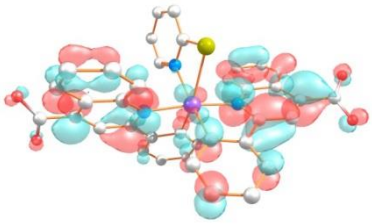	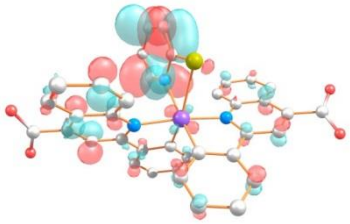
LUMO (-1.817 eV) Ir(4%), S^N(2%), C^N(94%)	LUMO+1 (-1.763 eV) Ir(5%), S^N(2%), C^N(93%)	LUMO+2 (-0.823 eV) Ir(4%), S^N(68%), C^N(29%)
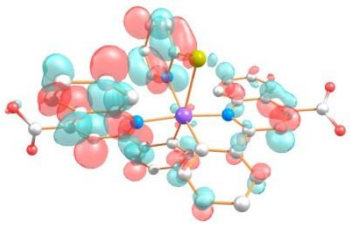	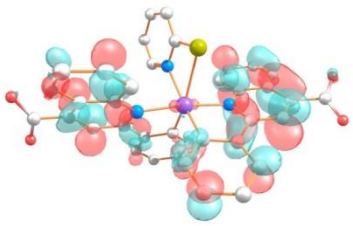	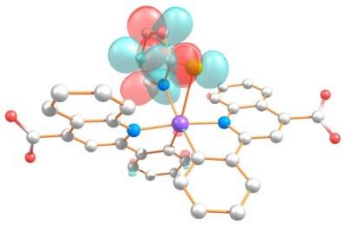
LUMO+3 (-0.767 eV) Ir(1%), S^N(27%), C^N(72%)	LUMO+4 (-0.680 eV) Ir(2%), S^N(1%), C^N(97%)	LUMO+5 (-0.246 eV) Ir(4%), S^N(84%), C^N(12%)

Figure S55. Molecular orbital plots for the optimized structure of **C1** in H_2O solution.

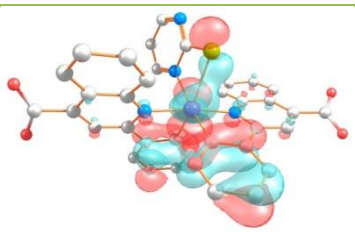	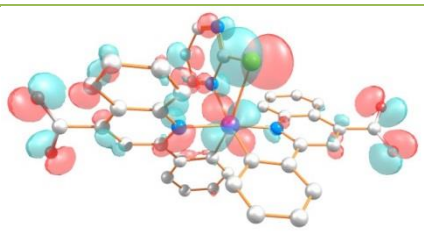	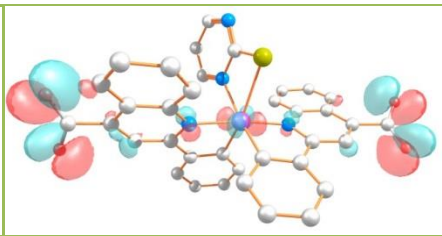
HOMO (-5.126 eV) Ir(46%), S^N(9%), C^N(45%)	HOMO-1 (-5.486 eV) Ir(20%), S^N(33%), C^N(47%)	HOMO-2 (-5.569 eV) Ir(3%), S^N(1%), C^N(96%)
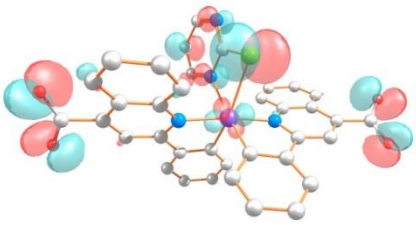	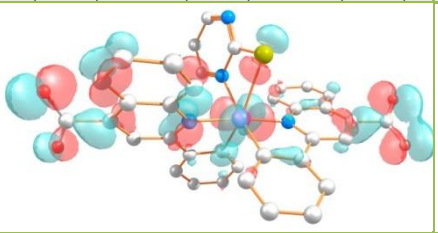	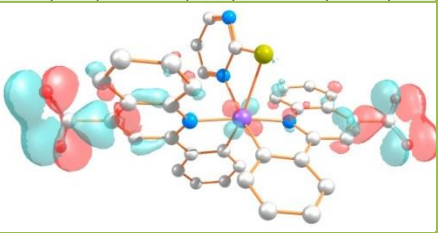
HOMO-3 (-5.601 eV) Ir(4%), S^N(31%), C^N(65%)	HOMO-4 (-5.825 eV) Ir(18%), S^N(5%), C^N(77%)	HOMO-5 (-5.857 eV) Ir(3%), S^N(2%), C^N(95%)
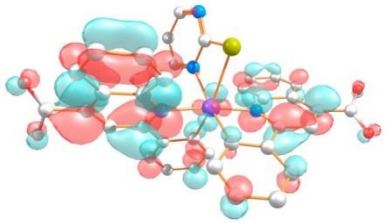	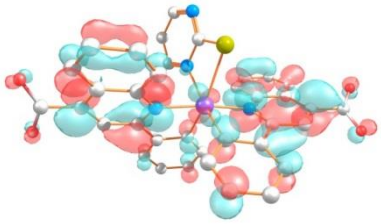	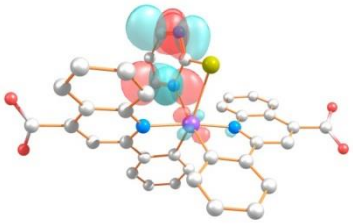
LUMO (-1.849 eV) Ir(4%), S^N(3%), C^N(93%)	LUMO+1 (-1.788 eV) Ir(4%), S^N(3%), C^N(93%)	LUMO+2 (-1.233 eV) Ir(4%), S^N(90%), C^N(6%)
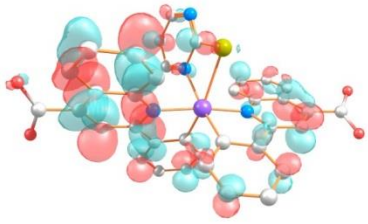	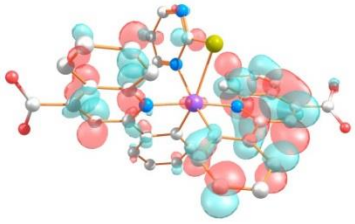	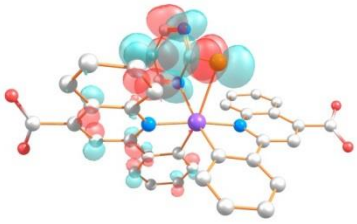
LUMO+3 (-0.805 eV) Ir(1%), S^N(9%), C^N(90%)	LUMO+4 (-0.706 eV) Ir(2%), S^N(6%), C^N(92%)	LUMO+5 (-0.613 eV) Ir(1%), S^N(80%), C^N(19%)

Figure S56. Molecular orbital plots for the optimized structure of **C2** in H_2O solution.

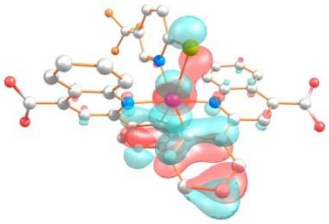	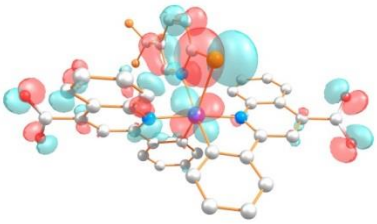	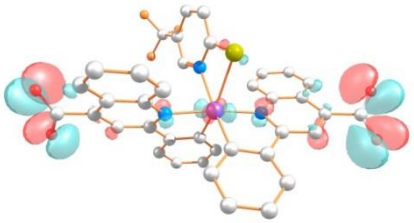
HOMO (-5.133 eV) Ir(45%), S^N(10%), C^N(45%)	HOMO-1 (-5.463 eV) Ir(19%), S^N(49%), C^N(32%)	HOMO-2 (-5.570 eV) Ir(2%), S^N(2%), C^N(96%)
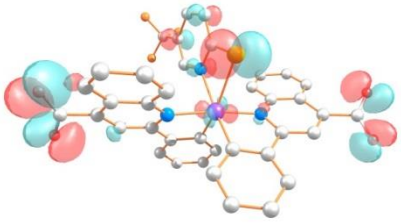	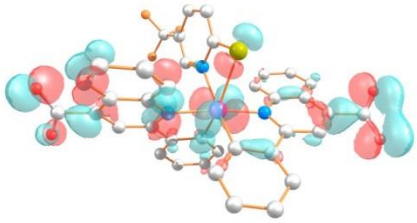	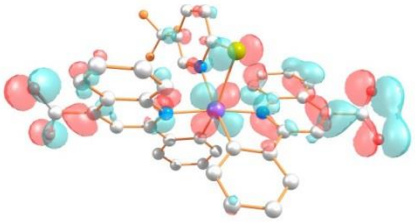
HOMO-3 (-5.582 eV) Ir(2%), S^N(20%), C^N(78%)	HOMO-4 (-5.824 eV) Ir(18%), S^N(6%), C^N(77%)	HOMO-5 (-5.850 eV) Ir(14%), S^N(8%), C^N(79%)
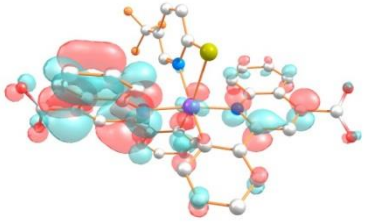	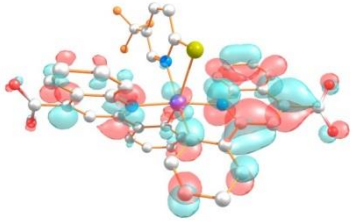	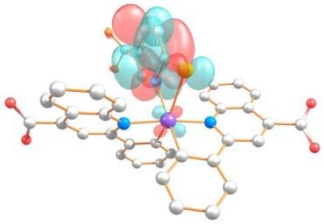
LUMO (-1.851 eV) Ir(4%), S^N(2%), C^N(94%)	LUMO+1 (-1.793 eV) Ir(4%), S^N(3%), C^N(93%)	LUMO+2 (-1.118 eV) Ir(3%), S^N(92%), C^N(5%)
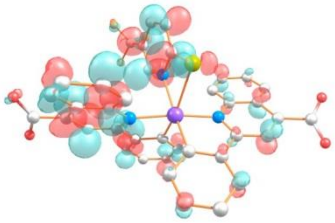	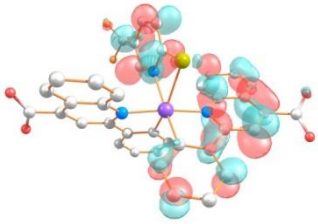	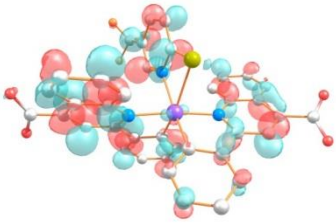
LUMO+3 (-0.850 eV) Ir(2%), S^N(38%), C^N(61%)	LUMO+4 (-0.728 eV) Ir(3%), S^N(37%), C^N(61%)	LUMO+5 (-0.690 eV) Ir(3%), S^N(23%), C^N(74%)

Figure S57. Molecular orbital plots for the optimized structure of **C3** in H_2O solution.

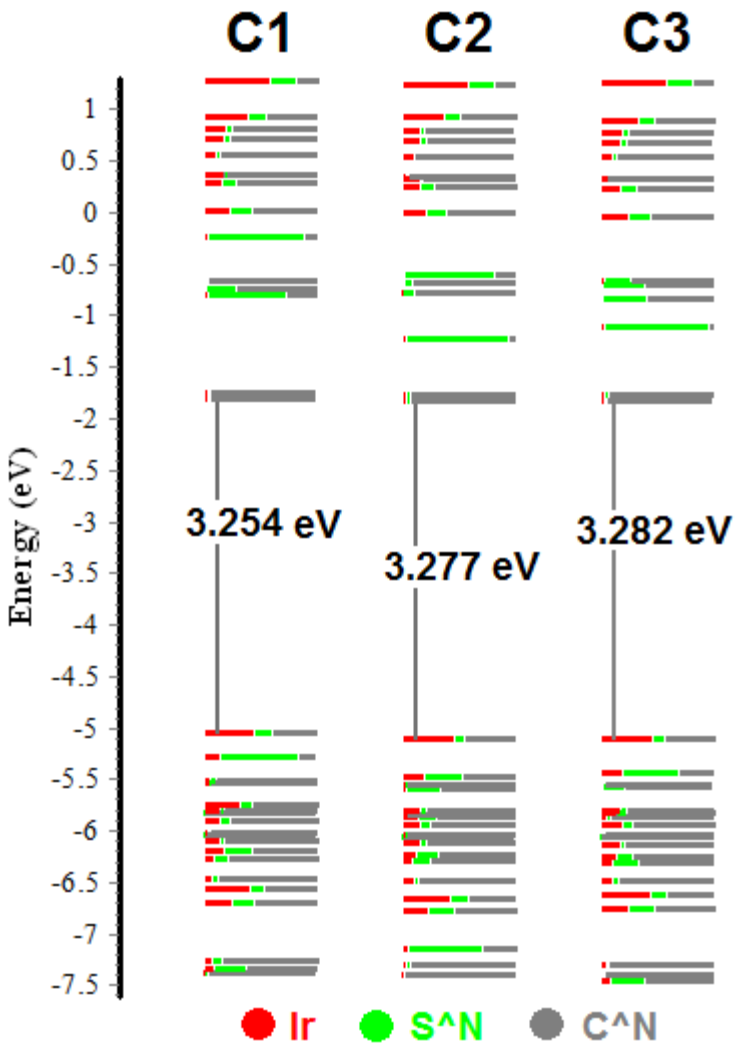

Figure S58. Comparative energy diagram for the molecular orbitals of **C1–C3**.

Table S9. Wavelengths and the nature of transitions for **C1** where M = Ir, L = C^N and L′ = S^N.

Excited state	Calculated λ (nm)	Oscillator strength	Transitions (Major Contribution)	Assignment
1	477.04	0.0057	HOMO→LUMO (98%)	ILCT/MLCT/L′LCT
2	475.72	0.0712	HOMO→L+1 (98%)	ILCT/MLCT/L′LCT
3	434.61	0.0386	H-1→LUMO (97%)	L′LCT/MLCT/ILCT
5	413.65	0.0334	H-3→LUMO (25%)	ILCT
			H-3→L+1 (24%)	ILCT
			H-2→LUMO (42%)	ILCT
12	354.70	0.0911	H-7→LUMO (15%)	ILCT/MLCT/L′LCT
			H-7→L+1 (15%)	ILCT/MLCT/L′LCT
			H-5→LUMO (19%)	ILCT/MLCT
			H-5→L+1 (17%)	ILCT/MLCT
16	343.43	0.0715	H-9→LUMO (31%)	ILCT
			H-9→L+1 (15%)	ILCT
			H-8→LUMO (30%)	ILCT/MLCT
			H-6→LUMO (11%)	ILCT
19	335.98	0.1242	H-10→LUMO (25%)	ILCT/MLCT
			HOMO→L+3 (46%)	ILCT/MLCT/ML′CT
22	329.29	0.0623	H-7→L+1 (19%)	ILCT/MLCT/L′LCT
			HOMO→L+4 (29%)	ILCT/MLCT/L′LCT
25	326.74	0.0469	H-1→L+2 (36%)	IL′CT/ILCT/MLCT
			HOMO→L+4 (37%)	ILCT/MLCT/L′LCT
32	309.13	0.0479	H-1→L+4 (54%)	L′LCT/MLCT/ILCT
			HOMO→L+6 (12%)	ILCT/IL′CT
45	285.97	0.0625	H-6→L+3 (15%)	ILCT/LL′CT
			H-6→L+4 (12%)	ILCT
			H-4→L+3 (19%)	ILCT/MLCT/IL′CT

Table S10. Wavelengths and the nature of transitions for **C2** where M = Ir, L = C^N and L′ = S^N.

Excited state	Calculated λ (nm)	Oscillator strength	Transitions (Major Contribution)	Assignment
1	473.50	0.0095	HOMO→LUMO (95%)	ILCT/MLCT/L′LCT
2	470.22	0.0702	HOMO→L+1 (95%)	ILCT/MLCT/L′LCT
3	418.38	0.0811	H-2→L+1 (25%)	ILCT
			H-1→LUMO (59%)	ILCT/MLCT/L′LCT
9	383.87	0.0256	H-5→LUMO (42%)	ILCT
			H-4→L+1 (25%)	ILCT/MLCT
11	366.19	0.0346	H-6→LUMO (25%),	ILCT/MLCT/L′LCT
			H-6→L+1 (13%)	ILCT/MLCT/L′LCT
			H-4→LUMO (19%)	ILCT/MLCT
			H-4→L+1 (15%)	ILCT/MLCT
17	344.24	0.0519	H-9→LUMO (40%)	ILCT
			H-9→L+1 (19%)	ILCT
			H-8→LUMO (17%)	ILCT
19	337.47	0.0559	H-10→LUMO (54%)	ILCT/MLCT/L′LCT
21	334.75	0.0779	HOMO→L+3 (77%)	ILCT/MLCT/IL′CT
23	329.85	0.0631	H-10→LUMO (10%)	ILCT/MLCT/L′LCT
			H-7→L+1 (15%)	ILCT/MLCT/L′LCT
			H-5→LUMO (13%)	ILCT
			HOMO→L+4 (13%)	ILCT/MLCT/L′LCT
28	320.25	0.0684	H-11→LUMO (11%)	ILCT/MLCT/L′LCT
			H-11→L+1 (38%)	ILCT/MLCT/L′LCT
35	304.38	0.0693	HOMO→L+6 (29%)	ILCT/IL′CT
39	299.88	0.0522	H-3→L+3 (12%),	ILCT/L′LCT
			H-2→L+3 (36%)	ILCT
			H-1→L+4 (12%)	ILCT/MLCT/L′LCT

Table S11. Wavelengths and the nature of transitions for **C3** where M = Ir, L = C^N and L′ = S^N.

Excited state	Calculated λ (nm)	Oscillator strength	Transitions (Major Contribution)	Assignment
1	473.09	0.0344	HOMO→LUMO (81%)	ILCT/MLCT/L′LCT
			HOMO→L+1 (17%)	ILCT/MLCT/L′LCT
2	469.11	0.0450	HOMO→LUMO (17%)	ILCT/MLCT/L′LCT
			HOMO→L+1 (81%)	ILCT/MLCT/L′LCT
3	419.79	0.0595	H-3→LUMO (22%)	ILCT/L′LCT
			H-2→LUMO (11%)	ILCT
			H-2→L+1 (11%)	ILCT
			H-1→LUMO (47%)	ILCT/L′LCT
4	415.45	0.0213	H-3→L+1 (12%)	ILCT/L′LCT
			H-2→LUMO (25%)	ILCT
			H-2→L+1 (10%)	ILCT
			H-1→LUMO (14%)	ILCT/L′LCT
8	383.98	0.0195	H-6→LUMO (13%)	ILCT/MLCT
			H-4→L+1 (47%)	ILCT/MLCT
12	366.41	0.0370	H-7→LUMO (17%)	ILCT/MLCT/L′LCT
			H-4→LUMO (27%)	ILCT/MLCT
			H-4→L+1 (11%)	ILCT/MLCT
15	349.23	0.0477	H-7→L+1 (26%)	ILCT/MLCT/L′LCT
			H-6→L+1 (18%)	ILCT/MLCT
			H-5→L+1 (13%)	ILCT/MLCT
19	337.14	0.0697	H-10→LUMO (47%)	ILCT/MLCT/L′LCT
21	334.27	0.0634	H-10→L+1 (21%)	MLCT/ILCT/L′LCT
			H-6→L+1 (12%)	ILCT/MLCT
			H-1→L+2 (25%)	IL′CT/LL′CT/ML′CT
24	327.02	0.0628	HOMO→L+4 (46%)	ILCT/MLCT/ML′CT
27	320.66	0.0500	H-11→L+1 (53%)	MLCT/ILCT/L′LCT
34	307.71	0.0729	H-2→L+2 (13%)	LL′CT
			H-1→L+3 (15%)	ILCT/IL′CT/MLCT/ML′CT
			HOMO→L+6 (25%)	IL′CT/ILCT
42	297.01	0.0826	H-2→L+4 (10%)	ILCT/LL′CT
			H-1→L+4 (13%)	ILCT/IL′CT/MLCT/ML′CT
			H-1→L+5 (35%)	ILCT/IL′CT/MLCT/ML′CT

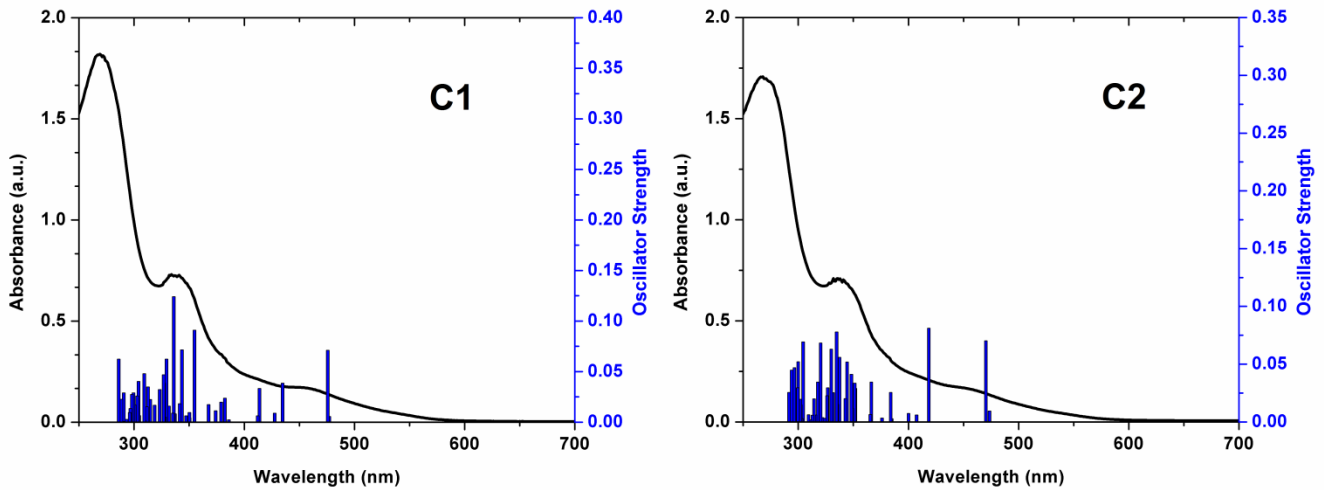

Figure S59. Overlaid experimental UV-Vis spectra and theoretical TD-DFT bars for **C1** and **C2**.

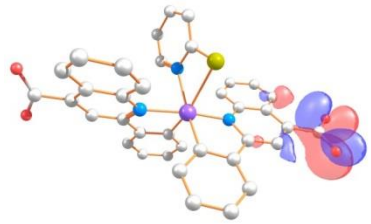	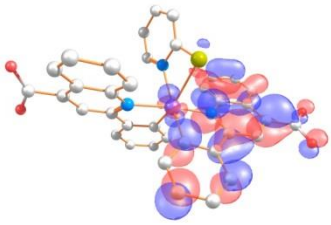
C1 LSOMO (-5.105 eV)	**C1** HSOMO (-2.986 eV)
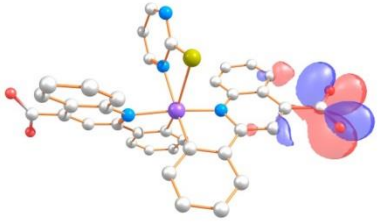	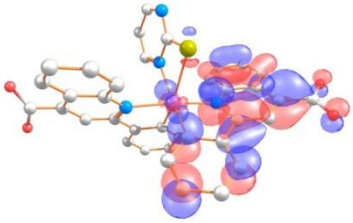
C2 LSOMO (-5.134 eV)	**C2** HSOMO (-3.065 eV)
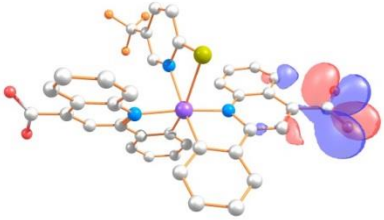	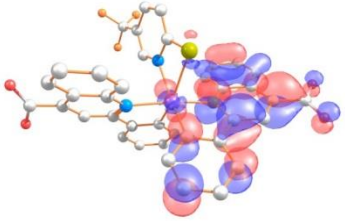
C3 LSOMO (-5.148 eV)	**C3** HSOMO (-3.092 eV)

Figure S60. LSOMO and HSOMO plots of **C1–C3** in T_1 states (H_2O solvent).

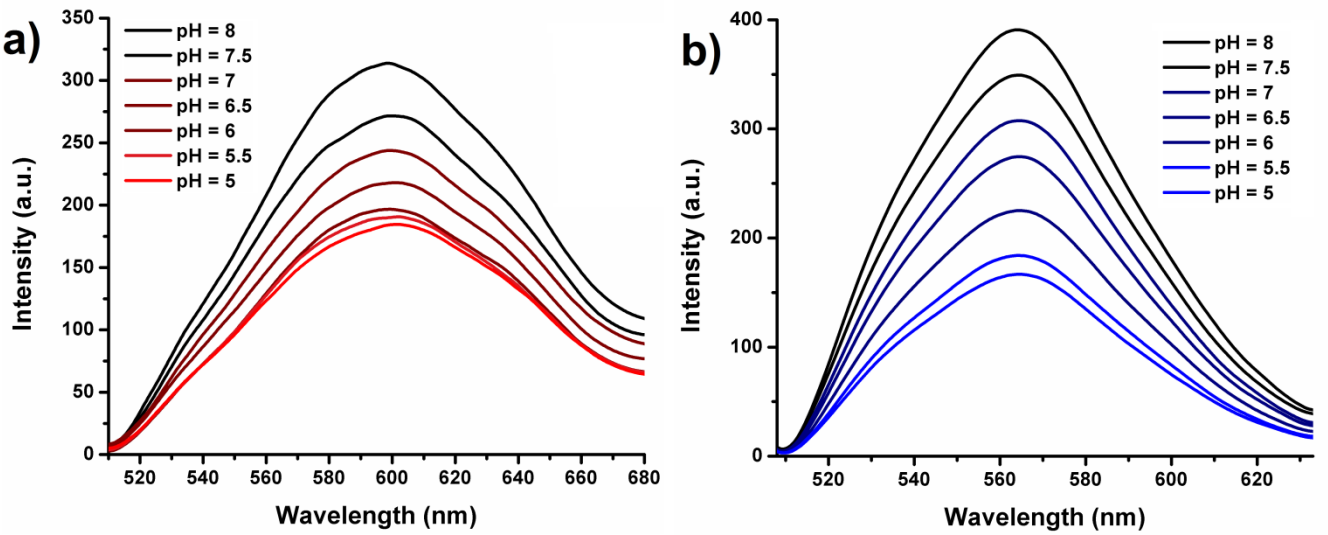

Figure S61. Change in the emission spectra of a) **C1** and b) **C2** in degassed phosphate buffer solutions with different pH values ranging from 5–8.

Table S12. Lifetime, QY, k_r and k_{nr} values for **C1–C3** in different pH ranging from 5–8.

	Lifetime (ns)			**QY**			**k_r (10^4) [s^{-1}]**			**k_{nr} (10^4) [s^{-1}]**		
pH	**C1**	**C2**	**C3**	**C1**	**C2**	**C3**	**C1**	**C2**	**C3**	**C1**	**C2**	**C3**
5	77	115	155	0.0007	**0.002**	**0.017**	0.90	1.73	10.96	1297.79	867.82	634.19
5.5	112	138	195	0.003	0.008	0.023	2.67	5.79	11.79	890.17	718.84	501.02
6	126	195	333	0.01	0.019	0.053	7.93	9.74	15.91	785.71	503.07	284.38
6.5	141	240	421	0.022	0.041	0.072	15.60	17.08	17.10	693.61	399.58	220.42
7	144	242	478	0.043	0.059	0.098	29.86	24.38	20.50	664.58	388.84	188.70
7.5	177	277	496	0.061	0.071	0.109	34.46	25.63	21.97	530.50	335.37	179.63
8	190	287	623	0.078	0.097	0.144	41.05	33.79	23.11	485.26	314.63	137.39

Table S13. Crystallographic and structure refinement data for **B2** and **B5**.

	B2	**B5**
Empirical formula	$C_{38}H_{29}IrN_4O_5S$	$C_{41}H_{28}I\ N_3O_4S_2$
Formula weight	845.91	882.98
Temperature	100(2) K	100(2) K
Wavelength	0.71073 Å	0.71073 Å
Crystal system	Triclinic	Triclinic
Space group	P -1	P -1
Unit cell dimensions	a = 9.1852(7) Å b = 12.9336(7) Å c = 13.8984(8) Å α= 96.688(2)°. β= 100.159(2)°. γ = 92.890(2)°.	a = 9.1594(1) Å b = 13.8302(2) Å c = 14.2302(2) Å α= 95.228(1)°. β= 101.461(1)°. γ = 97.684(1)°.
Volume	1609.89(18) $Å^3$	1737.92(4) $Å^3$
Z	2	2
Density (calculated)	1.745 Mg/m^3	1.687 Mg/m^3
Absorption coefficient	4.265 mm^{-1}	4.010 mm^{-1}
F(000)	836	872
Crystal size	0.14 × 0.11 × 0.09 mm^3	0.20 × 0.10 × 0.10 mm^3
Theta range for data collection	2.042 to 28.282°.	2.449 to 28.309°.
Index ranges	-12 ≤ h ≤ 12, -17 ≤ k ≤ 17, -18 ≤ l ≤ 18	-12 ≤ h ≤ 12, -18 ≤ k ≤ 18, -18 ≤ l ≤ 18
Reflections collected	74974	83823
Independent reflections	7583 [R(int) = 0.0286]	8614 [R(int) = 0.0205]
Completeness to theta = 25.242°	96.8 %	99.4 %
Absorption correction	Semi-empirical from equivalents	Semi-empirical from equivalents
Max. and min. transmission	0.7457 and 0.6233	0.7457 and 0.6376
Refinement method	Full-matrix least-squares on F^2	Full-matrix least-squares on F^2
Data / restraints / parameters	7583 / 0 / 446	8614 / 12 / 470
Goodness-of-fit on F^2	1.412	1.126
Final R indices [I>2sigma(I)]	R1 = 0.0284, wR2 = 0.0787	R1 = 0.0140, wR2 = 0.0351
R indices (all data)	R1 = 0.0306, wR2 = 0.0796	R1 = 0.0141, wR2 = 0.0352
Extinction coefficient	n/a	n/a
Largest diff. peak and hole	2.064 and -2.943 $e.Å^{-3}$	1.137 and -0.569 $e.Å^{-3}$

Experimental Section

General Procedures and Materials

^{1}H NMR, ^{13}C{^{1}H}APT NMR and 2D-NMR spectra (^{1}H^{1}H COSY, HMBC, HSQC) were recorded on a Bruker Avance 400 MHz instrument at 298 K. All chemical shifts (δ) are reported in ppm relative to their corresponding external standards ($SiMe_4$ for ^{1}H and ^{13}C) and the coupling constants (*J*) have been expressed in Hz. The instruments for HR ESI-Mass measurement were Q-TOF-MS (Bruker MicroTOF-Q mass spectrometer) in a positive ion electrospray ionization mode or High resolution or Thermo Fisher Scientific Exactive Plus Orbitrap MS System with an electrospray ionization (ESI) probe in a negative mode. 2-Phenyl-quinoline-4-carboxylic acid methyl ester (pqe ligand), iridium(III) chloride hydrate ($IrCl_3.nH_2O$), pyridine-2-thiol (HSpy), pyrimidine-2-thiol (HSpyN), 5-(trifluoromethyl)-pyridine-2-thiol ($HSpyCF_3$), benzothiazole-2-thiol (HSBt), 2-thiazoline-2-thiol (HStz) and all the other chemicals and solvents were purchased from commercial vendors. The reactions were carried out under air atmosphere in common solvents. The solvents were used without any further drying or purifications.

X-ray Structure Determination

The appropriate crystals of **B2** and **B5** were obtained for further characterization by X-ray crystallography technique. These crystals were formed by slow diffusion of a layer of *n*-hexane into CH_2Cl_2 solutions of the complexes. Single crystals of **B2** and **B5** were coated with fluorinated oil and mounted on the goniometer head. X-ray diffraction data were collected at 100(2) K with Mo Kα radiation (λ=0.71073 Å) using ω and fi rotations on a D8 VENTURE Bruker diffractometer. Measured intensities were integrated and corrected for absorption effects with SAINT+[1] and SADABS[2] programs, included in APEX4 package. The structures were solved by direct methods and refined using SHELXL-2018/3.[3] All non-H atoms were refined anisotropically. H atoms were constrained to idealized geometries and refined with a riding model. In the case of **B2**, one of the methyl groups (C13) was found to be disordered over two positions at half occupancy each. For **B5**, lattice CH_2Cl_2 (one molecule at 0.25 occupancy) was found in the asymmetric unit. The crystallographic and structure refinement data for **B2** and **B5** have been collected in Table S13. For both complexes the coordination geometry around the

iridium atom can be rationalized as an intensely distorted octahedron, since the S^N and pqe bite angles are around 65° and 80°, respectively, being much smaller than 90°. The pqe ligands in both crystal structures are not planar and show a relatively considerable curvature in their planes. The dihedral angles between the pqe planes are almost equal to 76° and 74° for the structures of **B2** and **B5**, respectively. The N atoms of the pqe ligands are *trans* to each other while the C ligating atoms are *trans* to S and N atoms of the S^N chelates. The Ir–C bond lengths in each structure are very similar and compare well with those reported for related five-membered iridacycles.

Computational Details

Density functional calculations were performed utilizing the Gaussian09[4] program suite. The optimization of the geometries in the S_0 and T_1 states were carried out without imposing any symmetry constraints using the B3LYP level of theory[5] and implemented in the Gaussian software. Frequency calculations also were performed with optimization to verify the optimized structures with minimum energy. The LANL2DZ basis set was chosen to describe Ir[6] and the 6-31G(d) basis set was chosen for other atoms. The calculations for the electronic absorption spectra by time-dependent DFT (TD-DFT) were performed at the same level of theory and basis sets. The compositions of molecular orbitals and theoretical absorption spectra were plotted using the "Chemcraft version 1.7" software.[7] The details of electronic transitions were obtained by GaussSum software.[8] Solvent effects have been considered by the conductor-like polarizable continuum model (CPCM).[9]

Photophysical Measurements

UV-Vis spectra were performed using a Perkin-Elmer Lambda 25 spectrophotometer. Photoluminescence spectra were recorded on a JASCO FP-8500 or a Jobin-Yvon Horiba Fluorolog 3-11 Tau-3 spectrofluorimeter at room and low temperatures. The luminescence lifetime values in degassed solvents at 25 °C were determined in a Jobin Yvon Horiba Fluorolog operating in the phosphorimeter mode. Luminescence quantum yield values (Φ) were evaluated at room temperature using a comparative method[10] with $[Ru(bpy)_3]^{2+}$ as the standard (Φ_s = 0.04 in water).[11] The pH-dependent luminescence spectra for **C1–C3** were performed in standard phosphate buffer solutions (PBS) with seven different pH values ranging from 5–8 (5, 5.5, 6, 6.5, 7, 7.5 and 8). To achieve the

desired pH values, the appropriate amounts of the KH_2PO_4 and K_2HPO_4 solutions in water (each 0.1 M) were mixed together. Then, for each complex, seven solutions with different pH values were provided at the concentration of 10^{-5} M. Prior to use, the final pH of the solutions were calibrated using a Metrohm 827 pH-meter by addition of very small amount of KH_2PO_4 or K_2HPO_4 solutions as acidic and basic phosphate salts, respectively. The aliquots of 3 mL were taken for the emission measurements in standard cuvette equipped with Teflon septum. The solutions in cuvettes were degassed by bubbling argon gas into the solutions for 15 minutes prior to the emission measurements. Finally, the emission spectra of **C1–C3** in aqueous solutions were yielded using the excitation wavelength of 365 nm.

References

1. Bruker, A., SAINT+ Ver. 6.01/NT: A computer program for data reduction. *Bruker Analytical X-ray systems, Madison, Wisconsin* **1999**, *53719*, 1173.

2. (a) Bruker, A., Inc. APEX3, SAINT, SADABS 2016, Madison. Wisconsin USA; (b) Krause, L.; Herbst-Irmer, R.; Sheldrick, G. M.; Stalke, D., Comparison of silver and molybdenum microfocus X-ray sources for single-crystal structure determination. *J. Appl. Crystallogr.* **2015**, *48*, 3-10.

3. Sheldrick, G. M., Crystal structure refinement with SHELXL. *Acta Crystallogr. C Struct. Chem.* **2015**, *71*, 3-8.

4. Frisch, M. J.; Trucks, G. W.; Schlegel, H. B.; Scuseria, G. E.; Robb, M. A.; Cheeseman, J. R.; Scalmani, G.; Barone, V.; Mennucci, B.; Petersson, G. A.; Nakatsuji, H.; Caricato, M.; Li, X.; Hratchian, H. P.; Izmaylov, A. F.; Bloino, J.; Zheng, G.; Sonnenberg, J. L.; Hada, M.; Ehara, M.; Toyota, K.; Fukuda, R.; Hasegawa, J.; Ishida, M.; Nakajima, T.; Honda, Y.; Kitao, O.; Nakai, H.; Vreven, T.; Montgomery, J. J. A.; Peralta, J. E.; Ogliaro, F.; Bearpark, M.; Heyd, J. J.; Brothers, E.; Kudin, K. N.; Staroverov, V. N.; Keith, T.; Kobayashi, R.; Normand, J.; Raghavachari, K.; Rendell, A.; Burant, J. C.; Iyengar, S. S.; Tomasi, J.; Cossi, M.; Rega, N.; Millam, J. M.; Klene, M.; Knox, J. E.; Cross, J. B.; Bakken, V.; Adamo, C.; Jaramillo, J.; Gomperts, R.; Stratmann, R. E.; Yazyev, O.; Austin, A. J.; Cammi, R.; Pomelli, C.; Ochterski, J. W.; Martin, R. L.; Morokuma, K.; Zakrzewski,

V. G.; Voth, G. A.; Salvador, P.; Dannenberg, J. J.; Dapprich, S.; Daniels, A. D.; Farkas, O.; Foresman, J. B.; Ortiz, J. V.; Cioslowski, J.; Fox, D. J., *Gaussian 09, Revision A.02*. 2016; p Gaussian, Inc., Wallingford CT.

5. (a) Becke, A. D., Density-functional Thermochemistry. III. The Role of Exact Exchange. *J. Chem. Phys.* **1993**, *98*, 5648-5652; (b) Miehlich, B.; Savin, A.; Stoll, H.; Preuss, H., Results obtained with the correlation energy density functionals of Becke and Lee, Yang and Parr. *Chem. Phys. Lett.* **1989**, *157*, 200-206; (c) Lee, C.; Yang, W.; Parr, R. G., Development of the Colle-Salvetti correlation-energy formula into a functional of the electron density. *Phys. Rev. B* **1988**, *37*, 785.

6. (a) Wadt, W. R.; Hay, P. J., Ab initio effective core potentials for molecular calculations. Potentials for main group elements Na to Bi. *J. Chem. Phys.* **1985**, *82*, 284-298; (b) Roy, L. E.; Hay, P. J.; Martin, R. L., Revised basis sets for the LANL effective core potentials. *J. Chem. Theory Comput.* **2008**, *4*, 1029-1031.

7. Chemcraft - Graphical Software for Visualization of Quantum Chemistry Computations. https://www.chemcraftprog.com.

8. O'boyle, N. M.; Tenderholt, A. L.; Langner, K. M., Cclib: a library for package-independent computational chemistry algorithms. *J. Comp. Chem.* **2008**, *29*, 839-845.

9. (a) Cossi, M.; Scalmani, G.; Rega, N.; Barone, V., New developments in the polarizable continuum model for quantum mechanical and classical calculations on molecules in solution. *J. Chem. Phys.* **2002**, *117*, 43-54; (b) Barone, V.; Cossi, M.; Tomasi, J., A new definition of cavities for the computation of solvation free energies by the polarizable continuum model. *J. Chem. Phys.* **1997**, *107*, 3210-3221.

10. Brouwer, A. M., Standards for photoluminescence quantum yield measurements in solution (IUPAC Technical Report). *Pure Appl. Chem.* **2011**, *83*, 2213-2228.

11. Suzuki, K.; Kobayashi, A.; Kaneko, S.; Takehira, K.; Yoshihara, T.; Ishida, H.; Shiina, Y.; Oishi, S.; Tobita, S., Reevaluation of absolute luminescence quantum yields of standard solutions using a spectrometer with an integrating sphere and a back-thinned CCD detector. *Phys. Chem. Chem. Phys.* **2009**, *11*, 9850-9860.